

## **General Disclaimer**

### **One or more of the Following Statements may affect this Document**

- This document has been reproduced from the best copy furnished by the organizational source. It is being released in the interest of making available as much information as possible.
- This document may contain data, which exceeds the sheet parameters. It was furnished in this condition by the organizational source and is the best copy available.
- This document may contain tone-on-tone or color graphs, charts and/or pictures, which have been reproduced in black and white.
- This document is paginated as submitted by the original source.
- Portions of this document are not fully legible due to the historical nature of some of the material. However, it is the best reproduction available from the original submission.

8

NASA CR-147439

Made available under NASA sponsorship in the interest of early and wide dissemination of Earth Resources Survey Program information and without liability for any use made thereof.

THE USEFULNESS OF SKYLAB/EREP S-190 AND S-192  
IMAGERY IN MULTISTAGE FOREST SURVEYS

E76-10197  
CR-147439

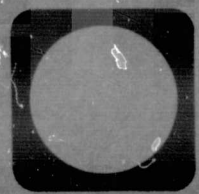
Dr. Philip G. Langley, Principal Investigator  
Dr. Jan van Roessel, Co-investigator  
Earth Satellite Corporation  
2150 Shattuck Avenue  
Berkeley, California 94704

(E76-10197) THE USEFULNESS OF SKYLAB/EREP S-190 AND S-192 IMAGERY IN MULTISTAGE FOREST SURVEYS Final Report (Earth Satellite Corp., Berkeley, Calif.) 134 p HC \$6.00 N76-18616  
CSCL 02F G3/43 00197 Unclas

January, 1976  
Final Report, Type III

Prepared for  
LYNDON B. JOHNSON SPACE CENTER  
Houston, Texas 77058

EARTH SATELLITE CORPORATION (EarthSat)  
7222 47th St. (Chevy Chase), Washington, D. C. 20015  
2150 Shattuck Avenue, Berkeley, California 94704  
(301) 652-7130 (415) 845-5140



1. Report No.	2. Government Accession No.	3. Recipient's Catalog No.	
4. Title and Subtitle The Usefulness of SKYLAB/EREP S-190 and S-192 Imagery in Multistage Forest Surveys		5. Report Date January, 1976	
		6. Performing Organization Code	
7. Author(s) Philip G. Langley, Jan van Roesel <i>mg</i>		8. Performing Organization Report No. G-091	
9. Performing Organization Name and Address Earth Satellite Corporation 2150 Shattuck Avenue Berkeley, California 94704		10. Work Unit No.	
		11. Contract or Grant No. NAS9-13289	
		13. Type of Report and Period Covered Final Report, Type III	
12. Sponsoring Agency Name and Address Lyndon B. Johnson Space Center Houston, Texas 77058		14. Sponsoring Agency Code	
15. Supplementary Notes <b>ORIGINAL CONTAINS COLOR ILLUSTRATIONS</b>			
16. Abstract This investigation examined the usefulness of SKYLAB/EREP S-190 imagery in increasing the precision of sampling for timber volume in multistage forest surveys. In the designs considered, primary sampling units are as small as one square as defined by the General Land Office Cadastral Survey of the Western United States. A precision annotation system was developed for delineating sample unit corners on S-190A and S-190B imagery and in the S-192 MSS digital tape system. The RMSE of corner location was 90 and 100 meters in the x and y direction, respectively, when annotating S-190A imagery. The potential gain in sampling precision was evaluated through image interpretation experiments utilizing the S-190A, S-190B, and high-flight aerial imagery. As expected, the largest gain was achieved with the high-flight aerial photography. The highest gain attributable to EREP data was achieved with a two-date composite of color IR images which yielded a gain in precision of 43.3 percent. There was no significant difference between the (continued next page)			
17. Key Words (Selected by Author(s))		18. Distribution Statement Original photography may be purchased from: EROS Data Center 10th and Dakota Avenue Sioux Falls, SD 57198	
19. Security Classif. (of this report) Unclassified	20. Security Classif. (of this page) Unclassified	21. No. of Pages 134	22. Price*

\*For sale by the Clearinghouse for Federal Scientific and Technical Information, Springfield, Virginia 22151.

## 16. Abstract (continued)

results obtained from S-190A color versus S-190B color, between S-190A color versus S-190A color IR or between two sampling methods evaluated. There was a significant difference in sampling precision between June and September imagery and between EREP and aircraft imagery.

## PREFACE

Objectives. This SKYLAB investigation had three main objectives. These were (1) to investigate the applicability of EREP S-190A, S-190B, and S-192 data for improving the precision of multistage forest inventories, (2) to develop a precision analytical annotation technique so that sample units as small as one mile square could be reliably located on S-190 images as well as in the coordinate system of the S-192 digital tapes, and (3) to develop an interpretive model capable of deriving forest-related variables from the above EREP data.

Background. The first application of multistage sampling using space and aerial photography for forest surveys was conducted with data obtained by the Apollo 9 astronauts in 1969 (Langley, et al., 1969). While lower altitude aerial photography had been used in forest surveys for many years, the advent of high-altitude aircraft and spacecraft generated an interest in the application of small-scale imagery to these surveys. While the Apollo 9 experiment demonstrated that space imagery could provide data to improve the precision of forest surveys, it remained to be determined if the methods (1) could be applied to sample units prespecified on the ground, (2) could be applied in other areas, and (3) could take advantage of the better resolution and multispectral characteristics of EREP data in forest surveys. Another relatively minor objective was to determine if the sampling method had any significant effect on the gain in precision and stability of timber volume estimates derived from space data. These questions were addressed in the present study.

Scope. The test site used in this investigation was the aggregation of nearly 200 land sections, one square mile in size, in Trinity County, California, owned by the Southern Pacific Land Company. These sections served as primary sample units in experiments aimed at evaluating the gain in sampling precision that could be achieved by introducing SKYLAB-EREP data into the sampling plan.

The first stage sampling methods evaluated for relative gains compared to simple random sampling were stratified, variable probability, and regression.

The precision image annotation system that was developed extended the existing capability of annotating the corners of primary sample units within the geometry of aerial photographs, LANDSAT imagery, and the LANDSAT MSS to SKYLAB-EREP S-190 imagery and S-192 data tapes. Image overlays were produced by computer methods for visually identifying the sample unit corners on each of the image types. Concurrently, the coordinates of the points in the computer tape system can be determined. Hence, specific sample units are addressable over spectral bands and time for interpretation purposes.

The annotation system is capable of correcting for image distortions caused by earth curvature, terrain relief, and systematic distortions inherent in the imaging system.

The image interpretation experiments included a machine-assisted technique using a density slicer and purely human techniques. A number of primary sample units (psu's) were examined and evaluated for the proportion of area exhibiting a specific tonal or color response.

These responses were used in correlation models to determine their relationship to the timber volumes present in each psu. From these data, the potential gain achievable from each image type in each of three sampling methods was determined.

### Results.

1. The RMSE of point location achieved with the annotation system on S-190A imagery was 100 meters and 90 meters in the x and y direction, respectively.

2. The potential gains in sampling precision attributable to space derived imagery ranged from 4.9 to 43.3 percent depending on the image type, interpretation method, time of year, and sampling method applied. These results can be compared with the 55.1 percent gain achieved by means of human interpretation methods applied to high-flight aircraft photography.

3. There was no significant difference in sampling gains achieved with the S-190B color imagery compared to the S-190A color imagery.

4. There was no significant difference in sampling gains when comparing S-190A color with S-190A color IR imagery.

5. Seasonal variation was significant. S-190A products obtained in September yielded higher gains than those obtained in June. S-190A color IR composites from both time periods yielded the highest results of all 190A and 190B products tried. However, no temporal combinations were possible with the S-190B imagery.

6. Using 100 primary sample units as a base under simple random sampling, the revenue made available for incorporating space acquired data into the sample design to estimate timber volume was as high as \$39,400.00.

## TABLE OF CONTENTS

1.0	INTRODUCTION . . . . .	1
1.1	BACKGROUND. . . . .	1
1.2	INVENTORY METHODS EMPLOYING AERIAL PHOTOGRAPHY. . . . .	4
1.2.1	Inventory Designs Using High- and Low-Altitude Photography . . . . .	8
1.2.2	Some Design Considerations . . . . .	9
1.3	THE APOLLO 9 FOREST SURVEY EXPERIMENT . . . . .	10
1.4	THE SOUTHERN PACIFIC TIMBER INVENTORY . . . . .	16
1.4.1	The Sampling Design. . . . .	18
1.4.2	The Second Stage . . . . .	21
1.4.3	The Third Sample Stage . . . . .	23
2.0	OBJECTIVES OF THIS SKYLAB/EREP INVESTIGATION . . . . .	30
3.0	COORDINATE TRANSFORMATIONS . . . . .	33
3.1	INTRODUCTION. . . . .	33
3.2	APPROACH. . . . .	33
3.3	IMAGE ANNOTATION OF 1/40,000 SCALE AERIAL PHOTOGRAPHS. . . . .	34
3.4	IMAGE ANNOTATION OF RB-57 HIGH-FLIGHT PHOTOGRAPHY . . . . .	34
3.4.1	Block Adjustment . . . . .	35
3.4.2	Production of Image Overlays . . . . .	36
3.5	IMAGE ANNOTATION OF SCANNER IMAGES. . . . .	38
3.5.1	Resection Theory . . . . .	38
3.5.2	Coordinate Systems . . . . .	42
3.5.3	Polynomial Fitting of the Residuals. . . . .	43
3.5.4	Experimental Results . . . . .	44
3.5.5	The Production of Image Overlays . . . . .	49

Table of Contents (continued)

4.0	S-190 SPACE AND HIGH-FLIGHT AERIAL INTERPRETATION MODELS. . . . .	52
4.1	INTRODUCTION. . . . .	52
4.2	MULTISPECTRAL COMBINING OF EREP IMAGES. . . . .	54
4.2.1	I <sup>2</sup> S Addcol . . . . .	54
4.3	VP-8 IMAGE ANALYZER . . . . .	57
4.3.1	Results of VP-8 Trials . . . . .	59
4.4	HUMAN INTERPRETATION MODELS . . . . .	60
4.4.1	Space Imagery. . . . .	60
4.4.2	High-Flight Aerial Photography . . . . .	62
4.5	SUMMARY OF RESULTS. . . . .	65
5.0	DIGITAL INTERPRETATION MODELS. . . . .	74
	APPENDIX A. . . . .	76
	APPENDIX B. . . . .	98
	APPENDIX C. . . . .	111
	REFERENCES. . . . .	120

## LIST OF ILLUSTRATIONS

### Figure

- 1 A reproduction made from Apollo 9 infrared color frame 3740 of the Mississippi River Valley . . . . . 11
- 2 Polaroid photography (1/60,000) was taken over each primary sampling unit selected for the first stage in the multistage sample . . . . . 12
- 3 The scaled diagram shows how the two 1/12,000 scale 70mm photo sample strips and 1/2,000 scale 70mm color samples are related to each other and to the 1/60,000 scale polaroid photography . . . . . 13
- 4 This 1/12,000 scale photography, enlarged approximately two times, was taken from one of the sample strips flown over the area shown in Figure 2, according to the configuration indicated in Figure 3. . . . . 14
- 5 A 1/2,000 scale photograph showing a portion of the area covered by Figure 4 . . . . . 15
- 6 An optical dendrometer was used to make bole measurements on four to six trees on each ground plot. . . . . 17
- 7 An example of the "checkerboard" layout of SP lands . . . . . 19
- 8 Three-stage sampling layout of the SP timber inventory. . . . . 22
- 9 Flow diagram of space and aerial overlay manufacture for delineating sample unit boundaries . . . . . 37
- 10 Examples of parcels annotated on a 1/126,000 scale high-flight photograph . . . . . 39
- 11 S-190A color, June, 1973 . . . . . 45
- 12 S-190A color IR, June, 1973. . . . . 45
- 13 S-190A color, September, 1973. . . . . 46
- 14 S-190A color IR, September, 1973 . . . . . 46

List of Illustrations (continued)

Figure

15	S-190A color IR, June/September, 1973 composite. . . . .	47
16	S-190B color, September, 1973. . . . .	47
17	Hypsocline chart of Digital Terrain Model. . . . .	51
18	Shade print of test area produced from S-192 digital tape . . . . .	75

APPENDICES:

A1	Apollo 9 timber inventory study, western Georgia. Estimated volume vs. photo volume at first stage . . . . .	91
A2	Apollo 9 timber inventory study, Atlanta area. Estimated vs. photo volume at first stage. . . . .	92
A3	Apollo 9 timber inventory study, Atlanta area. Estimated vs. photo volume after translation of X scale. . . . .	93
A4	Apollo 9 timber inventory study, Mississippi Valley pine stratum. Estimated vs. photo volume at first stage. . . . .	94
A5	Apollo 9 timber inventory study, Mississippi Valley bottomland hardwood stratum. Estimated vs. photo volume at first stage. . . . .	95
A6	Apollo 9 timber inventory study, Mississippi Valley bottomland hardwood stratum. Estimated vs. photo volume after translation of X scale. . . . .	96

## LIST OF TABLES

### Table

1	Selected statistics from the Southern Pacific timber inventory . . . . .	26
2	Optimum allocation data for one survey unit (Southern Pacific timber inventory). . . . .	27
3	RMSEs for resection of Landsat 1 MSS images 103 and 104. . . . .	48
4	Results of the high-flight photo interpretation experiment . . . . .	64
5	Selected statistics from the space and aerial image interpretation trials employing one-square-mile sample units and comparison of alternative sampling methods . . . . .	66
6	Revenue made available for image interpretation under three sampling methods compared to a base of 100 primary sample units under simple random sampling . . . . .	68

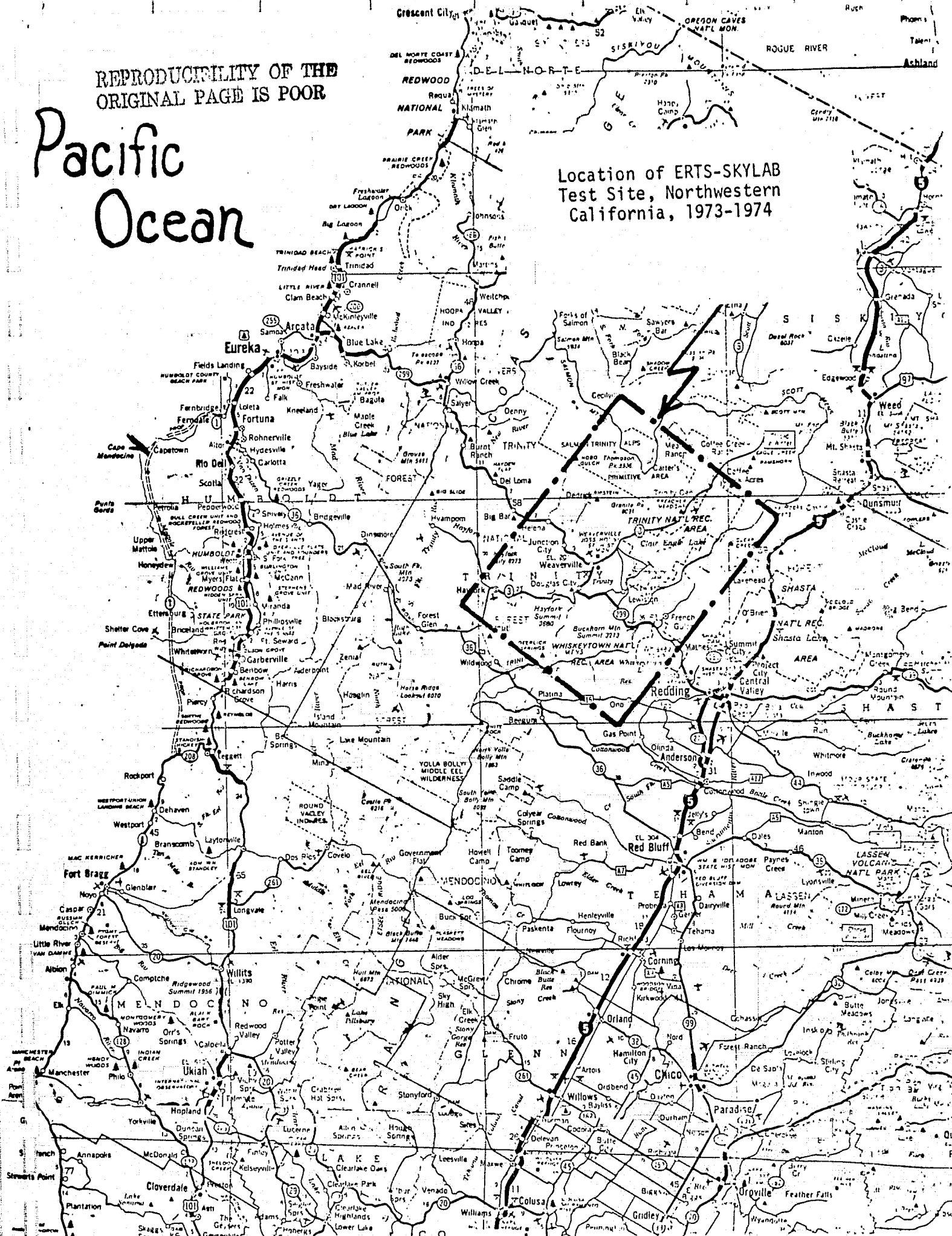
### APPENDICES:

A.1	Illustration of the reduction of the sample variance with variance probability sampling. . . . .	80
A.2	Rel-variances of $v_i/p_i$ from the first stage of the Apollo 9 inventory study. . . . .	90

REPRODUCIBILITY OF THE ORIGINAL PAGE IS POOR

# Pacific Ocean

Location of ERTS-SKYLAB Test Site, Northwestern California, 1973-1974



THE USEFULNESS OF SKYLAB/EREP S-190 AND S-192 IMAGERY  
IN MULTISTAGE FOREST SURVEYS

1.0 INTRODUCTION

1.1 BACKGROUND

One of the great potential benefits of remote sensing from space is the increased ability to inventory and evaluate earth resources. In forestry, as in other areas, this offers an opportunity to develop dynamic resource inventory systems to provide current statistics needed in management planning, economic development, and policy formulation.

Many private organizations, federal and state agencies, and foreign governments conduct forest surveys on a regular basis to determine the quantity, quality, and distribution of timber resources within areas of particular interest to them. Most of these surveys are conducted periodically at five-, ten-, or even twenty-year intervals. However, the increasing pace of wood utilization, coupled with the increasing pressure on available forest land from diverse user groups, particularly in the U.S., is making it increasingly difficult just to keep up with the changes in the forest resource picture. What will ultimately be needed to help ease this situation is a forest resource inventory system able to provide timely estimates efficiently. The advent of space acquired imagery, with its potential uniformity of coverage over large areas, should contribute significantly toward attaining this goal.

During the spring and summer of 1969, a multistage forest survey experiment was conducted on approximately 10 million acres in the

Mississippi Valley area and Georgia using Apollo 9 photography, three scales of aerial photography, and ground data. Among the objectives of that pilot survey were (1) to demonstrate in a preliminary fashion the applicability of a new sampling theory to resource surveys, and (2) to show how the information obtainable from space imagery could be profitably utilized to reduce the sampling error of the timber volume estimates obtained from the survey.

The sampling theory used in the Apollo 9 study, and extended in the present SKYLAB investigation, was developed by P. G. Langley, the principal investigator, as a needed addition to the body of general theory which deals with resource sample surveys using space- and aerial-derived information.<sup>1/</sup> Some of the theoretical properties of the multi-stage variable probability sampling estimator were developed also by Langley for the Earth Resources Survey Program, Office of Space Sciences and Applications, NASA. The investigation is titled, "The Development of an Earth Resources Information System Using Aerial Photographs and Digital Computers" (Langley, et al., 1970). The optimum allocation theory was completed during the present SKYLAB investigation.

While the Apollo 9 study proved successful in its objectives and the study clearly demonstrated the potential of space imagery in earth resources surveys and information systems, it also highlighted the fact that much

---

<sup>1/</sup> This general theory has proved particularly useful for management plan inventories that are developed in conjunction with resource information systems. The information stored in these systems is frequently used to generate supplementary variables for use in the sample design. The results of sample surveys may be subsequently used to improve the information system. Thus, the information system may continually improve and each resource survey may become more efficient.

development work must be conducted in multispectral image interpretation and processing before space imagery can be effectively utilized in operational earth resource survey systems. A subsequent paper (Langley, 1971) outlined some of the problems and opportunities in detail and was presented at the Earth Resources Session of the XXIst Congress of the International Astronautical Federation, Constance, West Germany. The concept of a broadly based resource information system with updating provided by satellite monitoring in conjunction with sampling data from aerial photographs and ground measurements was also outlined.

Simultaneously with the work on the development of applications of multistage sampling theory to resource surveys using satellite data, an investigation was being conducted on earth resources information systems by Dr. Jan van Roessel, co-investigator in the present investigation. The investigation, titled, "The Automatic Mapping of Forest Resources Using Digitized Stereopairs of Aerial Photographs," developed many of the basic algorithms and computer programs in analytic photogrammetry, coordinate transformations, and image transformations needed to complete the present work.

The multistage sampling method using space and aircraft imagery, evaluated in this investigation, was an extension of a timber inventory project previously completed by Earth Satellite Corporation for the Southern Pacific Land Company. The multistage inventory method employed that used variable probabilities of sample selection was itself an outgrowth of previous survey techniques that employed aerial photography in concert with field sampling. Therefore, before proceeding with the results of this investigation, we will first review some of the previous

methods most often used, the Apollo 9 survey, and the Southern Pacific Inventory design that was used as a base for the present SKYLAB/EREP investigation. The multistage variable probability theory, the derivation of the optimal allocation formulas, and the derivation of the variances are given in Appendices A and B.

## 1.2 INVENTORY METHODS EMPLOYING AERIAL PHOTOGRAPHY

There have been many techniques proposed for estimating timber volumes by means of aerial photograph. Most of the methods, employing medium- to small-scale aerial photography, have been well described and tested (Aldred, 1971). Double sampling is often employed in conjunction with point sampling where many photo points are marked on aerial photographs. These points, constituting the primary sample, are examined by photo interpreters and predictions relating to the volume of timber per unit of land area are made. Then a subsample is drawn according to one of several rules and these points are visited on the ground where actual volumetric measurements (or estimates) are obtained. This method of sampling is relatively efficient for surveying very large areas in a general way. The California Forest Survey, conducted by the Forest Service, U.S. Department of Agriculture, has used double sampling for stratification for the past several years. Other proposals for the use of double sampling include double systematic sampling for regression with multiple random starts (Shiue and John, 1962), double sampling with regression for estimating Douglas-fir mortality (Wear, 1964), and double sampling with pps (probability proportional to size) selection in the second phase (Schreuder, 1966).

While double sampling employing photo points on medium- to small-scale photography appears to be relatively efficient for general

surveys over large areas, it is usually not suitable for more intensive surveys obtained for management planning on specific tracts of land. Here, the forest manager desires not only information about the forest as a whole, he also desires information about the location of his resources parcel by parcel (or even stand by stand). One of the most commonly used methods for obtaining information to this degree of intensity is to partition the forest into stand categories. This is accomplished by delineating, on the imagery, forest areas that are relatively homogeneous in their makeup of forest trees. Treating the stand delineations as sampling units within strata, a sample is drawn from each stratum according to one of a number of sampling rules. Examples of these sampling rules are simple random, probability proportional to size (as measured by area or predicted timber volume), or simple random with optimum allocation among strata.

After a sample of timber stands is drawn, a subsample of trees or plots is usually located and the volume of timber is measured at each subunit. The measurements are converted to an average volume per unit of area which, when multiplied by the area of the stand, yields an estimate of the total timber volume in the stand.

The stratified stand method of sampling for [estimated] timber volume has generally been considered to be relatively efficient compared to sampling solely on the ground, at least in virgin forests. This is because the cost of stand delineation on aerial photos and the transfer of these delineations to maps of a known scale is relatively low (about \$0.20 to 0.30 per acre) compared to the cost of measuring a plot on the ground (\$40.00 or more per plot). Actual comparative data to substantiate this claim are hard to come by, however.

As logging has progressed across the countryside, the virgin forests have been cut over and many have been replaced by second growth forests. Residual and second growth forests are often more heterogeneous than virgin forests, however, consisting of clumps of trees here and there with a few old residual trees scattered about. In this situation, the possibility of reducing the variation of volume measurements by means of stand stratification on aerial photographs is greatly diminished. The authors have experienced situations in which no gain in sampling efficiency was achieved by stratifying cut-over stands by means of delineation on aerial photographs. This is an important consequence when considering whether or not to include space-acquired data in forest inventories.

In spite of the difficulties of partitioning forest areas into homogeneous stands in heterogeneous stand situations, the forest stand map is still a highly valued tool of the forest manager. If these maps, or their pictorial counterparts, known as orthophotos, are to continue to be used as bases for stratification, other procedures might be considered to counteract the high within-stratum variation often encountered. A second possible alternative to timber stand maps as bases for stratification is EREP S-190B space photography. While individual trees are not discernible, the boundaries of important vegetation categories, such as conifer and hardwood, can be accurately identified.

As mentioned earlier, medium-scale (1/15,000 to 1/20,000) aerial photographs have been used in timber inventories for many years as an aid to management planning. However, these medium-scale photographs

leave much to be desired in the overall efficiency of a resource survey. In many situations, such as the mixed conifer stands on the west slope of the Sierra Nevada mountains in California, the scale is too small for determining species or for pinpointing sample locations on the ground except in a broad way. At the same time, the scale of these photos is too large for survey efficiency because of the relatively small area covered per photo. For example, a 1/15,000 scale photo covers only 1/16 the ground area covered by a 1/60,000 scale photograph, and only 1/256 the ground area covered by a 1/120,000 scale photo such as obtained from the U-2 and RB-57 aircraft. Consequently, a large number of photos is required at 1/15,000 scale to cover an area of even moderate size, thus making handling and mapping costs unnecessarily high. Furthermore, the total information imaged on medium-scale photographs is seldom used except for forest stand mapping--a task which can now be performed using small-scale, high-altitude photographs.

The development of high-altitude aircraft and cameras with finer resolution of detail have made it possible to incorporate photographs of from 1/40,000 to 1/80,000 or even 1/120,000 scale in a forest inventory design. The detail in these photographs, if flown to proper camera-film-filter specifications, appears to be adequate for stand mapping and preliminary volume prediction.

Sample strips of large-scale (1/2,000 to 1/6,000) 70mm color photography drawn with probability proportional to predictions obtained from the high-altitude photographs, can then be re flown using large-scale photography. The large-scale 70mm photographs are easily registered with the high-altitude photos. Furthermore, interpretations can be made

as to tree size and species. From this information, ground samples can be drawn and precisely located on the ground.

### 1.2.1 Inventory Designs Using High-and Low-Altitude Photography

Aldred (1971) made very rigorous analyses of the suitability of various stratified double sampling estimators. In his work, large-scale sample photographs were used to define a large primary sample of photoplots with ground measurement on a relatively small subsample of these plots. Small-scale photos (up to 1/40,000) were used to define the strata. According to Aldred, both the small-and large-scale photos provided gains in sampling efficiency within the range of prescribed conditions he studied. Langley (1961) recognized the potential of high-quality small-scale aerial photos in extensive forest surveys and later developed and applied multistage variable probability sampling theory in a pilot forest survey which utilized Apollo 9 space photography, small-scale aerial imagery, and large-scale 70mm aerial imagery (Langley, et al., 1969). These experiments were also successful, in that a reduction in the estimated sampling error was attained at the high- and low-altitude levels by taking advantage of the additional information provided by the increasingly larger scales of photography. In both Aldred's and Langley's approaches, the high-altitude imagery was used to first partition the target population into strata corresponding to logical categories of distinctive features. Aldred then applied double sampling with large-scale photoplots of such dimensions that a subsample of these could be measured in their entirety on the ground. This was not feasible in the Apollo 9 experiment because the photography obtained from orbital altitudes was of insufficient resolution to allow direct

keying to large-scale aerial imagery. At least one intermediate scale had to be provided and the multistage sampling framework was a convenient method for doing so.

### 1.2.2 Some Design Considerations

In forest inventories using small-scale aerial photographs to make stand measurements and large-scale photographs for more detailed tree measurements, there remain many unanswered questions about the optimal design configuration. For example, the double sampling approach would assume a random drawing of the primary sample within strata. However, for operational efficiency, an aircraft, once on target, can traverse a long strip of a mile or more covering a cluster of ground plots for practically the same cost as covering only 1 plot. Photo interpreters can assess tree characteristics in all the plots in the cluster and select relatively few plots for ground measurement. When this procedure is followed, a gain in efficiency can be realized by selecting individual strips at random with probability proportional to some measure of size obtained from the high-altitude small-scale photography. Hence, one or more sample strips extending clear across the sample units can be drawn with varying probability and large-scale photographs can be obtained of these. After interpreting the large-scale photographs, a small subsample of field plots can be drawn within strips, again with a conditional probability proportional to a measure of size such as predicted volume of timber. Using this general procedure, the operational advantages of clustering are enjoyed at every step. Furthermore, easily obtained information is fully utilized from all levels of photography or other type of imagery.

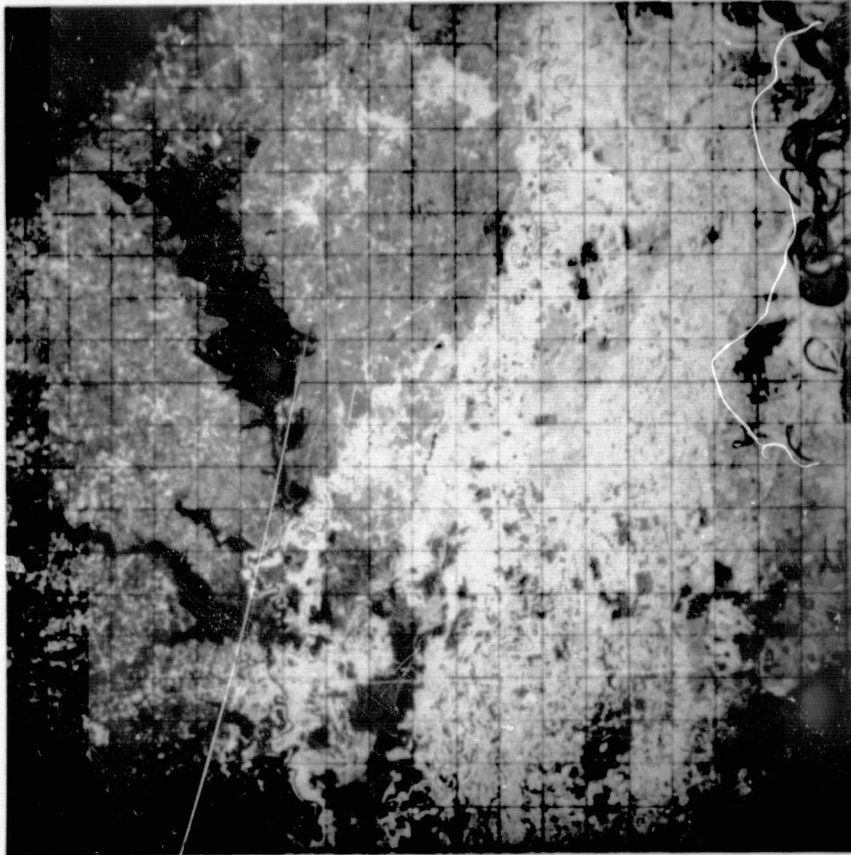
### 1.3 THE APOLLO 9 FOREST SURVEY EXPERIMENT

The flight of Apollo 9 in March of 1969 included photographic experiments (NASA designated Scientific Operation 65) which provided 70mm multispectral photographs of limited areas in the southern United States. These photographs were obtained at a scale of approximately 1/2,225,000 by means of Hasselblad cameras and provided synoptic coverage of approximately five million acres per frame. Four of these frames obtained from Apollo 9, two in the Mississippi Valley area and two in the Atlanta, Georgia area were taken at a time when the weather was clear. Consequently, they provided an outstanding opportunity to apply multistage variable probability (pps) sampling to a forest survey using space and aircraft photography.

The complete description of this trial has been described elsewhere (Langley, et al., 1969, Langley, 1971). The initial trial included the selection of five primary sample units in the Mississippi Valley area and five in the Georgia area. Each primary unit contained a square plot of land approximately four miles on a side and containing 10,240 acres. Within each primary unit, a subsample of two strips was drawn. Each strip was approximately a third of a mile wide and traversed the primary unit.

The third sample stage consisted of triplets of 1/2,000 scale 70mm color photographs within which a sample of one ground plot per strip comprised the fourth stage. Sample trees within the ground plots comprised the fifth stage. Figures 1 through 5 illustrate the nesting of successively larger photo scales that was used in the

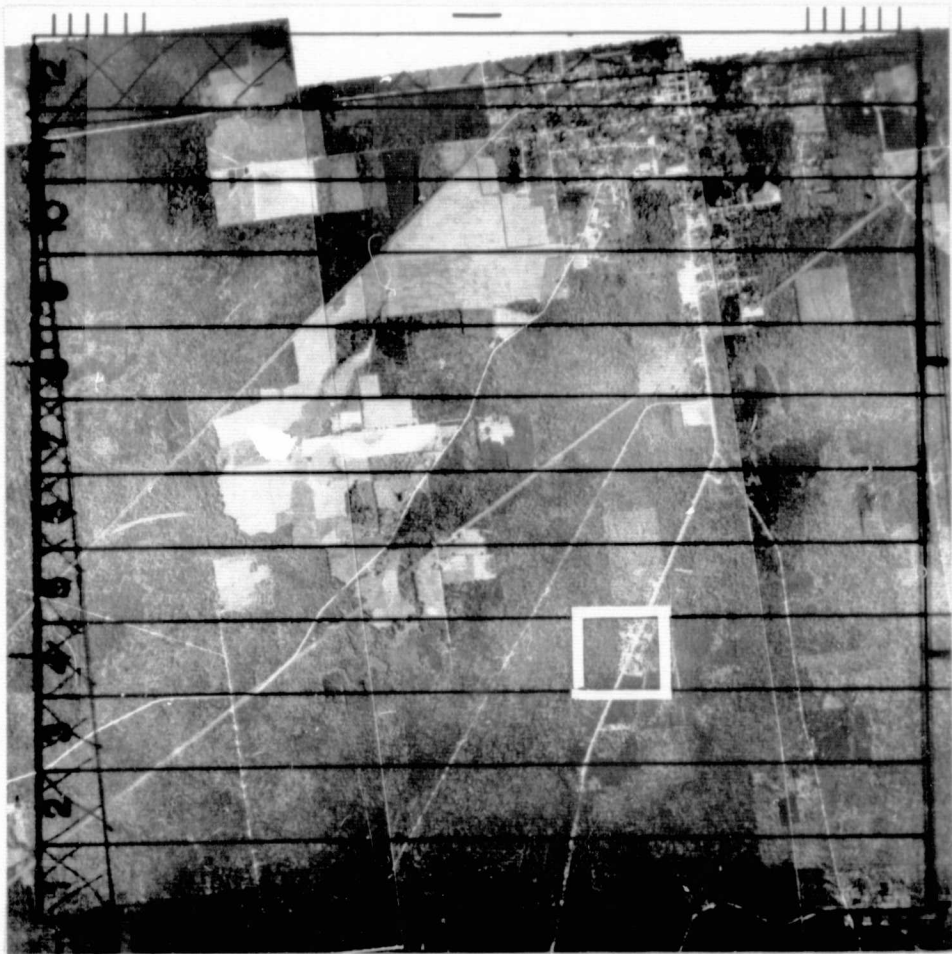
REPRODUCIBILITY OF THE  
ORIGINAL PAGE IS POOR



Courtesy of NASA and  
U.S. Forest Service

Figure 1. A reproduction made from Apollo 9 infrared color frame 3740 of the Mississippi River Valley. Forest areas consisting of upland pine and hardwood are discernible on the left while lowland hardwood areas are discernible on the right intermingled with agricultural lands. The grid of 400 four-by-four-mile squares was used to predict timber volumes for the first level of inventory information. A grid cell was defined as a primary sample unit.

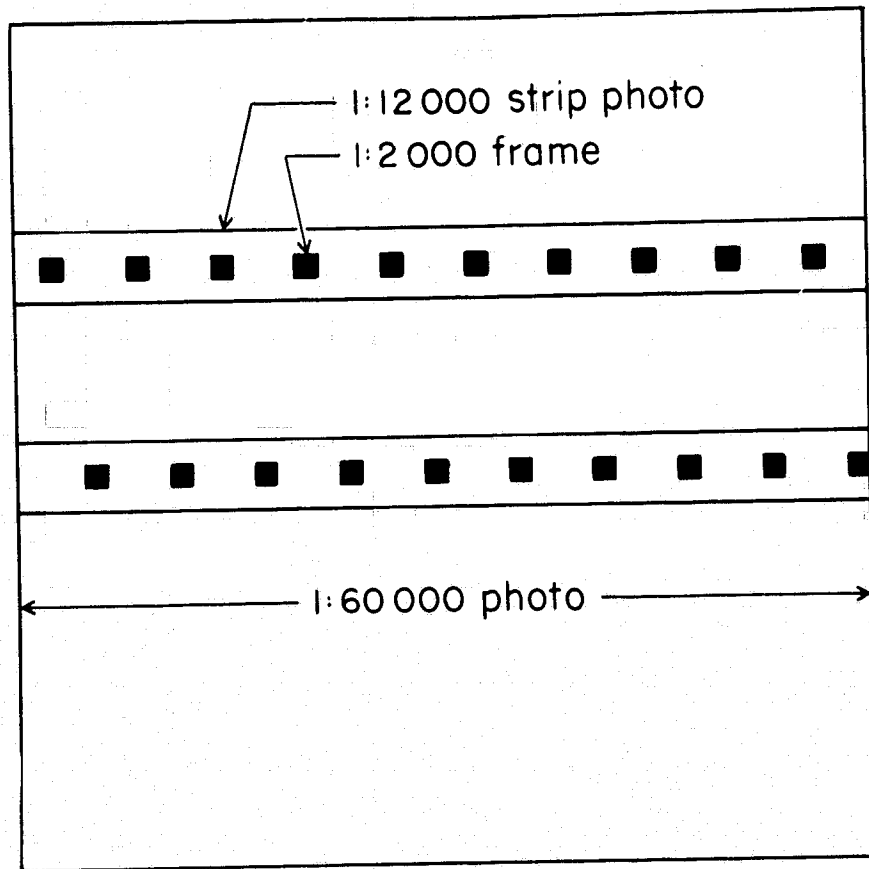
REPRODUCIBILITY OF THE  
ORIGINAL PAGE IS POOR



Courtesy of U.S. Forest Service

Figure 2. Polaroid photography (1/60,000) was taken over each primary sampling unit selected for the first stage in the multistage sample. The mosaic shown is for the four-by-four-mile square indicated by the arrow in the upper center of the space photo in Figure 1.

REPRODUCIBILITY OF THE  
ORIGINAL PAGE IS POOR



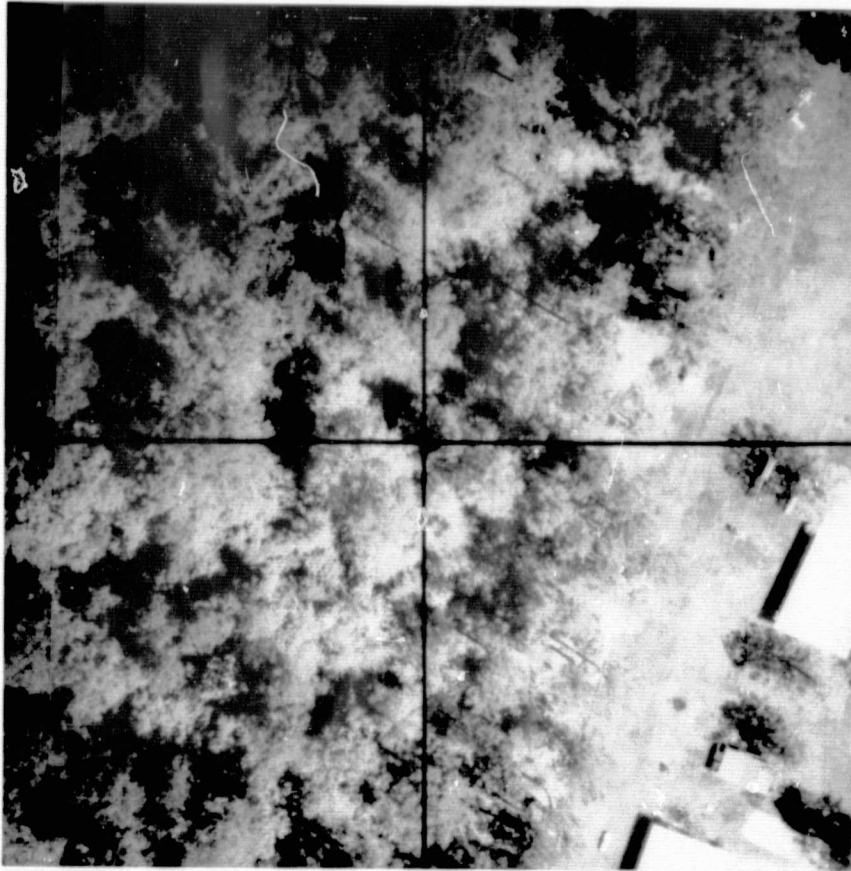
Courtesy of U.S. Forest Service

Figure 3. The scaled diagram shows how the two 1/12,000 scale 70mm photo sample strips and 1/2,000 scale 70mm color samples are related to each other and to the 1/60,000 scale polaroid photography.



Courtesy of U.S. Forest Service

Figure 4. This 1/12,000 scale photography, enlarged approximately two times, was taken from one of the sample strips flown over the area shown in Figure 2, according to the configuration indicated in Figure 3. The area covered is indicated by the square in the lower right-hand portion of the photo in Figure 2.



Courtesy of U.S. Forest Service

Figure 5. A 1/2,000 scale photograph showing a portion of the area covered by Figure 4. The grid divides the photograph into four sample plots approximately .63 acres in size which is convenient for location on the ground and subsequent timber volume measurements.

REPRODUCIBILITY OF THE  
ORIGINAL PAGE IS POOR

Apollo 9 inventory trial. The dendrometer in Figure 6 was used to obtain tree measurements on the ground plots.

The Apollo 9 forest survey experiment demonstrated that it was possible to undertake broad resource surveys beginning with information derived from imagery obtained at orbital altitudes. It also demonstrated that it was feasible to identify from an aircraft and rephotograph large sample areas by means of visual reference to the space imagery.

The information derived from the space photography provided an estimated reduction of 58 percent in precision in the Mississippi Valley area while no gain was achieved in the Georgia area. In evaluating these results, it is important to keep in mind that we had no previous experience in differentiating between forest trees and other vegetation from space imagery. Since that time, new equipments have been developed that allow the simultaneous analysis of several spectral bands. Experiments have been under way by several NASA sponsored investigators to develop new image interpretation techniques that should yield better predictions of forest variables by species groups from orbital altitudes. As these techniques are developed, sample surveys which utilize this information will be improved at the first stage.

#### 1.4 THE SOUTHERN PACIFIC TIMBER INVENTORY

Forest managers more concerned with short- and long-term management planning on specific tracts of land must have detailed resource information pertaining to those tracts. Volume, growth, and number of trees by species and tree size are examples of the kinds of information required.



Courtesy of U.S. Forest Service

Figure 6. An optical dendrometer was used to make bole measurements on four to six trees on each ground plot.

In 1970, the authors, under the auspices of the Earth Satellite Corporation, undertook a timber inventory of a portion of the forest holdings of the Southern Pacific (SP) Land Company. The half-million acre "alternate section" layout of the SP lands, scattered over nearly two million acres in several northern California counties, provided an almost ideal opportunity to implement multistage variable probability sampling using high- and low-altitude aerial photography. In addition to the extensive area covered by the survey, the properties were situated in some of the most rugged terrain in northern California including portions of Trinity County. An example of the "checkerboard" layout of the SP land is shown in Figure 7.

#### 1.4.1 The Sampling Design

The SP Land Company possessed records showing the estimated total volume of timber on each parcel of land within the area of interest. However, since much of the information had come from different sources, there was little indication of the reliability of the figures from parcel to parcel. So while individual parcels, many of which were 640 acres in size, might have made satisfactory primary sample units (psu's), it was decided to cluster them together in the hope of reducing the variation among psu's. The specification for the scale of the high-altitude aerial photography was set at 1/40,000 for several reasons: (1) the effective area of each stereo model would cover approximately 8 square miles of land area, a reasonable amount for timber mapping purposes, (2) individual trees would be discernible for effective timber stand delineation by tree size classes, and (3) when employing the desired focal length of 8-1/4" the required flying height of 27,500 feet

REPRODUCIBILITY OF THE  
ORIGINAL PAGE IS POOR



Courtesy of Earth Satellite Corp.  
and Southern Pacific Land Company

Figure 7. An example of the "checkerboard" layout of SP lands. The photo positions of the section corners, with the effects of tilt and topographic displacement added in, are determined from map data and plotted on the photography by computer methods. The group of four sections showing on this photo makes up one primary sample unit.

above terrain plus an average ground elevation of 5,000 feet put the propeller-driven aircraft at its operational ceiling of 32,500 feet. This latter was an important consideration because switching to a jet aircraft would have entailed a substantially higher cost. At the 1/40,000 photo scale, up to four or five 640-acre sections of SP land would be imaged on the effective area of each photo forming a cluster. Since individual photos were convenient to handle, it was decided to designate the SP lands falling within the effective area of 1/40,000 scale photographs as the psu's.

The company also wished to have the new inventory estimates reported by survey units as well as for the total area. To accomplish this, the survey units were treated as strata and variable probability sampling was undertaken independently within each stratum. The sampling rule was to select psu's with probability proportional to the timber volume shown on the company records. The primary units were drawn with replacement. One hundred ninety two primary units were drawn out of a finite population of nearly 400. As it was to be expected, several psu's were drawn twice. On these occasions, independent sub-sampling was undertaken for each primary draw.

New 1/40,000 scale aerial photography was obtained and the company land was delineated on these photographs (Figure 7). The timber volumes of record at that time were cumulated by photograph and by management unit; then they were transformed to sampling probabilities.

The overall design goal was to arrive at an estimated sampling error (standard error) of approximately 10 percent of total net volume

per management unit when evaluated at the 67 percent confidence level. However, to minimize overall variance, the primary samples were allocated to survey units in proportion to stratum size as measured in units of predicted volume. In this allocation, the error terms and the cost factors were considered to be constant and only the stratum sizes were allowed to vary. All primary sample units were allocated to survey units in this way. The primary sample was then drawn at random (with replacement) with probability proportional to the predicted timber volumes of record at the beginning of the survey.

#### 1.4.2 The Second Stage

The second stage of the sampling plan consisted of strips of 70mm color photography traversing across sample parcels. Because of the alternate section arrangement, each strip was one mile or less in length. To obtain the selection probabilities, each ownership parcel delineated on the high-altitude photographs included in the primary sample was partitioned into strips oriented in a North-South direction. The width of the strips was approximately eight chains so as to include 10 per mile. Figure 8 illustrates the layout of the primary, secondary, and tertiary sampling units.

By means of photo interpretation, a timber volume prediction was obtained for all strips delineated on a sample photograph. These predictions were translated into conditional probabilities and a subsample was drawn in each psu. The number of strips in each draw was approximately proportional to the square root of the size of the psu as measured in terms of predicted timber volume. This was the optimal allocation under the assumption that

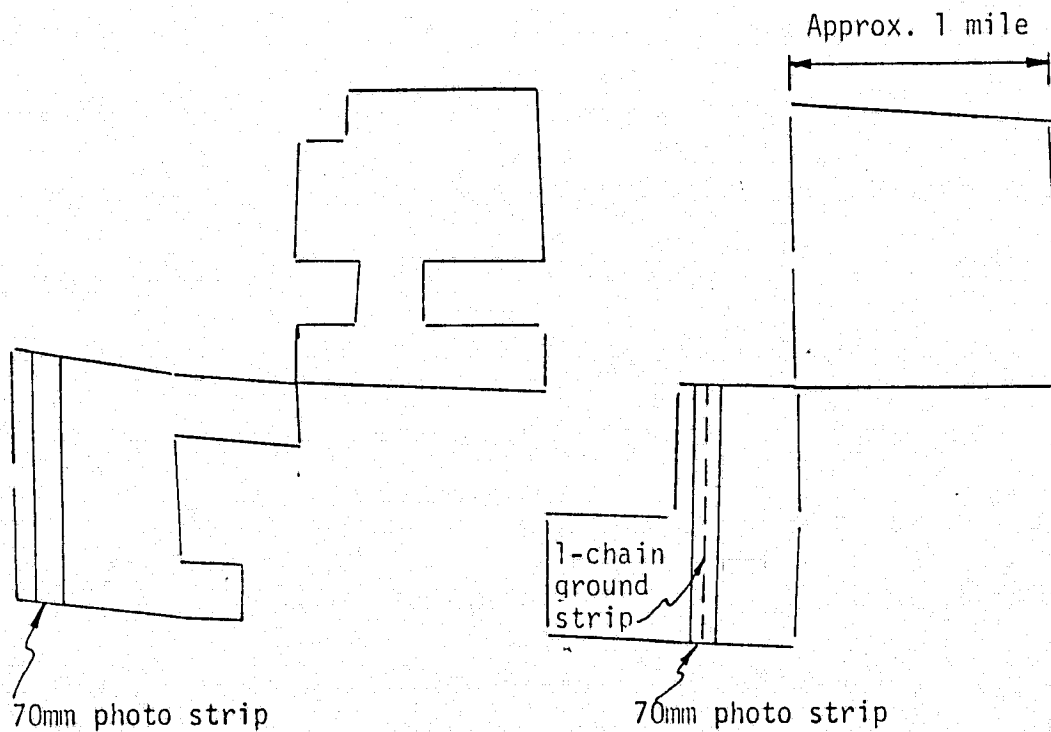


Figure 8. Three-stage sampling layout of the SP timber inventory. The aggregate of sections, such as in the above example, constitutes one primary sampling unit. The aggregate of 70mm photo strips constitutes a second-stage unit and the third-stage unit is the 1-chain ground strip.

the error terms and the cost of measurement were constant over all primary units. An average of two sample strips per primary unit were drawn and allocated as described. A completely optimal allocation was not possible because no estimates were available as to the magnitude of the first and second stage errors. The average number of two was decided on from intuition based on previous experience of Langley.

After having selected approximately 400 sample strips, they were rephotographed in color at a scale of approximately 1/4,000 by means of a Hasselblad 70mm camera. After obtaining the low-altitude photography, the boundaries of the 8 chain sample strips were delineated on them by visual comparison with the 1/40,000 scale photos when viewed through a magnifying stereoscope.

#### 1.4.3 The Third Sample Stage

According to theory, the 70mm sample photography would have been partitioned into plots or strips of such a size that a single plot or strip would be measurable on the ground. Then, by means of photo interpretation, sampling probabilities would be formulated so that selections would be made at random with probability proportional to timber volume as in the first and second stages. These selected plots or strips would then be located in the field and the trees would be measured for timber volumes.

Because of compelling limitations in available funds and a tight time schedule, it was not possible to conduct the sampling in the third stage strictly according to pps theory. However, the procedure followed closely approximated the theoretical plan and

at the same time resulted in some substantial savings in the form of increased field efficiency.

Because of cost constraints attributable in part to the rough terrain and inaccessibility of the land, we were able to visit on the ground only one second stage unit (8 chain strip) per primary unit. In addition, we were not able to interpret the 70mm photography before the time of the field work because of a tight schedule. This situation arose from a heavy snowpack which lasted late into the spring that year which prevented taking the low-altitude photos in time to interpret them prior to the field season.

Because of these problems, the procedure followed was to locate a ground strip 1 chain wide more or less down the center of one of the second stage eight chain strips in each primary unit (Figure 8). This configuration promised to traverse most of the varying conditions present in a strip and yield the largest number of trees measured in the least time. As for the problem of which second stage strip to choose for ground sampling, it was decided that one 8 chain strip would be drawn at random with probability proportional to the second stage volume prediction obtained from the high-altitude photography. Then after completing the interpretation of the large-scale 70mm photography, expansion factors would be derived that were identical to what the third stage probabilities based on volume would have been had the interpretation of the 70mm photos been done beforehand.

The weight (or expansion factor) that was applied to each one chain ground strip was the inverse of the ratio of the predicted timber volume (derived from photo interpretation) of the trees falling

within the one chain strip divided by the predicted volume of the trees falling in all the eight chain strips included in the secondary draw.

The interesting results of the survey from the sampling standpoint are the sample estimates by survey unit, the coefficients of variation observed at the first stage, the sampling errors, and the sample sizes. These figures are given in Table 1. Also of interest are the first, second, and third stage error terms and the optimum allocation of survey funds. All of these intermediate results are not available because the calculations were performed in total by means of an electronic computer. However, intermediate results were obtained for one survey unit for the purpose of checking out the program. From these intermediate results, the optimum allocation data shown in Table 2 were obtained.

In addition to having volume estimates summarized by survey unit, the company also wished to have the estimates reported for each parcel of land included in the sampling frame. The final estimates obtained for these parcels, which were mostly one square mile in size, were used in the present EREP investigation to evaluate the comparative gain in the precision (variance) of the same inventory had the S-190 imagery been used at the section level.

Obtaining the section estimates was accomplished by first partitioning each parcel into elevation-aspect compartments on the 1/40,000 scale photographs followed by further partitioning into major stand size-density groups which we labeled forest systems. As the field work progressed, the data were kept separately by forest system.

Table 1

## Selected Statistics From The Southern Pacific Timber Inventory

<u>Survey Unit</u>	<u>No. of psu's</u>	<u>Estimated Timber Volume (MM FBM)</u>	<u>First Stage Coefficient of Variation</u>	<u>Sampling Error (%)</u>
1	66	944.0	.45	5.57
2	11	250.3	.31	9.45
3	27	563.6	.35	6.73
4	12	223.5	.36	10.25
5	5	94.0	.10	4.64
6	14	204.4	.48	12.82
7	25	373.6	.62	12.37
8	28	372.6	.57	10.69
9	5	57.1	.16	6.98
<u>Total</u>	<u>193</u>	<u>3,083.1</u>		<u>3.29%</u>

Table 2

Optimum Allocation Data For One Survey Unit  
(Southern Pacific Timber Inventory)

<u>Sampling Stage</u>	<u>Error Terms</u>	<u>Cost Per Sample Unit</u>	<u>Total Cost Allocated to Unit</u>
1	$\hat{E}_1 = 3.0854 \times 10^{10}$	$D_1 = \$217.85$	$\bar{D}^* = \$58,800$
2	$\hat{E}_2 = 7.1763 \times 10^{10}$	$D_2 = \$267.24$	
3	$\hat{E}_3 = 1.0207 \times 10^{11}$	$D_3 = \$375.00$	

$$m^0 = \frac{\bar{D}^* \sqrt{\frac{E_1}{D_1}}}{\sqrt{E_1 D_1} + \sqrt{E_2 D_2} + \sqrt{E_3 D_3}} = 53.06 \Rightarrow 53$$

$$n_T^0 = m^0 n^0 = m^0 \sqrt{\frac{E_2 D_1}{E_1 D_2}} = 53.06(1.38) = 73.22 \Rightarrow 73$$

$$t_T^0 = m^0 n^0 t^0 = m^0 \sqrt{\frac{E_2 D_1}{E_1 D_2}} \sqrt{\frac{E_3 D_2}{E_2 D_3}} = m^0 \sqrt{\frac{E_3 D_1}{E_1 D_3}} = 53.06(1.39) = 73.56 \Rightarrow 74$$

Hence, the optimum allocations to sampling stages compared to the actual are:

<u>Optimum</u>	<u>Actual</u>
$m^0 = 53(D_1) = \$11,546$	$m = 66(D_1) = \$14,378$
$n_T^0 = 73(D_2) = 19,509$	$n_T = 68(D_2) = 18,172$
$t_T^0 = 74(D_3) = 27,750$	$t_T = 70(D_3) = 26,250$
Total Cost \$58,805	\$58,800

Table 2 (cont.)

Using equation (29) to approximate the relative gain in precision from optimum allocation, we have

$$[\text{Var}(v)]^{\text{opt.}} = \frac{E_1}{53} + \frac{E_2}{73} + \frac{E_3}{74} = 2.9445 \times 10^9$$

$$[\text{Var}(v)]^{\text{act.}} = \frac{E_1}{66} + \frac{E_2}{68} + \frac{E_3}{70} = 2.9810 \times 10^9$$

Hence the relative gain under optimum allocation would have been

$$\frac{[\text{Var}(v)]^{\text{act.}} - [\text{Var}(v)]^{\text{opt.}}}{[\text{Var}(v)]^{\text{opt.}}} \times 100 = 1.2\%$$

During the computation phase, the volume per acre by tree size group and species was determined for each forest system encountered in the sampling process.

The size-density coding system used to describe the forest system was a numerical one from which we developed regression coefficients to translate the size-density codes assigned to each forest system into volume predictions by three tree diameter groups (1) 12" to 19", (2) 20" to 35", and (3) 36" +. The equations were applied to the assigned codes for all forest systems in all land parcels. The species breakdown was derived by means of a nearest neighbor rule based on survey unit, elevation, aspect, and slope. The estimated volumes for each forest system were summed by parcel within each survey unit and adjusted to the totals obtained from the multistage sampling plan. Finally, the estimates for each forest system were written into a computer file making them available for more detailed analyses later on. Furthermore, the data are available for deriving new sampling probabilities for the purpose of conducting special purpose surveys to obtain improved estimates of selected components of the timber resource base. Therefore, the SP Land Company achieved the major first step in establishing a timber resource information system which can be used in day-to-day decision-making and at the same time provide data for improving the efficiency of updating the file through new sample surveys.

## 2.0 OBJECTIVES OF THIS SKYLAB/EREP INVESTIGATION

The events of the recent past, outlined in Section 1 above, point to a logical sequence in the development of forest sampling techniques that are applicable to projects covering large areas. Early techniques employed aerial photography of medium-scale, usually 1/20,000, then later to 1/15,840 on National Forests, and finally to 1/12,000 scale on some private lands. As aerospace technology progressed, there developed an increased interest in utilizing high resolution photography obtained from high-flying aircraft. Photography obtained from Apollo 9 gave the first indication that space-acquired data, even though of relatively coarse resolution, might be employed advantageously in forest surveys covering large areas. The main advantages of imagery acquired from space seemed to be that (1) entire forest populations could be covered nearly instantaneously, (2) multispectral data with good registration among spectral bands could be obtained, and (3) a standard of uniformity could be established in the data base that would allow meaningful comparisons over space and time.

It was apparent from the Apollo 9 experiment that further work was needed in at least three areas before space-acquired data could be effectively employed in operational forest sampling applications. Firstly, the sampling procedure needed to be examined in more detail from several standpoints: (1) to obtain an impression of its generality, it had to be applied to a different area, (2) it needed to be determined if primary units smaller than four miles square, as used in the Apollo 9 experiment, could be effectively employed at the space level, and (3) a method for optimally allocating survey funds to various stages in the sample design needed to be developed.

Secondly, since estimates of forest parameters are usually reported by ownership class, and often by political subdivisions, a capability was required to identify the space-acquired data by these categories for survey purposes. Therefore, a system was required to locate boundary points as accurately as economically feasible on the imagery and in the digital data base. The algorithm to be used had to account for image displacements caused by topography, earth curvature, spacecraft attitude, and the imaging systems.

Thirdly, an investigation of image interpretation and analysis techniques for forest survey purposes was required (1) to determine the feasibility of incorporating the multispectral and temporal characteristics of the data into the design and (2) to determine the extent to which these data could be employed to improve the precision of forest inventory estimates.

To satisfy the above requirements, the objectives of this EREP investigation were to (1) develop transforms for the location and transfer of boundaries, areas, and points of interest from topographic maps or coordinate descriptions to high-flight aerial photographs and satellite imagery, (2) further develop multistage sampling techniques to inventory forest resources, and (3) if possible, identify interpretation techniques which take advantage of the multispectral and temporal characteristics of the data.

After obtaining the techniques, they would be applied to a test area for which timber volume estimates are available to develop new timber volume estimates which incorporate the satellite data, and determine the gain in efficiency attributable to the S-190A, S-190B,

and S-192 systems. The test area for this investigation is defined as the collection of land parcels, one square mile in size, owned and operated by the Southern Pacific Land Company (SP) in the portion of Trinity County, California, covered by the EREP imagery.

### 3.0 COORDINATE TRANSFORMATIONS

#### 3.1 INTRODUCTION

The development of a system to locate sample unit boundaries in the various kinds of aerial and space imagery was an integral part of our investigation to finalize a multistage forest inventory technique. The necessity for such a subsystem was demonstrated by the Apollo 9 multistage inventory trial (Langley et al., 1969). At that time the sample units were simply defined by superimposing a uniform grid on the satellite image (Figure 1). Thus, to obtain greater spatial correspondence between sample units in the various stages and to insure that the image interpretive data would in fact relate to the alternate section layout of the Southern Pacific lands, we developed a computational method for transferring the corner coordinates of sample units from topographic-ownership maps to the RB-57 and EREP data.

#### 3.2 APPROACH

The common approach taken for all three kinds of imagery, aerial, EREP S-190, and S-192, was to perform an analytical resection for each individual image or subimage. The input to such a resection consists of the image coordinates and ground coordinates of a set of commonly identifiable points. The spatial location of the image center and the orientation parameters of the image are the outputs of the procedure.

To transfer points from topographic maps to space platform imagery, we developed a generalized resection program in which any resection parameter can be enforced in the solution to any desired extent. This allows for the use of orbital parameters in the resection solution.

In addition to the resection program, we developed a technique applicable to space platform photography in which elevations can be assigned to digitized map points through the use of digital terrain models. Using this technique tedious manual elevation assignment for thousands of digitized points can be avoided.

With estimates of these parameters in hand, other points such as property corner points can be projected onto the images using analytical methods.

### 3.3 IMAGE ANNOTATION OF 1/40,000 SCALE AERIAL PHOTOGRAPHS

In the SP forest inventory we obtained good results with individual spatial resections of 1/40,000 scale aerial photographs. We developed a production program with a semiautomatic quality control that could process a large number of aerial photographs. The inputs to this program were the coordinates of a set of photo points which had been identified on USGS topographic maps and put into digital form with a map digitizer, as well as the set of digitized points defining the property boundaries.

The computed results were plotted with a Hewlett-Packard 9100A plotter on transparent stable material. The resultant overlay was then composited with the aerial negative and a combined print made. An example of such an annotated print is shown in Figure 7.

### 3.4 IMAGE ANNOTATION OF RB-57 HIGH-FLIGHT PHOTOGRAPHY

To annotate the U-2 RC-10 1/126,000 scale high-flight photographs in our ERTS investigation, we had the option to either find a set of individual ground control points for each photograph or to use ground

control for only a few points and then to extend this control to each photo by means of photo-triangulation and block adjustment. The latter approach was taken for the following two reasons. First, a block adjustment would yield greater precision than using control points from USGS planimetric maps, and second we could obtain precise coordinates for points which could both be defined on the high-flight aerial photographs and the satellite images.

Since it is somewhat difficult to identify map features on space imagery in rugged, mountainous terrain, we set out to identify a set of natural landmarks on the high-flight aerial photographs that could also be readily identified on the space images. We then used the aerial photographs to determine the ground coordinates of these points by executing a block adjustment. This block adjustment also provided the control for resectioning the aerial photographs. This approach was thought more desirable for the aerial stage because of its inherent greater accuracy due to simultaneous adjustments and the use of a precision MANN TA1/P monocomparator for coordinate measurement.

To minimize the programming effort, ground coordinates determined with the block adjustment, together with their measured plate coordinates, were fed into the existing resection program to perform the final transformation of the digitized SP section corners for the aerial stage.

#### 3.4.1 Block Adjustment

The block adjustment was performed after the two strips of high-flight aerial photographs with ten photos each had been triangulated. Schuts triangulation and block adjustment programs were used for this

purpose. Coordinates were expressed in a secant plane system, with its origin in the test areas, to remove the influence of earth curvature. The standard errors computed with the control points and tie points used in the adjustment proved to be 12.8, 10.3 and 4.4 m for Easting, Northing, and height, respectively. The planimetric errors correspond to a point identification error of about 0.1 mm on the photographic plate. The results can be considered very good in view of the 1/126,000 scale of the aerial photography.

#### 3.4.2 Production of Image Overlays

The production of image overlays with annotated sample units both for the aerial photographs and for the EREP S-190 images took place as indicated in the flow diagram of Figure 9. The differences between procedures for space and aerial images are indicated by the appropriate boxes.

Three types of points were annotated on the aerial and space images. These were (1) the primary and secondary sample unit corner points, (2) the county line points, and (3) the management unit boundary points. The units outlined on the aerial images were GLO land sections and fractions thereof. All points were digitized from 10 USGS maps at a scale of 1/62,500. Geographic coordinates were assigned to each digitized point by means of an interpolation method, using a set of map control points with known coordinates. The geographic coordinates were subsequently converted to secant plane coordinates. Elevations were read from the contour maps for all data points and were then added to the secant plane coordinates of the digitized points. Separate resections for the 20 high-flight aerial photographs were calculated

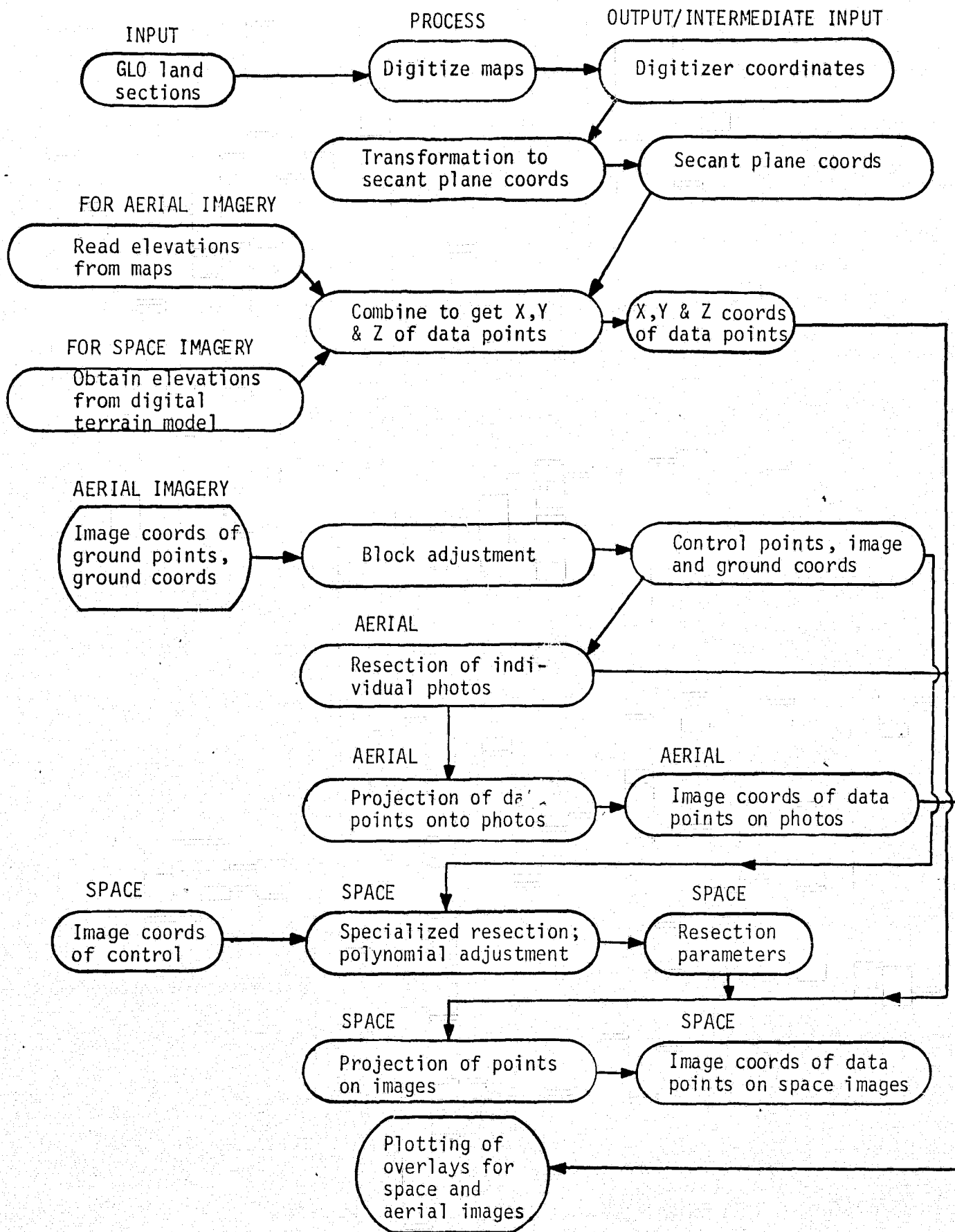


Figure 9. Flow diagram of space and aerial overlay manufacture for delineating sample unit boundaries.

using the control results from block adjustment. The data point coordinates were transformed to image coordinates by means of the resection results. The image coordinates were finally plotted on stable material templates using a Hewlett-Packard 9100A calculator plotter. An example of a high-flight aerial photo overlay is shown in Figure 10.

As it turned out, there was a high degree of similarity between the U-2 images used in the ERTS investigation and the RB-57 images taken one year later for this EREP investigation. Both data sets were obtained at approximately the same time of year and both were available in the 9" x 9" color IR format. Therefore, rather than doing a separate resectioning on the RB-57 imagery, the SP corner points were visually transferred from the U-2 to the RB-57 imagery (Figure 10). A transferscope was used for this process.

### 3.5 IMAGE ANNOTATION OF SCANNER IMAGES

#### 3.5.1 Resection Theory

In contrast to the resectioning of aerial photographs, EREP S-192 and Landsat images present two problems: (a) the image is produced by a multispectral scanner with a geometry different than that of aerial cameras, and (b) the imaging system has a very narrow perspective bundle.

The first problem is in part solved by the NASA data processing facilities where the geometry of the MSS images is partially shaped to resemble the geometry of an aerial photograph, not considering relief displacement, but taking into account earth curvature. The second problem causes an instability in the resection. It can be

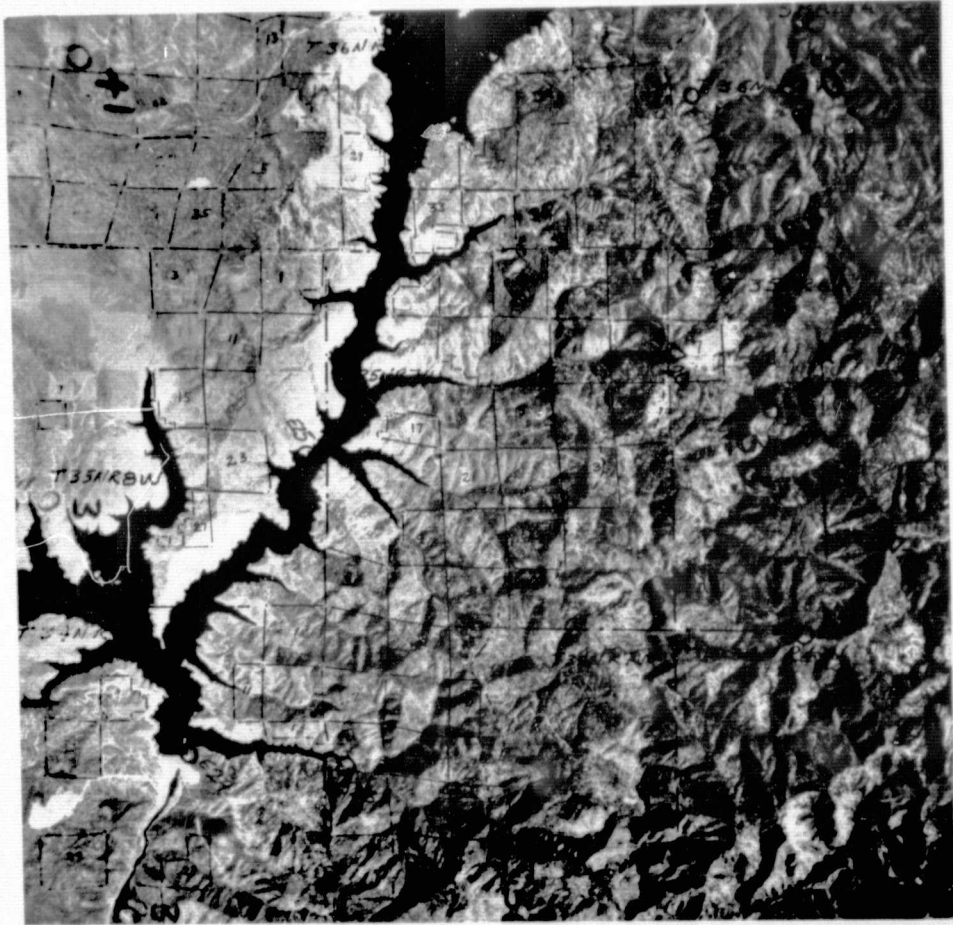


Figure 10. Examples of parcels annotated on a 1/126,000 scale high-flight photograph.

REPRODUCIBILITY OF THE  
ORIGINAL PAGE IS POOR

circumvented by enforcing some of the basic resection parameters, which must be determined from accurate outside sources such as the ephemeris data in the case of space images. We enforce the position of the simulated exposure station by assigning it the coordinates of the scanner picture center.

To make the resection program for the annotation of the scanner images completely general, so that it could be applied to S-190 images as well, we took the approach in which any parameter can be enforced at the value of its initial approximation by assigning appropriate weights. This approach can be implemented by using the parameter approximations in auxiliary equations in the linearized equation system:

$$\Delta p = p^{oo} - p^o + \epsilon \quad (1)$$

where:

$\Delta p$  is the correction to the approximation at the  $i$ th iteration

$p^{oo}$  is the approximation of the parameter value

$p^o$  is the parameter estimate to be enforced in the solution, and

$\epsilon$  is the difference between the least squares adjusted value of the parameter and the value to be enforced in the solution.

For the first iteration,  $p^{oo}$  is taken equal to  $p^o$ . Then, if we place a large weight on the auxiliary equation,  $\epsilon$  will be close to zero,  $\Delta p$  will be close to zero, and the initial approximation, which is equal to the desired parameter value, will not receive any corrections in the iterative process. Thus, the initially assigned parameter value will remain unchanged throughout the solution.

The normal equations take on the following form for n data points:

$$\left( \underline{X} \underline{W}^{-1} \underline{X}' \right)^{-1} \Delta = \underline{X} \underline{W}^{-1} \underline{Y} \quad (2)$$

with  $X'$  of the following form:

$$X' = \begin{bmatrix} a_x^1 & a_x^2 & \dots & a_x^9 \\ a_y^1 & a_y^2 & \dots & a_y^9 \\ 1 & 0 & \dots & 0 \\ 0 & 1 & \dots & 0 \\ \cdot & & & \cdot \\ \cdot & & & \cdot \\ \cdot & & & \cdot \\ 0 & \dots & & 1 \end{bmatrix} \quad \begin{array}{l} \text{(the third dimension} \\ \text{is not shown)} \end{array}$$

(11,9,n)

where  $a_x^1, a_x^2, \dots, a_y^1, a_y^2$  are the partial derivatives of the collinearity equations with respect to the nine resection parameters for a particular point.

The matrix has the following elements (only the first row is shown):

$$Y' = \left[ \begin{array}{cccc} \epsilon_x & \epsilon_y & (p_1^{oo} - p_1^o) & (p_2^{oo} - p_2^o) & \dots & (p_g^{oo} - p_g^o) \end{array} \right] \quad (3)$$

(9xn)

where  $\epsilon_x$  and  $\epsilon_y$  are the discrepancies resulting from an evaluation of the collinearity equations for the point under consideration with the current set of parameter approximations.

The matrix  $W$  is a diagonal  $11 \times 11$  weight matrix with unit weights in the first two positions, zero weights for those parameters that need to be estimated, and large weights (for instance, 100 unit weights) for those parameters that are to remain constant.

Thus, with the indicated solution we are free to fix or estimate parameters as needed. As the orbital path of the satellite is known quite accurately, the likely parameters to be enforced in the solution are the exposure station coordinates for the center of the image. For this purpose, the indicated latitude and longitude of the photocenters are taken from the best available source. For our Landsat investigation, we used the ERTS catalogue. To obtain the ERTS altitude, we prepared a program that computes the exposure station coordinates from orbital data furnished by NASA, given the Greenwich Mean Time (GMT) pertaining to the image center. However, we anticipated that the latitude and longitude indicated in the catalogue would be more accurate than the estimates computed by our program, since we only included first-order harmonic terms. In the solution, either the artificial focal length or the altitude needs to be enforced. We selected the altitude, since we assumed that scale change would be introduced in the bulk process through the introduction of an artificial focal length.

### 3.5.2 Coordinate Systems

The same secant plane coordinate system used for the block adjustment of the high-flight aerial photographs is used for the resection of the EREP and other space images. The conversion from the geographic coordinate system to the secant plane coordinate system yields coordinates of the control points in a cartesian coordinate system. The XY plane

of this system slices through the reference ellipsoid, so that the point elevations also reflect earth curvature.

The earth curvature accounts for part of the perspective displacement encountered in MSS images so that the use of the collinearity equation for the along-track direction in conjunction with the secant plane elevations is, therefore, partly justified.

### 3.5.3 Polynomial Fitting of the Residuals

To eliminate systematic trends remaining in the point residuals after the resection has been performed, we included in the resection program a general polynomial fitting routine with which we could fit separate trend surfaces through the x and y residuals of the plate coordinates. This part of the program can then account for the unexplained remaining systematic distortions.

For the polynomial surface fitting we use hybrid orthogonal polynomials in the x and y plate coordinates, generated with a recurrence relation. The maximum power of the polynomials is automatically determined by the program and then discounted to evaluate all possible power surface fits. For each power, Root Mean Square Errors (RMSEs) can be computed to assess the goodness of fit.

In the testing phase of the program we discovered that the polynomial fitting routine is general enough that, in terms of the residuals, almost identical results can be obtained by either performing a resection or by keeping all parameters fixed and then making the polynomial adjustment. Thus with the present program one can either opt for the classical resection technique or obtain the optimum polynomial fit.

#### 3.5.4 Experimental Results

To perform the resectioning and produce the sampling unit overlay for the first S-190A image, we used the generalized program package described above, even though, here, we were not dealing with scanner imagery. The 70 mm image was enlarged to a scale of 1/843,526 and transferred to a glass plate on which 34 control points were measured with a MANN TAPI comparator. The coordinates of these points, and ground control point coordinates obtained from the Coast and Geodetic survey were then used in the spatial resectioning program. This program is capable of doing a classical resection as well as an empirical polynomial adjustment. The overall RMSE of the resectioning proved to be 106 m on the ground. With an additional 2<sup>nd</sup> power polynomial adjustment RMSEs of 100 and 90.2 m were obtained in the x and y directions, respectively. These results are better by a magnitude of 2 than those obtained from ERTS, due to a better defined geometry, the use of SKYBET parameters, and a better ground resolution for control point identification. Examples of the annotation of the sample unit corners (GLO section and interior corners) can be seen in Figures 11 through 16.

A similar procedure was used on all of the S-190A and S-190B images. Unfortunately, because of delays in receiving the final S-192 data, combined with problems at our local computer center and cost limitations, we were unable to produce overlays for the S-192 images and data base. However, the process was successfully applied to Landsat imagery in our test area, and the qualities of this resectioning are given in Table 3.

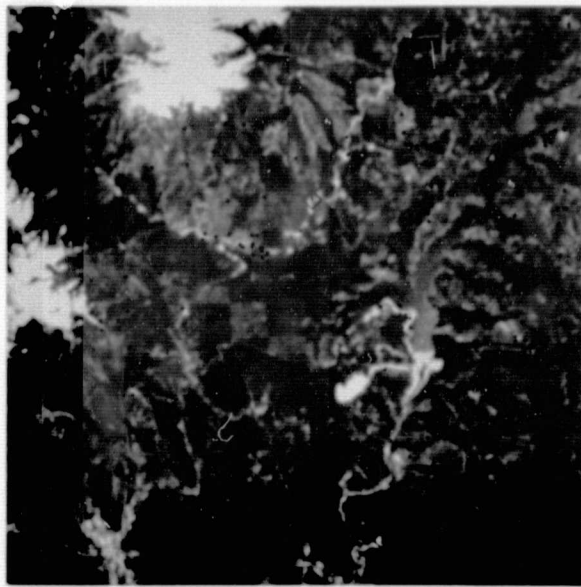


Figure 11. S-190A color, June, 1973.



Figure 12. S-190A color IR, June, 1973.

REPRODUCIBILITY OF THE  
ORIGINAL PAGE IS POOR.

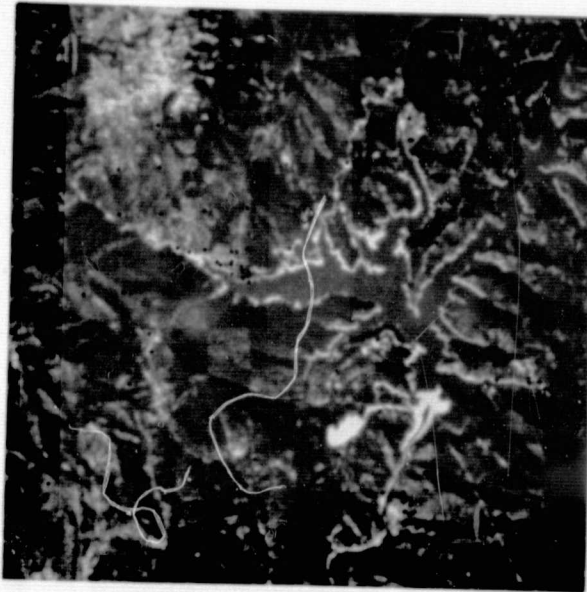


Figure 13. S-190A color, September, 1973.

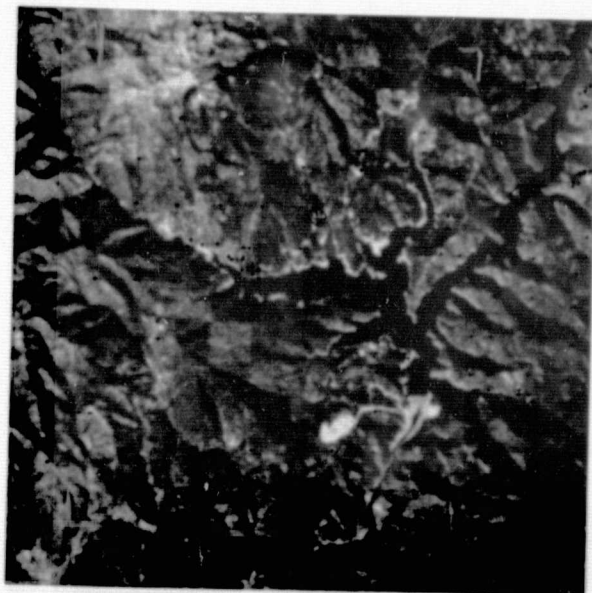


Figure 14. S-190A color IR, September, 1973.

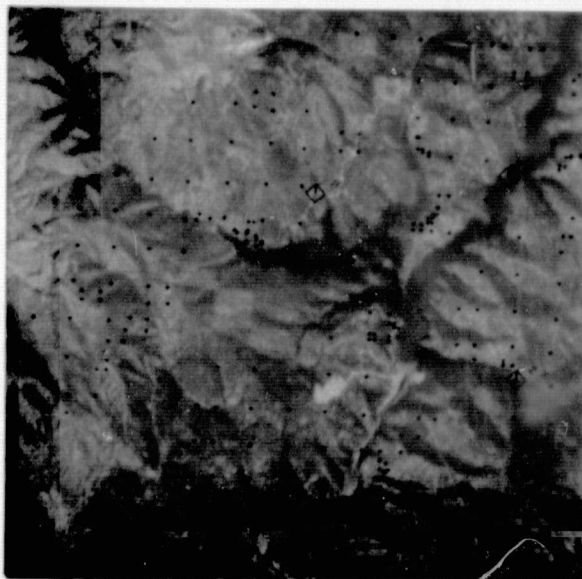


Figure 15. S-190A color IR, June/September, 1973 composite.

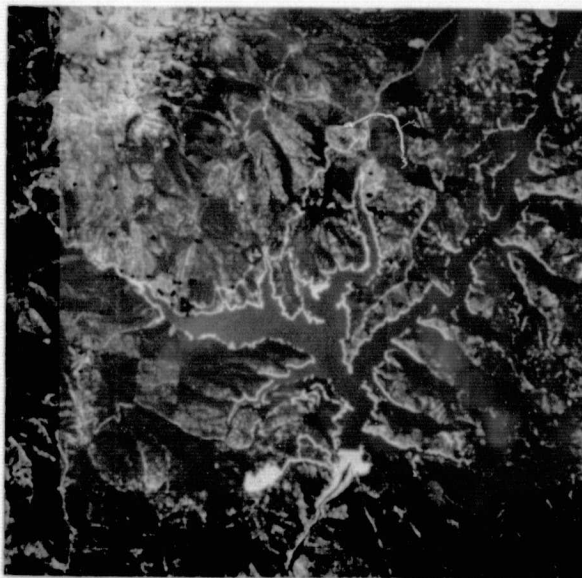


Figure 16. S-190B color, September, 1973.

Table 3

RMSEs for Resection of Landsat 1 MSS Images 103 and 104  
 (millimeters)  
 (x 1000: meters on the ground)

Image	Resection Result	After polynomial adjustment		
		1	Power 2	3
<u>Image 103</u> (18 points)				
RMSE for x	0.142	0.129	0.123	--
RMSE for y	0.146	0.138	0.116	--
Resultant	0.144	0.133	0.119	--
<u>Image 104</u> (30 points)				
RMSE for x	0.233	0.225	0.217	0.187
RMSE for y	0.196	0.181	0.176	0.146
Resultant	0.215	0.204	0.198	0.167

We can see in Table 3 that the RMSEs vary from 0.119 to 0.233 mm. This variation ranges from one to two times the identification accuracy of the U-2 RC-10 photography (0.1 mm), which is reasonable considering that the resolution of the Landsat MSS images is considerably less than that of the RC-10 photographs. Thus we can conclude that the point identification accuracy is the limiting factor with respect to the resection quality. Extending this argument to the S-192 data, we can hypothesize that the RMSEs would fall between those for the high-flight aerial photography and the Landsat MSS images. On the other hand, the circular scanning mode of the S-192 instrument, with the need to convert to a rectangular coordinate system for resectioning purposes may introduce additional

errors into the process, thus degrading the point identification accuracy to near the level of Landsat MSS imagery. Because of the problems stated above, we were not able to establish the exact accuracy attainable with the S-192 scanner, unfortunately.

### 3.5.5 The Production of Image Overlays

After the resectioning of the S-190 images was completed, the results were stored for subsequent use in the production of the image overlays. In producing the overlays, we used a second-degree residual estimation. Even though the benefits of this estimation were not clear-cut, we were convinced that the accuracy would not be degraded because of it.

At the beginning of our investigation we decided to take 4x4 blocks of one-square-mile GLO land sections as the primary sampling units. Thus, one primary unit would cover approximately 16 square miles. This was consistent with the size of the psu's used in the earlier Apollo 9 experiment.

Later on in our investigation, after having performed several resections of space images, we concluded that there was sufficient geometric accuracy for the primary sampling unit to be as small as a one-square-mile GLO land section. Consequently, we used the point data base developed for the annotation of the high-flight aerial photographs and projected these section corner points onto the S-190 images. All points were digitized from three maps at a scale of 1/2-inch to the mile. Geographic coordinates were then assigned to each point by means of an interpolation method using a set of map control points with known

coordinates. The geographic coordinates were subsequently converted to secant plane coordinates. At this time no elevations had yet been assigned to the digitized map points.

To produce elevations for the digitized points, we developed a digital terrain model of which a hypsocline chart is shown in Figure 17. This model covers an area of 125x125 km of our test area and includes part of the Sacramento Valley, the Trinity Alps and the Mount Shasta regions. In this region, the maximum terrain variation is 14,000 ft. because of the presence of Mt. Shasta. Elevations for the model were obtained by sampling an aeronautical chart with an 18x18 grid.

A test of the model showed that the RMSE of the actual terrain around the model surface amounted to 330 m. Under the assumption that the space image has a perspective geometry (including relief displacement), it can be shown that elevation errors in the order of 330 m would induce plate position errors of 37 micrometers on Landsat imagery, whereas errors of 111 micrometers would be incurred by assuming a mean terrain elevation.

After the elevations were assigned to the digitized points, they were processed through a program that sorts the points by frame number and projects them onto the space images in a rectangular coordinate system defined by the registration marks, if they exist. These coordinates were then plotted on stable transparent material with a Hewlett-Packard 9100A calculator-plotter at an enlargement ratio calculated by measuring a set of known distances. The resulting overlays were then attached to the S-190A and S-190B images in preparation for photo interpretation.



REPRODUCIBILITY OF THE  
ORIGINAL P/

Figure 17. Hypsocline chart of Digital Terrain Model.

## 4.0 S-190 SPACE AND HIGH-FLIGHT AERIAL INTERPRETATION MODELS

### 4.1 INTRODUCTION

In the type of multistage sampling scheme described in this report, measurements made at adjacent stages of the design are tied together by models that ultimately related remote sensor data to resource measurements obtained on the ground in sample areas. For example, in variable probability sampling, the model provides predictions which are used to determine unequal probabilities for drawing a sample in the next stage. In regression sampling, the model is used to adjust extensive but relatively inexpensive measurements made at the aerial stage with fewer data obtained from the more expensive ground stage. In stratified sampling, it is used to define strata in which independent ground sampling will take place.

Certainly the sampling method used is an important factor with regard to the overall level of precision obtained in the survey. But the interpretation model is of crucial importance since it governs the transfer of information from the image into the sampling design, and thus makes or breaks the quality of the survey assuming the transient data is adequate.

Colwell (1965) observed that photo interpretation entails two kinds of operations: (a) observing such photo-image characteristics as size, shape, shadow, tone, texture, and location, and (b) judging the significance of the features, based in large measure on their inter-relationships or "association."

Colwell noted that while a machine may have the capability to do the former, rarely is it capable of doing the latter sufficiently well. On the other hand, while a human being excels at judging associations, he may not be able to do a consistent job of interpreting features such as tone and texture from large amounts of image data, as he is soon overcome by boredom and fatigue.

At the beginning of our investigation we were aware that image features most highly correlated with biomass volume would be the spatial distribution of tone and texture, and that large amounts of data would have to be interpreted. In addition, human interpretation would not be entirely capable of extracting the maximum amount of information from multi-channel images such as provided by the S-192 scanner system.

In view of these considerations, most of the human image interpretation effort was concentrated on relatively simple interpretive models appropriate to the S-190A, S-190B, and the high-flight aerial photography. Photo interpreters were able to see individual trees on the aerial photographs and they were able to associate their observations with ground experience obtained in the area. Vegetation boundaries could be seen on the S-190 photography. Even so, the interpretation process was sometimes difficult since it required a substantial amount of subjective judgment both for the aerial and space system photography.

Before embarking on the human image interpretation effort, however, we deemed it advisable to subject a sample of the imagery types, including those from the S-192 scanner, to a simple multispectral additive viewer and a density slicer. The purpose of this was to

determine, in a cursory way, the possibility for achieving gains in sampling precision by virtue of obtaining better quality interpretive data related to forest variables. These simple trials and their results are described in the next section.

#### 4.2 MULTISPECTRAL COMBINING OF EREP IMAGES

We examined S-190A photographic and S-192 scanner type images from Skylab passes #34 and #37 over our Trinity County, California test area. Instruments used during the image analysis were the I<sup>2</sup>S (International Imaging Systems) Addcol and the VP-8 Image Analyzer from ISI (Image Systems International). In this section, we will describe the techniques used with each machine, the image materials used and the results obtained.

##### 4.2.1 I<sup>2</sup>S Addcol

This machine projects light through four color optical glass filters, one for each of four image samples. The samples consist of selected bands of the multispectral coverages of the S-190A imaging system.

The four image samples (70 mm black-and-white positive transparencies) are viewed first as one composite image without filters on a diffuse glass viewing screen. A color optical filter is then placed between each of the projection lights and corresponding image sample. The result is a color composite image on the viewing screen. For enhancement purposes the light intensity and filter color can be varied for each image sample. When the desired image is produced on the viewing screen the image is copied from the screen photographically using Ektacolor or other comparable film. Our experience with the S-190A imagery

indicated that the following combinations of light intensity setting and color filter were best for interpreting forest areas:

<u>S-190A</u> <u>Sample Image</u>	<u>Bandwidth (<math>\mu</math>)</u>	<u>I<sup>2</sup>S Addcol</u> <u>Light</u> <u>Intensity</u>	<u>Filter</u>
Roll 1	.69 - .80	9.1	Red
Roll 2	.77 - 1.00	8.7	Red
Roll 5	.58 - .80	8.5	Green
Roll 6	.47 - .58	10.0	Blue

The resulting image provided the greatest contrast and enhancement, as judged visually, which could be obtained with the sample images. Our objective was to enhance the existing forest stands in contrast to non-timbered and barren lands over our test area.

The same procedure was used with S-192 screening images from SKYLAB pass #37. In this case we had only three image samples which represented the spectral bands and bandwidths of concern to us in this investigation. Light intensity settings and filter combinations used for each image sample were as follows:

<u>S-192</u> <u>Sample Image</u>	<u>Bandwidth (<math>\mu</math>)</u>	<u>I<sup>2</sup>S Addcol</u> <u>Light</u> <u>Intensity</u>	<u>Filter</u>
Band 7	.78 - .88	8.7	Green
Band 11	1.55 - 1.75	8.5	Red
Band 2	.46 - .51	7.8	Blue

Our observations of the composite images produced for the S-190A and S-192 image sample have led us to the following conclusions. In the case of the S-190 composite image we observed a loss of resolution by combining the images and projecting them onto a ground diffuse

glass viewing screen. Second or third generation color infrared transparencies delivered as a SKYLAB product are several orders of magnitude better for interpreting photographic detail in the forested areas of Trinity County. In addition, we found that color enhancement of the several bands via the I<sup>2</sup>S machine did not produce equally as good or better color contrasts for interpretation of forest vegetation over our test area as did the color infrared film transparencies.

In case of the S-192 images, the photographic quality of the images received was fair to poor. However, we can make a few comments regarding our observations of the utility of the S-192 scanner as an imaging system.

Band 2 (.46 - .51  $\mu$ ) has wavelengths too short to be useful in forest vegetation analysis. Detail is obscured and contrast among features is almost nil.

Band 7 (.78 - .88  $\mu$ ) was the best of the three bands tried for vegetation analysis. Detail is clearer and contrasting vegetation features are interpretable by carefully studying the image.

Band 11 (1.55 - 1.75  $\mu$ ) seems to produce an image similar in appearance to a radar image of terrain. Geographic features show some contrast, water bodies and water courses show sharp contrast and detail. Detail in these features is readily interpretable, but for vegetation analysis this portion of the spectrum did not appear to be appropriate for our test site in California.

### 4.3 VP-8 IMAGE ANALYZER

The ISI VP-8 density slicer utilizes a video camera and television monitors. Between the camera and receivers are the electronics which convert the video signal to digital mode and measure the film density responses from several variable-width bands (slices). In addition to obtaining measurements of the proportion of an image exhibiting each density level, one can make point density measurements at any point on the image by means of an electronic cursor. Each point is uniquely identified by a pair of X, Y coordinates that can be read on the instrument panel. Hence, any point on the image can be measured for density so long as the image is not moved with respect to the video camera.

The more usual method of employing a density slicer in vegetation analysis work is to partition the image into grey levels by means of the system electronics. Beginning at the light or dark end of the density scale, one can "paint" the screen with light, progressing from one end of the scale to the other by means of a knob on the panel. In the VP-8 system used in this investigation, there are eight separate knobs with the accompanying electronics. Hence, the image can be partitioned into eight separate grey levels simultaneously. In addition, each of the eight density levels can be displayed in a unique color on a video screen. After properly adjusting the density levels, the proportion of screen occupied by each color can be read on the machine console. Therefore, the relative area of each vegetation type that can be uniquely incorporated within a density slice is measurable. It was by using this technique that we evaluated the usefulness of the VP-8

in forest sampling when applied to a single EREP S-190B black-and-white infrared image.

The S-190A frame number 058 from the black-and-white infrared film strip was the photographic medium used. This frame was first enlarged to a scale of 1/500,000 and printed on a transparent film base for use on the VP-8 light table. The control points used in the previous resectioning of this frame were located on the image. Then a resectioning overlay was produced showing the corner locations of the one-square-mile sampling units. The overlay was positioned on the image and placed on the VP-8 light table.

The next step was to calibrate the instrument to the density range of the transparency and the number of density bands desired, four in our case. A color is assigned to each level, and, finally, the proportional readouts on the instrument are calibrated to an area of known size on the image.

After calibrating the instrument to the image, we read the proportion of each sample unit occupied by each of four chosen colors. The density threshold levels were set to conform to four classes of timberland categories based on a small training set of sample units within the area of the inventory. The definitions of density level, assigned color, and corresponding expected timberland classes are given below.

<u>Density Level</u>	<u>Color</u>	<u>Expected Timberland Class</u>
1 (lightest)	Orange	Bare land
2	Green	Low volume--scattered trees
3	Violet	Med. volume--open stands
4 (darkest)	Blue	High volume--dense stands

The proportions of a sample unit in each of the three colors were recorded and considered as possible independent (X) variables in a regression model. The estimated volume of timber as determined from the SP inventory was entered as the dependent (Y) variable. The data format and sample unit identification is shown in the following example:

<u>Sample Unit</u>	<u>Estimated Timber Vol. (FBM) Y</u>	<u>% Orange X<sub>1</sub></u>	<u>% Green X<sub>2</sub></u>	<u>% Violet X<sub>3</sub></u>	<u>% Blue X<sub>4</sub></u>
T37N R9W S5	10,959	32	26	18	14

#### 4.3.1 Results of VP-8 Trials

Two trials were made, each one consisting of 34 primary sample units, one square mile in size, using a linear multiple regression model of the general form  $Y = X\beta + \epsilon$ . These two regression trials yielded the following statistics.

<u>Trial</u>	<u>Explained Variability (<math>\gamma^2</math>)</u>	<u>Significance of X Variables</u>				<u>Tabled Value of <math>t_{30}</math></u>
		<u>Orange</u>	<u>Green</u>	<u>Violet</u>	<u>Blue</u>	
1	.11	1.36	.76	-1.2	.17	1.70
2	.17	2.12	.45	-.56	-.98	1.70

As it can be seen in the above table, the maximum percentage of the total variability explained by this simple model was 17 percent, a value generally too low to be economically useful in sampling applications. The variable of highest significance was "orange" which corresponds to the light tone on the black-and-white infrared transparency which would relate to healthy vegetation.

The model was also evaluated for the gain in sampling precision that can be achieved under different sampling procedures using a method developed by Zarkovic (1964). The results are tabled below:

<u>Sampling Method (First Stage)</u>	<u>Percent Gain in Precision</u>	
	<u>Trial 1</u>	<u>Trial 2</u>
Stratified	5.93	12.98
Variable probability (pps)	2.27	7.49
Regression	11.48	16.53

In the above analysis, the gain in precision is analogous to the reduction in the sample size required to obtain the same variance. It appears from the above that regression sampling would be best when using the VP-8 instrument in the manner described above. The relatively low gain from pps sampling could be attributable to (1) a lack of sensitivity of the VP-8 responses to variations in tree sizes, or (2) the regression of Y on X not passing the origin. Under sensitive but stable conditions, the pss estimator is capable of greater gains than regression or stratified sampling and is applicable with small sample sizes, which is not the case with regression sampling. The economic significance of these results in relation to sampling efficiency is given in section 4.5 below.

#### 4.4 HUMAN INTERPRETATION MODELS

##### 4.4.1 Space Imagery

Throughout the course of the investigation, and as S-190 imagery was received from NASA, Houston, human image interpretation trials were conducted in the Trinity County test area. The technique used was

parallel to that used with the VP-8 image analyzer, except that color images were employed by the human interpreters.

The first human interpretation trials which were applied to the imagery received from SKYLAB II utilized 1/500,000 scale enlargements. Later on, a more complete analysis was made of SKYLAB II and SKYLAB II color imagery enlarged to a scale of 1/125,000.

In all of these trials, the approach was the same. First, transparent overlays were generated showing the location of the one-square-mile primary sample units on each image. Second, interpretations were made of the proportion of each sample unit exhibiting each of three or four distinct color tones. Regression models were formulated using the proportion of the sample units in each color as the independent variables. The results of these runs were screened and the ones showing the most promising results were tabled. These are shown below.

Even though up to four color class separations were made during the course of the investigation, three only seemed to be the maximum number that contributed significantly to any model. Also, the intercept was removed from all models without any significant reduction in the multiple correlation coefficients.

In interpreting the color imagery, the color classes showing the most significant relationship to our estimated timber volumes are:

<u>Emulsion Type</u>	<u>Most Significant Colors</u>
Conventional color	Dark green, light green, tan
Color infrared	Deep red, bright red, blue

#### 4.4.2 High-Flight Aerial Photography

During the course of our SKYLAB and ERTS investigations, we also conducted human photo interpretation trials to evaluate the usefulness of high-flight aerial photography in forest inventory work and to compare these results with those obtained with the SKYLAB EREP S-190A S-190B photography.

Our aim was to develop a regression type interpretation model for which the independent variables could be interpreted from the high-flight photographs. The dependent variable used was timber volume per square mile as determined from our survey of SP timberlands in Trinity County. In comparing the results of these trials with those obtained from interpreting EREP S-190 data, it should be kept in mind that individual trees are discernible on high-flight aerial photography and not on the EREP photography.

We started out with the interpretation of eight variables. These were (1) the percentage of a parcel on southern exposure, (2) the percentage of southern exposure covered with coniferous forest, (3) crown density of the conifer covered portion, (4) percentage of large trees on this portion, and the variables (5) through (8) being a repeat of the first four variables for the northern exposure.

In this first interpretation experiment we interpreted black-and-white prints of the U-2 color infrared photographs. Two interpreters estimated the 8 variables for the 40 sections twice. The initial idea was to average the four sets of interpreted data to reduce their variability and to reduce interpreter bias. For this purpose we did an analysis of

variance to determine if there was a significant difference between interpreters, and to test the homogeneity of variance among the different data sets. The outcome of these tests showed that the data could be averaged. Special care was taken to make the data consistent by using the conference interpretation system, where common standards for the interpretation were continually established.

Using the averaged eight variables, we tried six different models incorporating linear and non-linear combinations of the variables. The outcomes did not differ significantly from model to model. The multiple correlation coefficient was in the order of 0.65 and the standard error of the estimate was of the magnitude of 2.5 million board feet (bd. ft.) per square mile. We discovered, however, that we could economize on the interpretation effort by averaging the variables for the northern and southern exposures, as this distinction apparently did not contribute to the overall result.

In the next experiment the number of variables was reduced to three; namely: (1) percentage of the section covered by coniferous forest (C), (2) crown cover density of the coniferous forest (D), and (3) the percentage of the stand in large trees (L).

In addition, we investigated two other factors: the difference between the use of black-and-white or color infrared photographs, and the difference between interpreters. The results of the second experiment in which we tried three models, two interpreters, and two kinds of photography are given in Table 4.

Table 4

## Results of the High-Flight Photo Interpretation Experiment

Model	Black-and-White		Color Infrared	
	Int. 1	Int. 2	Int. 1	Int. 2
	Multiple correlation coefficient			
1. $V=M+CD+CD^2+CL+CL^2$	0.71	-	0.74	0.64
2. $V=M+CD+CD^2$	0.58	-	0.58	0.53
3. $V=M+C(D+D^2+L+L^2)$	0.72	-	0.74	0.65

In Table 4 there are no entries for the second interpreter under black-and-white photography, since this interpreter was no longer available. However, it can be concluded from the color infrared interpretation that there was indeed a significant difference between interpreters.

The second conclusion that can be drawn from the experimental outcomes is that the difference between color infrared and black-and-white photography is very small, so that the type of photography used does not seem to be an important consideration in this case.

The variable percentage of large trees (L) was a source of complaint during the interpretation work. Highly subjective judgment was required for its interpretation. We, therefore, omitted this variable (model 2) to determine its influence on the multiple correlation coefficient. The decrease in this coefficient, however, indicated that

the variable made an important contribution and, thus, it was included in the final model.

The third model was the final one selected for testing in a sample survey situation.

#### 4.5 SUMMARY OF RESULTS

In Table 5, we have summarized the most significant results of the S-190 and high-flight aerial image interpretation trials as they relate to timber volume estimation in Trinity County employing one-square-mile primary sampling units.

The most important results from the sampling standpoint are the relative gains that could be achieved using the different sampling methods, (1) stratified, (2) probability proportional to size (pps), and (3) regression. The gains listed in the table are in relation to what would be achieved under simple random sampling. The reason for this comparison is that under simple random sampling, primary sample units would be drawn without benefit of any prior information concerning the resource base, in other words, without taking advantage of the interpretive data available from the aircraft or space imagery. All of the three plans listed do take advantage of the image data but in different ways. Therefore, any one of the three methods may be most appropriate in specific situations. Interactions among sample units, the interaction between the remote sensor and ground data, the sample size, and even the experience of the interpreter in the local area can affect the best selection of sampling method. Nevertheless, it can be seen from the table that all three of the sample methods shown do take some advantage

Table 5

Selected Statistics from the Space and Aerial Image Interpretation Trials Employing  
One-Square-Mile Sample Units and Comparison of Alternative Sampling Methods

Image Type	Month of Acquisition	Image Scale	Inter. Method	Sample Size	Proportion of variability explained by the model ( $r^2$ )	Average % Gain in Sampling Precision Compared to Simple Random		
						Stratified	pps.	Regression
S-190A B&W IR	June	1/500,000	VP-8	34	.14	9.5	4.9	14.0
S-190A Color IR	June	1/500,000	Human	114	.38	23.4	30.5	38.4
S-190A Color	June	1/125,000	"	170	.24	15.0	21.3	24.4
S-190A Color IR	June	1/125,000	"	184	.25	17.3	22.8	25.3
S-190A Color	Sept.	1/125,000	"	184	.38	28.1	32.1	38.8
S-190A Color IR	Sept.	1/125,000	"	185	.36	25.2	31.9	36.2
S-190A Color IR	June/Sept. Composite	1/125,000	"	140	.43	35.1	39.5	43.3
S-190B Color	Sept.	1/125,000	"	186	.37	27.8	35.6	37.3
High-Flight Aerial Color IR	June	1/125,000	"	40	.55	43.4	49.9	55.1
Average Gain (Human Interpretation of Space imagery)						24.6	30.5	34.8
Standard Deviation						6.8	6.5	7.1

of all kinds of imagery in increasing the precision of a forest inventory for a given sample size.

In evaluating the economic benefit of EREP S-190 imagery when used in this manner, one must consider the cost of obtaining and interpreting the imagery in relation to the cost savings achieved by virtue of the reduction in the required sample size.

From Table 2, page 27, it can be determined that in 1972, the cost of utilizing two 70 mm strips and one crew day, to obtain tree measurements, per one-square-mile primary unit was \$909.48 ( $2(267.24) + 375.00$ ). Therefore, an allowable reduction of 20% in the sample size in a situation requiring 50 primary sample units would result in a sampling cost saving of \$9,094.80 that could be credited toward obtaining and interpreting the space acquired data. Table 6 lists the revenues that would be available for image acquisition and interpretation when employing selected S-190 products into the design, assuming a base of 100 psu's under simple random sampling.

On the other hand, there are other data types that are sometimes available, such as aerial photography, that can be used instead of space acquired data. Therefore, the feasibility of implementing a satellite remote sensor program must heavily depend on the multidisciplinary aspects of the program, the size of the area covered, the consistency of the data, and the frequency of coverage. It might be appropriately noted here that, in the forest inventory business, there is always a shortage of good quality imagery covering the right area at the right

Table 6

Revenue Made Available for Image Interpretation under Three Sampling Methods Compared to a Base of 100 Primary Sample Units under Simple Random Sampling  
(Figures assume a subsampling plan of 2 low altitude 70 mm strips and one crew day on the ground per psu, 1972 data)

Image Type	Month of Acquisition	Cost of Data Acquisition* within Primary Units (Thousands of Dollars)			Revenue Made Available for Image Interpretation (Thousands of Dollars)		
		Stratified	pps	Regression	Stratified	pps	Regression
S-190A Color	June	77.3	71.6	68.8	13.6	19.4	22.2
S-190A Color IR	June	75.2	70.2	67.9	15.7	20.7	23.0
S-190A Color	Sept.	65.4	61.8	55.7	25.6	29.2	35.3
S-190A Color IR	Sept.	68.0	61.9	58.0	22.9	29.0	32.9
S-190A Color IR	June & Sept. Composite	59.0	55.0	51.6	31.9	35.9	39.4
S-190B Color	Sept.	65.7	58.6	57.0	25.3	32.4	33.9

\*Cost under simple random sampling for 100 psu's is 90.9 thousand dollars.

time. Amelioration of these problems alone would go a long way in advancing the art of resource information management.

There are several significant results that can be observed in Table 5.

- a. The results from the VP-8 experiments were disappointing. Although some gain was achieved, considerably more effort would be needed to develop this type of instrument into a viable competitor in forest survey work of the type investigated here.
- b. The S-190A products obtained in September yielded significantly higher gains than the products obtained in early June. This was because of a greater spectral difference between commercial conifers (evergreen) and noncommercial broadleaves, brush, and grass in September compared to June.
- c. The color composite incorporating June and September S-190A imagery yielded the highest gains of any of the space acquired data tried. Therefore, temporal variations were important in our analysis (i.e., two timely coverages are significantly better than one).
- d. There was no significant difference between the gains achieved with S-190B imagery compared to S-190A imagery.
- e. There was no significant difference between S-190A color versus S-190A color IR.

- f. The gains in sampling precision were significantly better with the high-flight aerial imagery than with any of the space acquired data. This is even more significant when considering that the June S-190A imagery, when the aircraft data was acquired, gave poorer results than the September S-190A products. Therefore, the capability to resolve trees yields significantly better results and is more important than seasonal variations.

We have concluded that some of the reasons for the similarity in the results of the S-190A and S-190B image interpretations is that significant vegetation type boundaries can be delineated on all the space imagery used and trees are discernible on none of them. Because of this, important data concerning the density of commercial species, bole sizes, and tree heights cannot be ascertained. Therefore, the conclusion must be drawn that the EREP S-190 data is of significant but limited usefulness in forest inventories using human interpretation methods. The general conclusion is that the number of primary sample units required to achieve a given level of variance can be reduced from 24 percent to 43 percent by introducing EREP type information into the sampling design. This general conclusion was indicated in the Apollo 9 experiment, our ERTS investigation, and re-verified in the present investigation. To achieve further gains from space systems, and to obtain a capability for forest stand mapping for management purposes, it would be necessary to increase the resolution to a point where trees are discernible. At that point, a new plateau in capability would be reached.

There are a few other important points, both pro and con, that come out of the investigation that are narratively commented on below. These comments are in line with Mr. Ryborn Kirby's letter of April 1, 1975 to the Principal Investigator.

(a) The higher spatial resolution of the S-190B appears to us to have definite advantages over the S-190A system both from the vegetation mapping standpoint and from the operational standpoint. From the mapping standpoint, vegetation boundaries are more clearly defined and hence could be mapped to a greater degree of accuracy. As a result of this, acreage measurements would be more accurate. This may or may not increase the precision of timber volume estimates depending on the sampling method used.

(b) The improved spectral discrimination of the S-190A system did not seem to contribute significantly to our investigation. All of the major vegetation type differences could be discriminated on all the image types. The differences were simply a matter of degree. By and large, the infrared color imagery is the best single product. It cuts the haze best and differentiates between commercial conifer areas and non-commercial hardwood and brush areas. Color infrared with a capability to resolve trees, such as with RB-57 high-flight photography, would be super.

(c) The consistency of sun angle is probably one of the more important attributes attainable with space imagery for forest survey work. Consistency over space and time is extremely important in allowing the development of machine assisted interpretation models

and techniques. In past experiments aimed at determining the feasibility of automating forest photo interpretation with aerial photography, the variations in reflectance attributable to variation in sun angle and topography were always a major cause of variability. Therefore, maintaining a steady sun angle by latitude would be beneficial. Seasonal variations, however, are an aid to forest image interpretation because grass, brush, broadleaf, and conifer vegetation all undergo differential changes in their reflectance characteristics over time. These differences can be capitalized on in developing machine-assisted interpretation models. In our investigation, we found significant differences due to seasonal variation as shown in Table 5.

(d) Improvements in resolution, particularly if trees could be resolved, formatted to a larger scale, say 1/125,000, would probably be of more benefit in forest surveys than further improvements in spectral discrimination. High resolution also contributes to the operational efficiency by facilitating the identification of sample areas from aircraft and on the ground in multistage surveys. This is an important consideration from the standpoint of operational efficiency.

(e) There is no established standard of precision for forest surveys. It usually varies by the size of the area to be surveyed and the cost of making a wrong decision. The Forest Survey maintained a standard of precision of 5 percent per million acres for area estimates and 10 percent per billion board feet for volume estimates evaluated at the 67 percent confidence level. Many private owners try for a standard of 10 percent on total volume evaluated at the 95 percent confidence level. The main significance attributable to the level of precision

is the survey cost to achieve that precision balanced against the cost of a wrong decision that may be attributable to inadequate information.

(f) We feel that the most useful single SKYLAB-type product for forest surveys is the S-190B imagery enlarged to a scale of about 1/125,000. If better resolution could be obtained, color enlargements to a scale of 1/63,360 (1" = 1 mile) would be extremely useful in forestry work, particularly if they could be supplied at frequent intervals of once or twice a year. This type of product would assist managers in updating harvest areas and generally keeping track of changes in the resource base. This is one of the biggest single problems in resource information management.

(g) SKYLAB-type data can almost provide a remote sensor program geared to land management but not quite. We feel that an increase in resolution is necessary for widespread application. Then, the application would be tremendous for resource mapping, monitoring, inventorying, and management.

## 5.0 DIGITAL INTERPRETATION MODELS

One of the initial objectives of this investigation was to develop S-192 digital interpretation models expressly for timber volume estimation by one-square-mile sample units. We did, in fact, develop the programs to the point where the sample units can be isolated in the computer ready for analysis. And we did produce shade prints covering our test area (Figure 18). Unfortunately, a change from the Univac 1108 Exec II to the Exec VIII monitor system at the ISD computer center, at the crucial time when the S-192 tapes were finally received from Houston, made it impossible for us to complete the digital model investigation within the remaining time and available funding.

The description of the analysis system, which is now nearly ready to be implemented using S-192 data, was included in our ERTS report to Goddard Space Flight Center, Greenbelt, Maryland. For a complete description of the digital MSS timber volume interpretation system, see section 4.3, pages 39 through 56 of the final report, "Investigation to Develop a Multistage Forest Sampling Inventory System Using ERTS-1 Imagery," ERTS Investigation #174.

Since the S-192 scanner system employs many more channels than the ERTS system, the task of screening to isolate the channels most appropriate for forest inventory purposes could be a formidable one. On the other hand, the greater selectivity of channels and the greater resolution of the S-192 scanner compared to the LANDSAT MSS could result in a more significant interpretive system. This would be an appropriate subject for a future investigation.

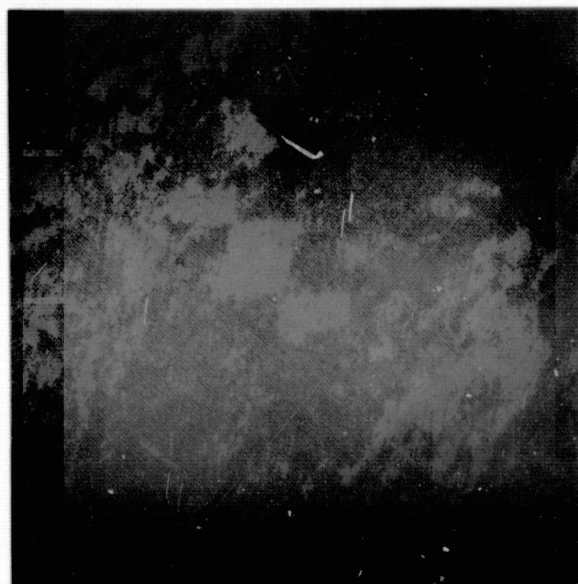


Figure 18. Shade print of test area produced from S-192 digital tape.

## APPENDIX A

### THE THEORY OF MULTISTAGE VARIABLE PROBABILITY SAMPLING WITH REPLACEMENT

#### General Description

Sampling with unequal probabilities has been known to statisticians for some time. It is often referred to as sampling with probability proportional to size (pps). Hansen and Hurwitz (1949) applied it to census surveys and since that time various forms of the method have been described and used by many people. A notable example in forestry is due to Groesenbaugh (1958) who demonstrated that Bitterlich point sampling with a prism or angle gauge selects trees with probability proportional to basal area. Several years ago, Langley envisioned the use of pps sampling in timber management inventories and taxation surveys when prior information concerning the target population was available from file records or aerial photographs.

In the early 1960's Langley suggested the use of high altitude photographs as a means of increasing the efficiency of forest surveys that covered large areas (Langley, 1961). Later, he thought about the possibilities of incorporating photointerpretation data in timber inventories by means of one-stage pps sampling. In about 1965, he considered the possibilities of incorporating multistage pps sampling into forest surveys. However, it was not until the Douglas-fir mortality surveys of 1967 (Wert and Roettgering, 1968) that a pressing incentive was provided to

develop the idea more fully. The Apollo 9 experiment in 1969, the Southern Pacific Inventory of 1971, the NASA ERTS-1 experiment, and finally the present SKYLAB/EREP investigation provided the incentives to complete the derivation of the optimum allocation procedures as presented in Appendix C.

In the context of this paper, sampling with replacement in the multistage case means that each time a unit is drawn repetitively in any stage, a new independent subsample must be drawn in all subsequent stages.

#### One-Stage Variable Probability Sampling

To illustrate the method, suppose we write a one-stage random sampling estimator for total forest volume on a tract of land as

$$v = \frac{N}{n} \sum_{i=1}^n v_i \quad (1)$$

in which

$v_i$  is the measured timber volume on the  $i^{\text{th}}$  sample unit,

$n$  is the number of units included in the sample and

$N$  is the number of units in the target population. Formula (1) is, of course, equivalent to

$$v = \frac{1}{n} \sum_{i=1}^n v_i / \frac{1}{N}$$

From sampling theory, we know that  $\frac{1}{N}$  is the probability of selecting the  $i^{\text{th}}$  population unit at any given draw. Therefore

$$v = \frac{1}{n} \sum_{i=1}^n \frac{v_i}{p}$$

in which  $p = \frac{1}{N}$  is the constant probability of selection. Each ratio  $v_i/p$  estimates the population total.

If the probability of selection is derived from some other criterion, such as predicted timber volume derived from aerial photographs, we may write

$$P_i = C_i / \sum_{i=1}^N C_i$$

in which  $C_i$  is the predicted volume of timber in the  $i^{\text{th}}$  population unit. Since  $\sum_{i=1}^N P_i = 1.0$ , we satisfy the requirements of a probability distribution. The new estimator, known as the pps estimator, may be written as

$$v = \frac{1}{n} \sum_{i=1}^n \frac{v_i}{P_i} \quad (2)$$

This estimator is unbiased as long as the observations are physically drawn according to the prescribed probabilities. This is

shown by evaluating the expected value, i.e.

$$\begin{aligned}
 E(v) &= E\left[\frac{1}{n} \sum_{i=1}^n \frac{v_i}{p_i}\right] \\
 &= E\left(\frac{v_i}{p_i}\right) \\
 &= \sum_{i=1}^N p_i \frac{v_i}{p_i} \\
 &= \sum_{i=1}^N v_i \\
 &= V
 \end{aligned}$$

where  $V$  is the population parameter sought.

The sample selection is easily made by drawing  $n$  uniformly distributed random numbers with equal probability from a list of numbers in the interval 1 to  $\sum_{i=1}^N C_i$ . When selection is with replacement, a forest unit is included in the sample once each time a random number falls within its range on a cumulative list of the  $C_i$ 's (Table A.1, Col. 4); i.e. whenever

$$\sum_{i=1}^k C_i < r_j \leq \sum_{i=1}^{k+1} C_i$$

where  $r_j$  is the number selected at the  $j^{\text{th}}$  draw. For example, if we select three numbers at random between 1 and 154 (154 is  $\sum_{i=1}^N C_i$  in Table 1), and happen to draw 12, 85, and 130, we have selected units 2, 5, and 7 to be measured. This can be seen by referring to Col. 4 of the table. The first number, 12, is greater than 10, the upper bound for unit 1 but less than 40, the upper bound for unit 2 and so on. Furthermore, the samples have been

Table A.1

## Illustration of the Reduction of the Sample Variance with Variance Probability Sampling

				Variable Probability Sampling				Equal Probability Sampling			
(1) Unit (i)	(2) Timber Volume (V <sub>i</sub> )	(3) Predicted Volume (C <sub>i</sub> )	(4) Cum. Sum <sup>†</sup> $\sum_{i=1}^N C_i$	(5) $P_i = \frac{C_i}{\sum C_i}$	(6) V <sub>i</sub> /P <sub>i</sub>	(7) (V <sub>i</sub> /P <sub>i</sub> - V) <sup>2</sup>	(8) P <sub>i</sub> (V <sub>i</sub> /P <sub>i</sub> - V) <sup>2</sup>	(9) P = 1/12	(10) V <sub>i</sub> /P	(11) (V <sub>i</sub> /P - V) <sup>2</sup>	(12) P(V <sub>i</sub> /P - V) <sup>2</sup>
1	8	10	10	.0649	123	729	47	.0833	96	2916	243
2	34	30	40*	.1948	175	625	122	"	408	66564	5545
3	18	15	55	.0974	185	1225	119	"	216	4356	363
4	14	20	75	.1298	108	1764	229	"	168	324	27
5	45	50	125*	.3247	139	121	39	"	540	152100	12670
6	2	1	126	.0065	308	24964	162	"	24	15876	1322
7	8	10	136*	.0649	123	729	47	"	96	2916	243
8	3	5	141	.0325	92	3364	109	"	36	12996	1083
9	6	5	146	.0325	185	1225	40	"	72	6084	507
10	7	5	151	.0325	215	4225	137	"	84	4356	363
11	0	1	152	.0065	0	22500	146	"	0	22500	1874
12	5	2	154	.0130	385	55225	718	"	60	8100	675
Total	150 = V	154		1.00			1915				24,915

†The C<sub>i</sub>'s shown in column 3 are closer to the V<sub>i</sub>'s in column 2 than would normally be obtained in practice unless they had been corrected by, say, regression. However, the correlation coefficient R which is equal to .97 in this example, is of the same magnitude reported by Wear et al (1964) and therefore serves as a valid, though optimistic, example for demonstrating the use of photo predictions in variable probability sampling.

selected with probability proportional to the photo estimates  $C_i$  because unit 2 has  $40 - 10 = 30$  chances out of 154 of being selected, unit 5 has a  $50/154$  chance and unit 7 has a  $10/154$  chance of being selected. In other words, the sampling probabilities are equal over units of predicted volume rather than by the frequency of forest units as indicated by formula (1). Note that in neither case is it necessary to know the area of the forest units. When sampling is with replacement, the variance of the pps estimator  $v$ , over all possible samples of size  $n$  is (Cochran 1963, p. 253)

$$\text{Var}(v) = \frac{1}{n} \sum_{i=1}^N P_i \left( \frac{V_i}{P_i} - V \right)^2 \quad (3)$$

in which

$n$  is the sample size,

$N$  is the number of units in the population,

$P_j$  is the probability of selecting the  $i^{\text{th}}$  unit at the  $j^{\text{th}}$  draw,

$V_i$  is the timber volume in the  $i^{\text{th}}$  unit,

$V$  is the total volume in the forest.

Clearly,  $\text{Var}(v)$  is dependent on the squared deviations of the ratios  $V_i/P_i$  from  $V$ . The higher the linear correlation between the  $V_i$ 's and the  $P_i$ 's, the less variability there is among the ratios  $V_i/P_i$ . If the  $V_i$ 's and the  $P_i$ 's exhibited perfect proportionality the variance of  $v$  would be zero because the values of  $V_i/P_i$  would be the same for all population units and would equal  $V$ . Needless to say, this is never the case, for if it were, sampling would be unnecessary.

Using the values in Table A.1, the  $\text{Var}(v)$  can be calculated for a sample size of, say, three for both variable probability sampling and equal probability (simple random) sampling, respectively. Accordingly,

$$\text{Var}(v_{\text{pps}}) = \frac{1}{3}(1915) = 638$$

$$\text{Var}(v_{\text{sr}}) = \frac{1}{3}(24,915) = 8305$$

The sampling error (standard deviation) in each case is the square root of the variance.

$$\text{S.E.}_{(\text{pps})} = \sqrt{638} = 25.3 = 17\% \text{ of } V$$

$$\text{S.E.}_{(\text{sr})} = \sqrt{8305} = 91.1 = 61\% \text{ of } V$$

An unbiased estimate of the variance may be computed from a single sample using the formula (Cochran 1963, p. 254)

$$\text{var}(v) = \frac{1}{n(n-1)} \left[ \sum_{i=1}^n \left( \frac{v_i}{p_i} \right)^2 - nv^2 \right] \quad (4)$$

This is verified in Appendix B for two-stage sampling.

#### Two-Stage Variable Probability Sampling

When the primary sample units are too large for measuring the total attribute on the ground, as when measuring the volume of a large number of trees, a second stage may be added to the design yielding a new estimator

$$v = \frac{1}{m} \sum_{i=1}^m \frac{v_i}{p_i}$$

$$v = \frac{1}{m} \sum_{i=1}^m \frac{1}{p_i n_i} \sum_{j=1}^{n_i} \frac{v_{ij}}{p_{ij}} \quad (5)$$

in which

$v_{ij}$  is the measured volume in the  $j^{\text{th}}$  subunit in the  $i^{\text{th}}$  primary unit,

$p_{ij}$  is the conditional probability of drawing the  $j^{\text{th}}$  subunit given the  $i^{\text{th}}$  primary unit,

$p_i$  is the probability of drawing the  $i^{\text{th}}$  primary unit,

$n_i$  is the number of observations drawn from the  $i^{\text{th}}$  primary unit, and

$m$  is the number of primary units drawn from the population.

The two-stage pps estimator is unbiased if the observations are drawn as indicated by the selection probabilities. The second stage selection probabilities -- conditional on the first stage unit having been drawn -- may be defined as

$$P_{ij} = C_{ij} / \sum_{j=1}^{N_i} C_{ij}$$

in which  $C_{ij}$  is the criterion value assigned to the  $j^{\text{th}}$  subunit in the  $i^{\text{th}}$  primary unit and  $N_i$  is the number of secondary sample units in the population of the  $i^{\text{th}}$  primary unit. Then  $\sum_{j=1}^{N_i} P_{ij} = 1.0$  for each  $i^{\text{th}}$  primary unit. If the sum of the second stage predictions are adjusted such that  $\sum_{j=1}^{N_i} C_{ij}$  is equal to  $C_i$  from the

first stage selections, the two-stage estimator may be simplified to

$$v = \frac{C}{m} \sum_{i=1}^m \frac{1}{n_i} \sum_{j=1}^{n_i} \frac{v_{ij}}{c_{ij}} \quad (6)$$

in which  $C = \sum_{i=1}^M C_i$  where  $M$  is the total number of primary units in the target population.

As derived in Appendix B, the variance of  $v$  over all possible samples of  $m$  primary units and  $n_i$  second stage units when sampling with replacement is

$$\text{Var}(v) = \frac{1}{m} \left[ \sum_{i=1}^M \frac{V_i^2}{P_i} - V^2 \right] + \frac{1}{m} \sum_{i=1}^M \frac{1}{P_i n_i} \left[ \sum_{j=1}^{N_i} \frac{v_{ij}^2}{P_{ij}} - V_i^2 \right] \quad (7)$$

$$= \frac{1}{m} \sum_{i=1}^M P_i \left( \frac{V_i}{P_i} - V \right)^2 + \frac{1}{m} \sum_{i=1}^M \frac{1}{P_i n_i} \sum_{j=1}^{N_i} P_{ij} \left( \frac{v_{ij}}{P_{ij}} - V_i \right)^2 \quad (7a)$$

in which

$v_{ij}$  is the timber volume (or other attribute) in the  $j^{\text{th}}$  subunit of the  $i^{\text{th}}$  primary unit,

$V_i$  is the volume in the  $i^{\text{th}}$  population unit, and

$V$  is the total volume of timber in the population.

The other terms are as defined earlier.

As shown in Appendix B, an unbiased estimate of  $\text{Var}(v)$  for two- (or more) stage variable probability sampling may be calculated from the first stage estimates as with one-stage pps sampling (formula 4).

### Three-Stage Variable Probability Sampling

It often happens in forest sampling problems that even second stage sample units are too large for complete enumeration on the ground. This situation may arise when (1) very high altitude or space photography are used at the first stage, (2) the second stage units consist of long strips of large scale photography extending a mile or more, or (3) precise tree volumes are obtained on a subsample of trees in a plot by means of an optical dendrometer. In these cases, three stages or more may be included in the sample design.

The three-stage variable probability sampling estimator is simply an extension of the two-stage estimator (formula 5). It may be written as

$$v = \frac{1}{m} \sum_{i=1}^m \frac{1}{p_i n_i} \sum_{j=1}^{n_i} \frac{1}{p_{ij} t_{ij}} \sum_{k=1}^{t_{ij}} \frac{v_{ijk}}{p_{ijk}} \quad (8)$$

in which

$v_{ijk}$  is the measured volume in the  $k^{\text{th}}$  third stage unit in the  $j^{\text{th}}$  second stage unit in the  $i^{\text{th}}$  primary unit,

$p_{ijk}$  is the selection probability associated with  $v_{ijk}$ , defined as  $c_{ijk}/c_{ij}$ ,

$t_{ij}$  is the number of third stage units in the  $ij^{\text{th}}$  first and second stage units, and the other terms are as defined earlier.

When the predicted values are adjusted so that their sum equals the values at the next higher stage, i.e., when

$$\sum_{k=1}^{t_{ij}} C_{ijk} = C_{ij}$$

$$\sum_{j=1}^{N_i} C_{ij} = C_i$$

$$\sum_{i=1}^M C_i = C$$

the three-stage estimator may be simplified to

$$v = \frac{C}{m} \sum_{i=1}^m \frac{1}{n_i} \sum_{j=1}^{n_i} \frac{1}{t_{ij}} \sum_{k=1}^{t_{ij}} \frac{v_{ijk}}{c_{ijk}} \quad (9)$$

If  $n_i$  and  $t_{ij}$  always equal one, formula (9) further simplifies to

$$v = \frac{C}{m} \sum_{i=1}^m \frac{v_{ijk}}{c_{ijk}} \quad (10)$$

The reasonableness of this final simplification would depend, of course, on the outcome of optimum allocation. From early trials, it appears that large scale aerial photographs contain sufficient information to control the second or third stage variation within comparatively narrow limits compared to the first stage variance. One particular calculation of optimal allocation in a small two-stage trial survey in Shasta County, California showed that  $n_i$  should average about 1.6 for each first stage unit drawn. It may turn out that improved photo interpretation techniques for large and small scale color photography will result in optimum  $n_i$ 's of 1. However, optimum allocation depends on cost in addition to the variance (see Appendix C).

The variance of  $v$  for three-stage variable probability sampling with replacement is

$$\begin{aligned} \text{Var}(v) &= \frac{1}{m} \left[ \sum_{i=1}^M \frac{V_i^2}{P_i} - V^2 \right] + \frac{1}{m} \sum_{i=1}^M \frac{1}{P_i n_i} \left[ \sum_{j=1}^{N_i} \frac{V_{ij}^2}{P_{ij}} - V_i^2 \right] \\ &+ \frac{1}{m} \sum_{i=1}^M \frac{1}{P_i n_i} \sum_{j=1}^{N_i} \frac{1}{P_{ij} t_{ij}} \left[ \sum_{k=1}^{T_{ij}} \frac{V_{ijk}^2}{P_{ijk}} - V_{ij}^2 \right] \end{aligned} \quad (11)$$

$$\begin{aligned} &= \frac{1}{m} \sum_{i=1}^M P_i \left( \frac{V_i}{P_i} - V \right)^2 + \frac{1}{m} \sum_{i=1}^M \frac{1}{P_i n_i} \sum_{j=1}^{N_i} P_{ij} \left( \frac{V_{ij}}{P_{ij}} - V_i \right)^2 \\ &+ \frac{1}{m} \sum_{i=1}^M \frac{1}{P_i n_i} \sum_{j=1}^{N_i} \frac{1}{P_{ij} t_{ij}} \sum_{k=1}^{T_{ij}} P_{ijk} \left( \frac{V_{ijk}}{P_{ijk}} - V_{ij} \right)^2 \end{aligned} \quad (12)$$

in which all the terms are analogous to the first and second stage estimators defined earlier. The derivation of this variance is given in Appendix B.

### Stratified Sampling

In situations where the forest is partitioned into strata, consisting of forest stands delineated on high altitude aerial or space photographs, stratified sampling would be employed before the first stage. The estimator for total forest volume using stratified three-stage variable probability sampling is simply the sum of the individual stratum estimates, symbolically described as

$$\begin{aligned} v &= \sum_{h=1}^H v_h \\ &= \sum_{h=1}^H \frac{1}{m_h} \sum_{i=1}^{m_h} \frac{1}{P_{hi} n_{hi}} \sum_{j=1}^{n_{hi}} \frac{1}{P_{hij} t_{hij}} \sum_{k=1}^{t_{hij}} \frac{v_{hijk}}{P_{hijk}} \end{aligned} \quad (13)$$

in which all the terms are as before except for  $h$  and  $H$  denoting the individual stratum and number of strata respectively.

### The Gain from Sampling with Variable Probabilities

According to Murthy (1967, p. 197), the variance of  $v$  for one-stage simple random sampling with replacement may be estimated from a pps sample from the formula

$$\text{Var}(v)_{\text{srs}} = \frac{1}{n^2} \left( N \sum_{i=1}^n \frac{y_i^2}{p_i} - n \hat{y}_{\text{pps}}^2 \right) + \frac{1}{n} \text{Var}(v)_{\text{pps}}$$

If we substitute the estimated variance from pps sampling in the second term and also subtract it out and simplify, we obtain the estimated gain of pps sampling over equal probability sampling. The result may be expressed as

$$\hat{G}_{\text{pps}} = \frac{1}{n^2} \sum_{i=1}^n \frac{y_i^2}{p_i} \left( N - \frac{1}{p_i} \right) \quad (14)$$

As it can be seen from the formula, the gain decreases substantially as  $n$  gets large. Hence it would appear that the greatest gains are possible with small sample sizes and more particularly when  $N$  is large. Therefore, under certain conditions pps sampling may provide better estimators than regression or ratio sampling when the sample size is small.

### Transformations on Supplementary Variables

As it is shown earlier, the pps estimator is unbiased as long as the observations are drawn as prescribed by the predetermined

selection probabilities.

Even though the estimator is unbiased, however, the most precise results are obtained when the scatter is tight and the relationship between the prediction and measurement variables is linear through the origin (proportional). It often happens in forest photointerpretation work that measurement variables, such as timber volume, are curvilinearly related to prediction variables such as tree crown diameter. Curvilinearity of this kind would certainly lead to a higher variance. By subjecting the prediction variable to a suitable transformation, the relationship can be made nearly linear through the origin yielding significantly better results. For example, Aldred (1971) reports the following model can be used to predict white spruce volume in Eastern Canada from large scale air photographs.

$$\hat{V} = a + b(H \log(CA))$$

in which  $a$  and  $b$  are regression coefficients,  $H$  is photo-measured tree height,  $CA$  is photo-measured crown area and  $\hat{V}$  is the predicted volume of the tree in cubic feet. Similar functions are widely used to predict stand volumes from aerial photographs which in turn can be used as selection probabilities in variable probability sampling. Translating the  $X$  scale so as to remove the  $X$  intercept can improve the proportionality between the  $X$  and  $Y$  variables and lower the variance in pps sampling. Some examples, taken from the Apollo 9 forest inventory experiment, are given in the following pages.

Figures A1 through A2 show the relationships between the timber volume per primary sample unit as estimated from subsampling and the volume per psu as determined from the space photos by means of photointerpretation. Figures A1 and A2 show these relationships for the two strata in the state of Georgia. Figure A3 shows the same data as Figure A2 after translating the X scale to the right by an amount equal to the estimated X intercept from linear regression. After making this translation, the estimated rel-variance of the ratios  $v_i/p_i$  for that stratum is substantially reduced as shown in Table A.2. While the sample size here is too small to draw any general conclusions, it is conceivable that in situations where the regression line between the Y and the X variates does not pass through the origin, a translation of the X scale to make it so can improve the overall proportionality of the two variates and hence improve the pps estimator.

Table A.2  
Rel-Variations of  $v_i/p_i$  from the First Stage  
of the Apollo 9 Inventory Study

	<u>Georgia Area</u>	<u>Mississippi Valley Area</u>
Unstratified	.4409	.2125
Stratified (2 strata)	.0507	.0424
Stratified and translated (X-axis)	.0033	.0563

Figures A4 through A6 show the relationships between the Y and X variates for the two strata in the Mississippi River Valley. Figure A6 shows the regression through the origin in the bottomland

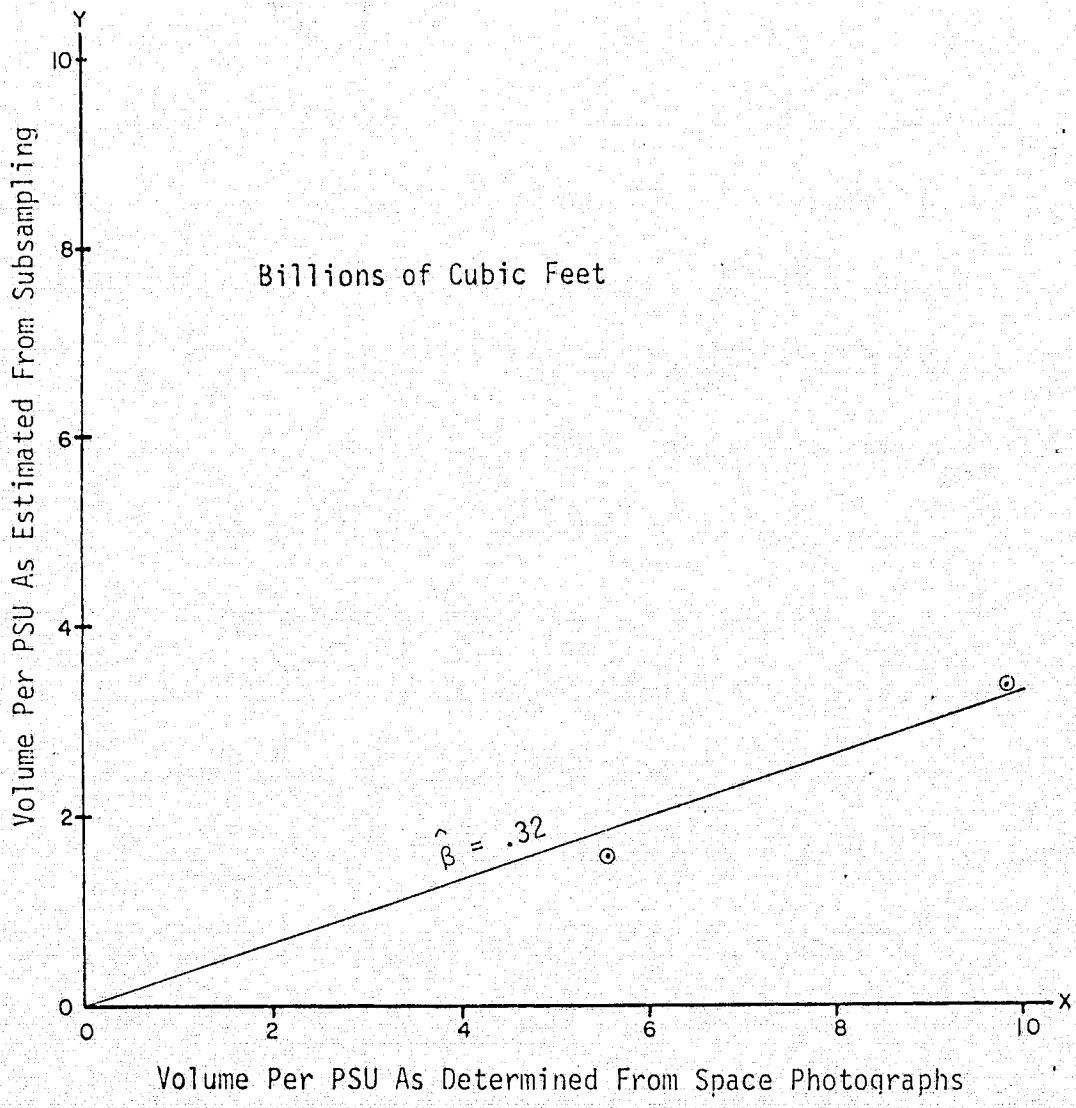


Figure A1. Apollo 9 Timber Inventory Study, Western Georgia. Estimated volume vs. photo volume at first stage.

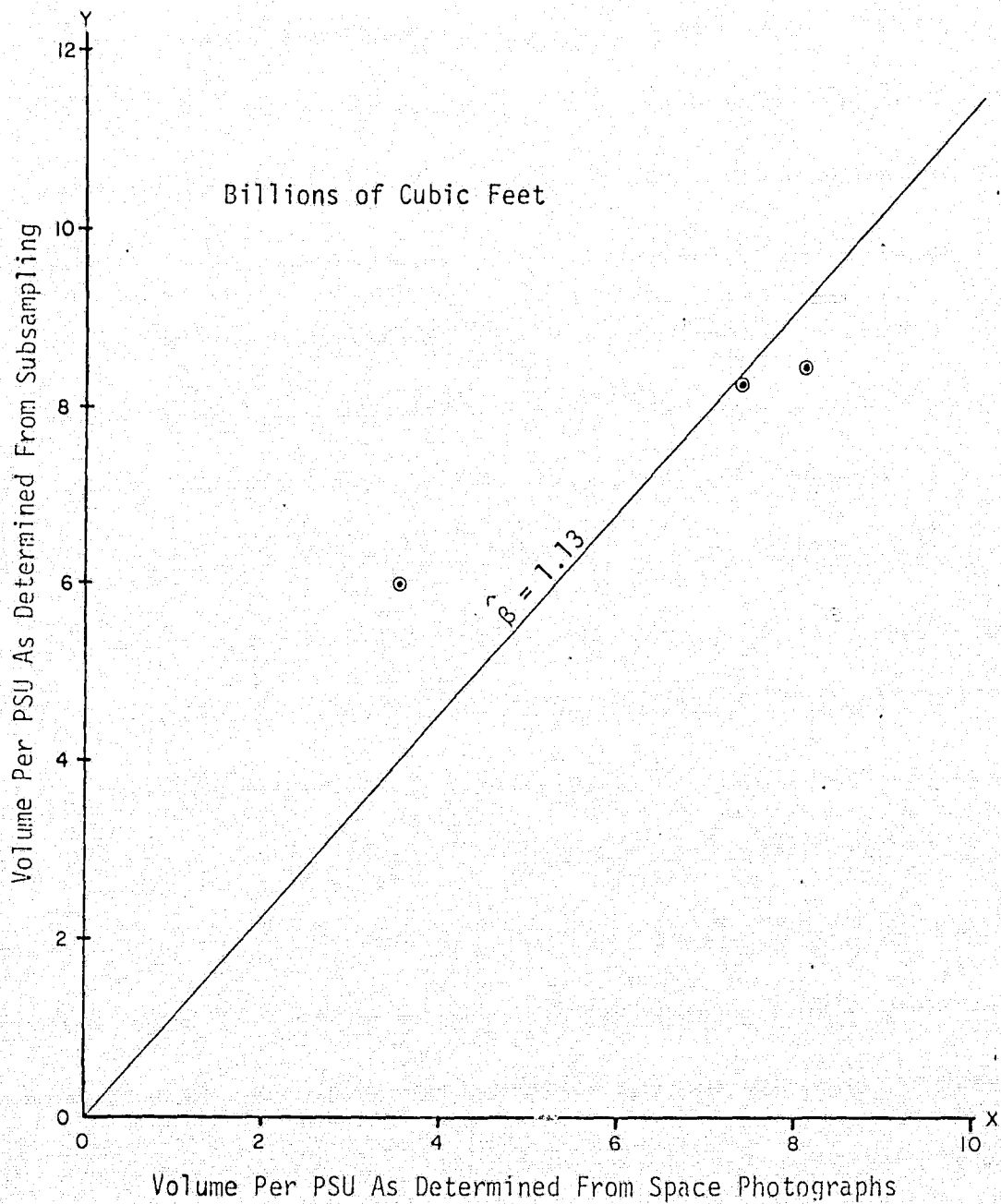


Figure A2. Apollo 9 Timber Inventory Study, Atlanta Area. Estimated vs. photo volume at first stage.

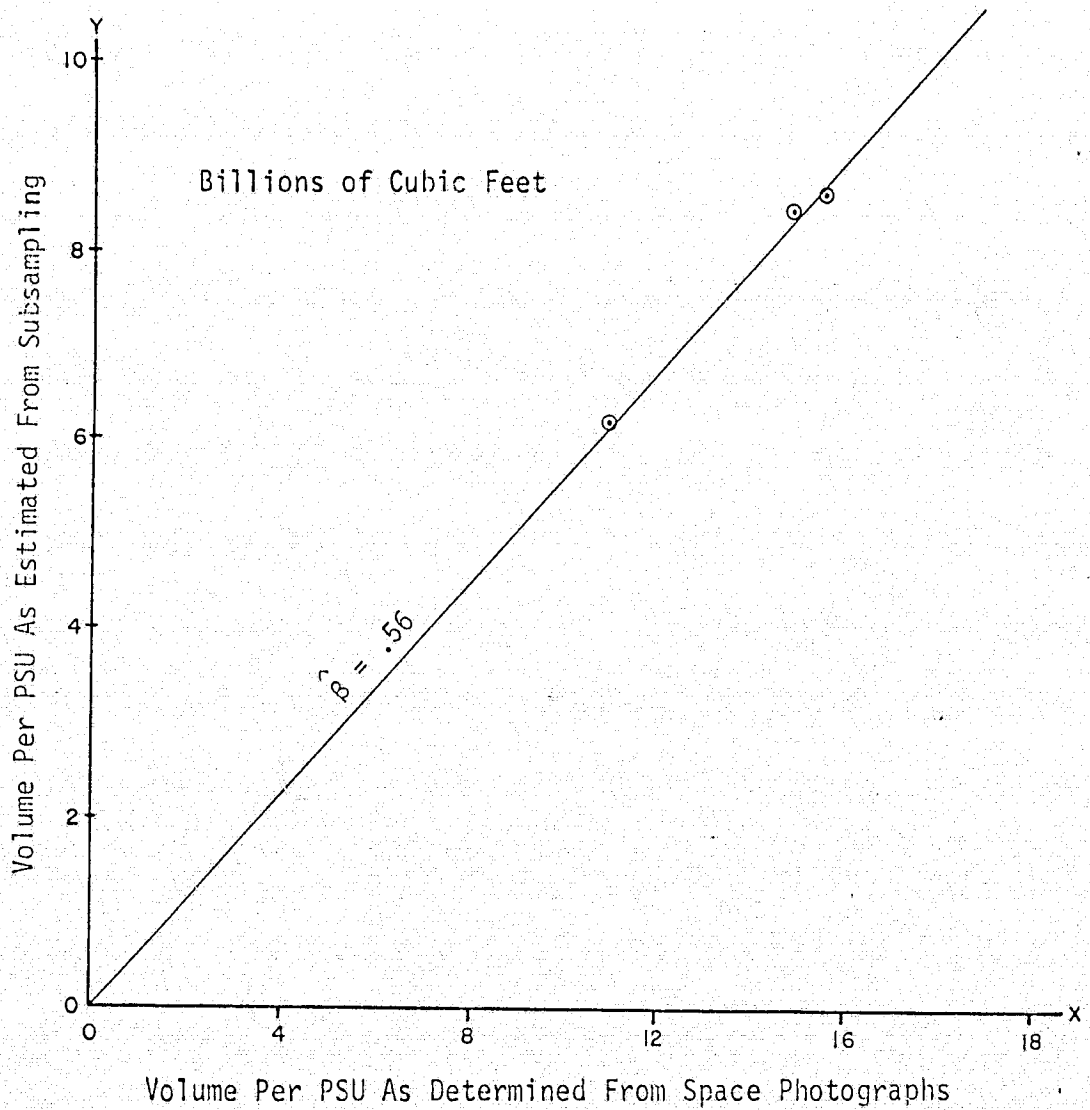
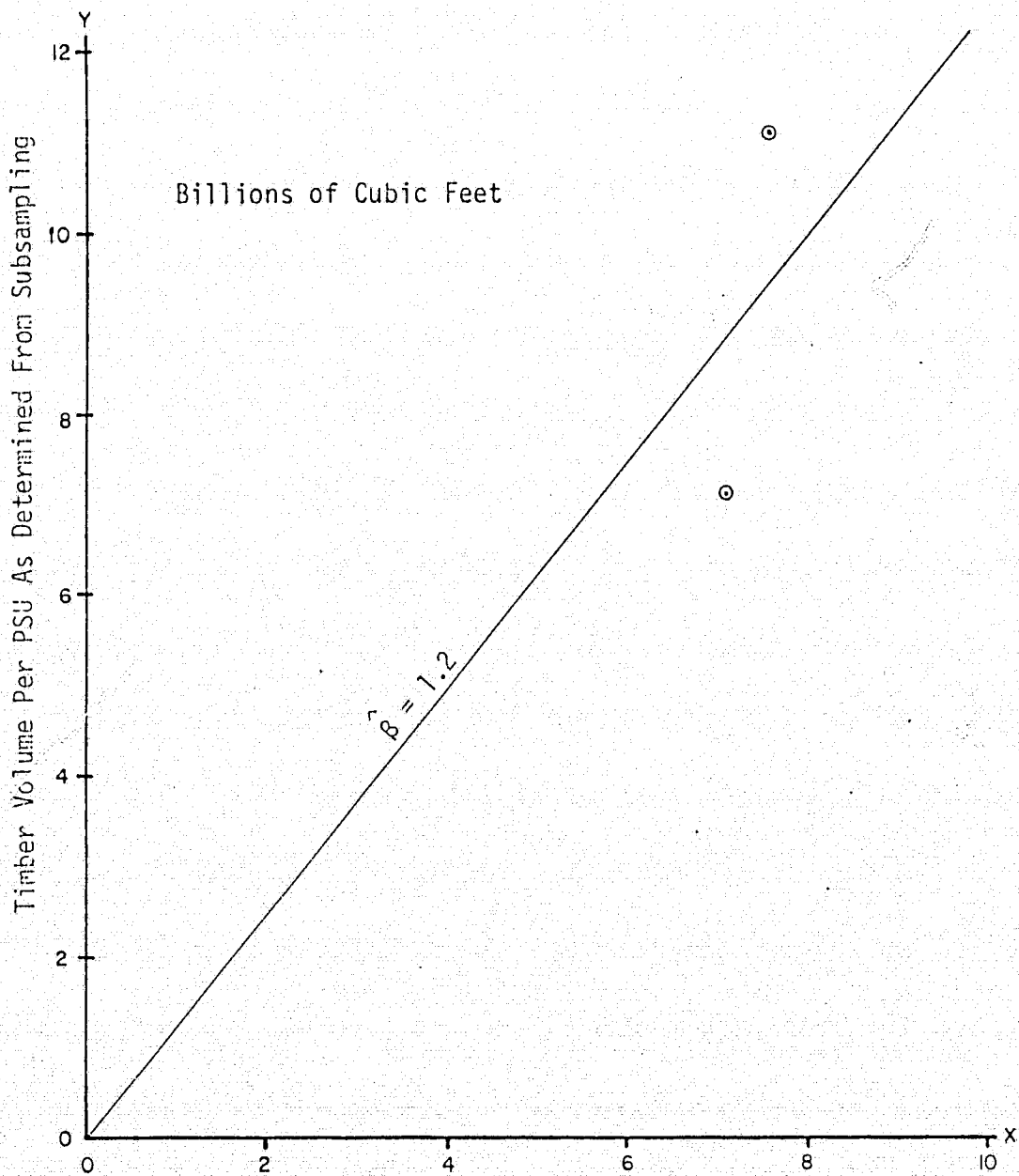


Figure A3. Apollo 9 Timber Inventory Study, Atlanta Area. Estimated vs. photo volume after translation of X scale.



Timber Volume Per PSU As Determined From Space Photographs

Figure A4. Apollo 9 Timber Inventory Study, Mississippi Valley Pine Stratum. Estimated vs. photo volume at first stage.

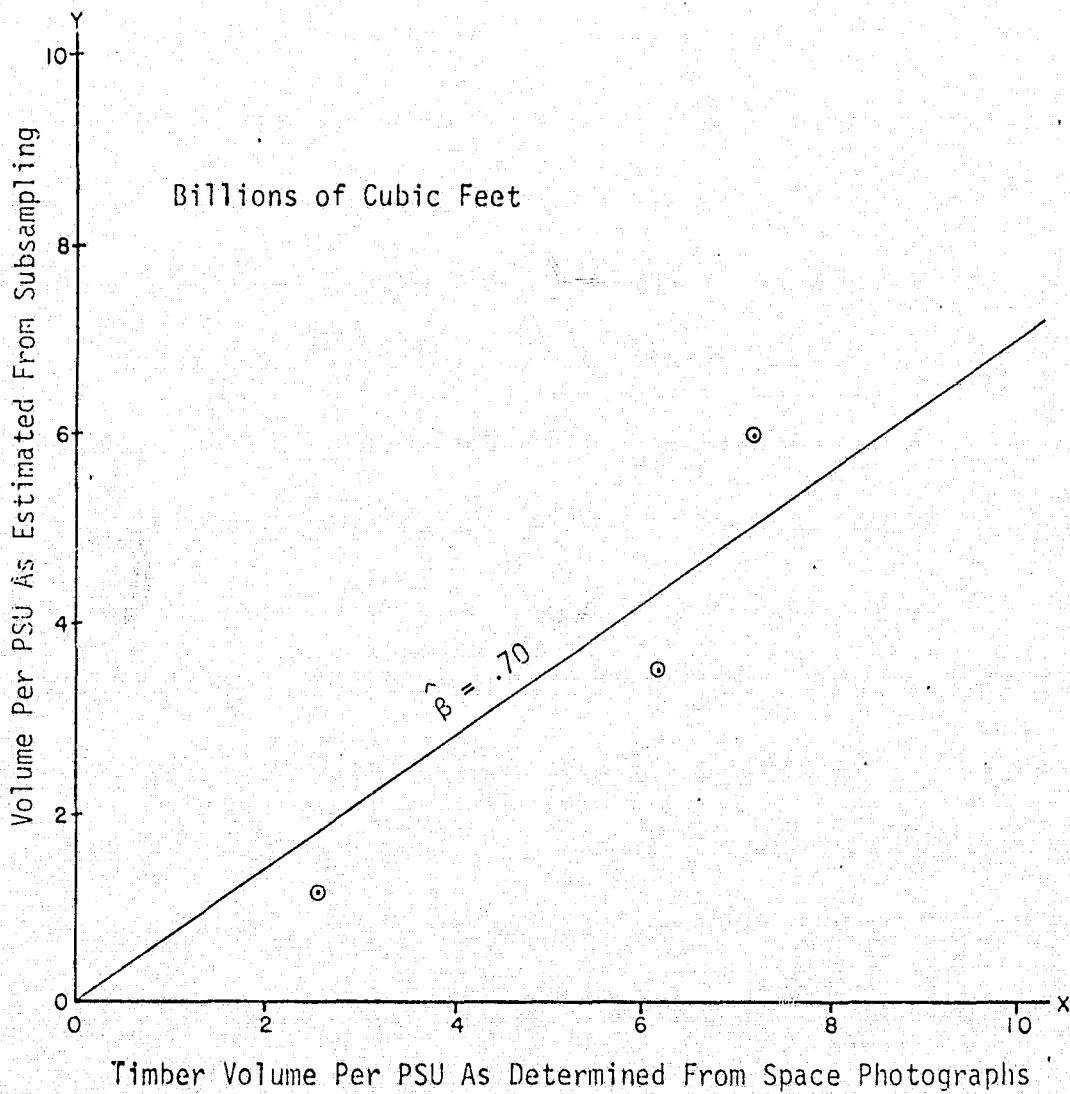


Figure A5. Apollo 9 Timber Inventory Study, Mississippi Valley Bottomland Hardwood Stratum. Estimated vs. photo volume at first stage.

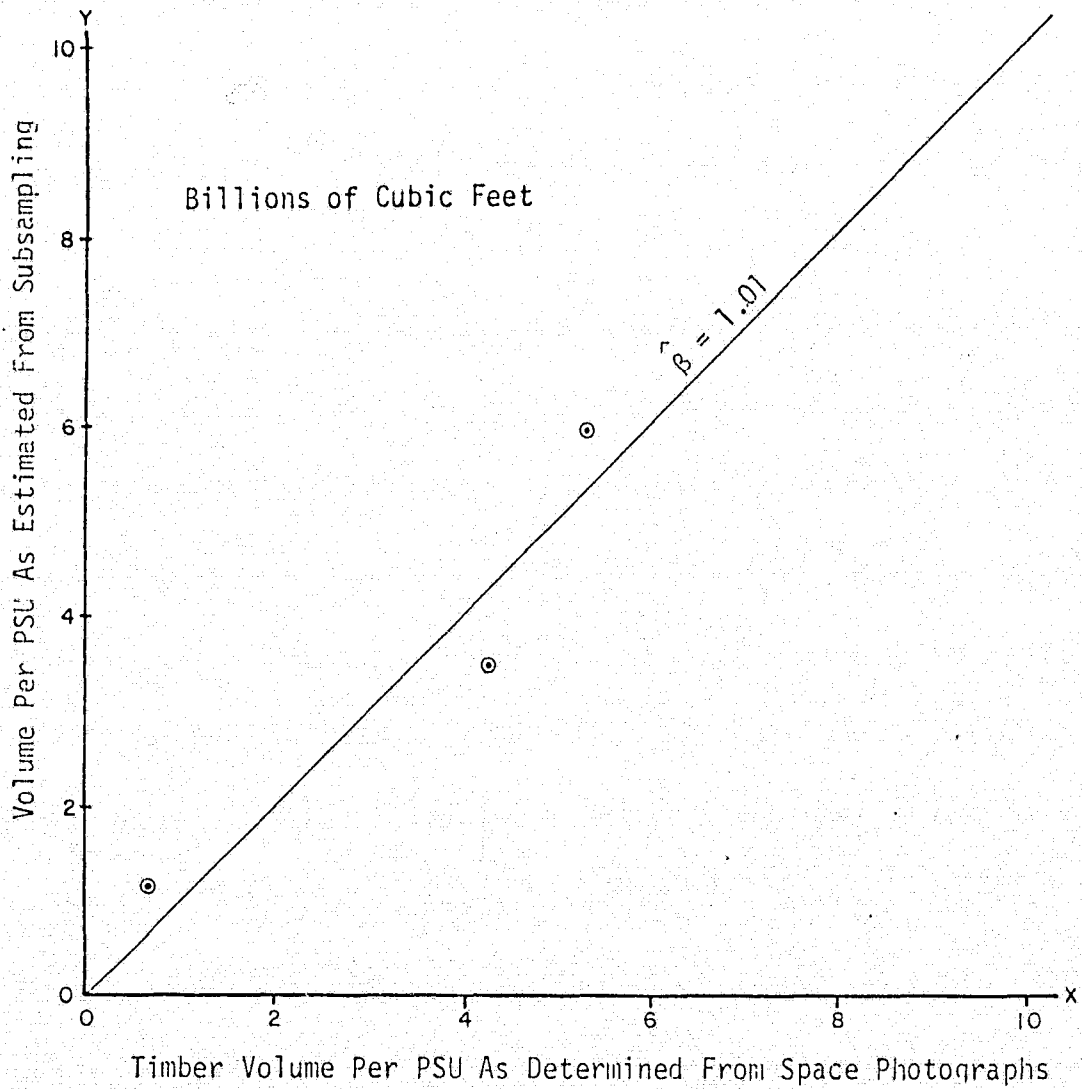


Figure A6. Apollo 9 Timber Inventory Study, Mississippi Valley Bottomland Hardwood Stratum. Estimated vs. photo volume after translation of X scale.

hardwood stratum after translating the X scale to the left. In this case, however, no gain in the rel-variance can be shown after the translation (Table A.2). On the other hand, no significant harm appears to be done by the translation.

APPENDIX B  
OPTIMUM ALLOCATION

In order to take maximum advantage of the funds expended for a timber survey using aerial photographs, it is helpful to have some idea about the relative sample size required in each stage of the design. Optimum allocation may be approached from two directions: (1) to minimize variance for a specified cost or (2) to minimize cost for a specified variance. The former approach is pursued herein.

Murthy (1967, p. 335) discusses optimum allocation in two- and three-stage designs of various configurations of sample selection. In his derivation of the optimal number of sample units to use in each stage, Murthy uses Lagrange multipliers, which is the method used here. However, this author presents the derivation for the cases where pps sampling is used in all stages of two- and three-stage designs. In addition, an approximate procedure is presented here for a variable allocation of samples in three-stage sampling which depends on the size of the units drawn in the first and second stages.

Two-Stage Sampling

Drawing from formula (7a), we can write the variance of the two-stage pps estimator as

$$\begin{aligned} \text{Var}(v) &= \frac{\sigma_1^2}{m} + \frac{1}{m} \sum_{i=1}^M \frac{1}{n_i} \frac{\sigma_{2i}^2}{P_i} \\ &= \frac{\sigma_1^2}{m} + \frac{1}{m} \sum_{i=1}^M \frac{\tilde{\sigma}_{2i}^2}{n_i} \end{aligned} \quad (15)$$

in which

$$\tilde{\sigma}_{2i}^2 = \sigma_{2i}^2 / P_i$$

In introducing the cost constraint, we assume the simplest linear function

$$D = mD_1 + \left( \sum_{i=1}^M n_i \right) D_2$$

in which

- $D$  is the cost of the survey excluding overhead costs,
- $D_1$  is the average cost of measuring a first stage unit and includes the cost of enumerating the predictions (i.e., the cost of obtaining the  $C_i$ 's),
- $D_2$  is the average cost of measuring a second stage unit, including travel costs.

Then,

$$\begin{aligned} \bar{D}^* &= E(D) = mD_1 + m \left( \sum_{i=1}^M P_i n_i \right) D_2 \\ &= mD_1 + m\bar{n}D_2 \end{aligned} \quad (16)$$

in which  $\bar{n} = \sum_{i=1}^M P_i n_i$ , the expected average number of second stage units per first stage unit. Now let  $N = M\bar{n}$ . Then by extracting from (15) and forming the Lagrange multiplier, define

$$L = \sum_{i=1}^M \frac{\sigma_{2i}^2}{P_i n_i} + \lambda \left( M \sum_{i=1}^M P_i n_i - N \right)$$

Differentiating with respect to a particular  $n_i$ , and equating to zero, we have for the  $r^{\text{th}}$  first stage unit

$$\frac{\partial L}{\partial n_r} = \frac{-\sigma_{2r}^2}{P_r n_r^2} + \lambda M P_r = 0$$

from which

$$n_r = \frac{1}{\sqrt{\lambda}} \frac{\sigma_{2r}}{P_r \sqrt{M}} \quad (17)$$

$$\bar{n} = \sum_{i=1}^M P_i n_i = \frac{1}{\sqrt{\lambda}} \frac{\sum_{i=1}^M \sigma_{2i}}{\sqrt{M}}$$

and finally,

$$\frac{1}{\sqrt{\lambda}} = \frac{\bar{n} \sqrt{M}}{\sum_{i=1}^M \sigma_{2i}}$$

Then substituting for  $1/\sqrt{\lambda}$  in equation (17) and simplifying, we obtain

$$n_r^0 = \bar{n} \frac{\sigma_{2r}}{P_r \sum_{i=1}^M \sigma_{2i}}$$

Hence

$$\begin{aligned} \sum_{i=1}^M \frac{\sigma_{2i}^2}{P_i n_i^0} &= \sum_{i=1}^M \frac{\sigma_{2i}^2}{P_i} \cdot \frac{P_i \left( \sum_{i=1}^M \sigma_{2i} \right)}{\bar{n} \sum_{i=1}^M \sigma_{2i}} \\ &= \frac{1}{\bar{n}} \left( \sum_{i=1}^M \sigma_{2i} \right)^2 \end{aligned}$$

Consequently, after "optimal" allocation of secondary units,

$$\text{Var}(v) = \frac{\sigma_1^2}{m} + \frac{\left( \sum_{i=1}^M \sigma_{2i} \right)^2}{m \bar{n}} = \frac{\sigma_1^2}{m} + \frac{\sigma_2^2}{m \bar{n}}$$

Now minimizing  $\text{Var}(v)$  with respect to  $m$  and  $\bar{n}$  subject to the expected cost constraint of formula (16), we define

$$L = \frac{\sigma_1^2}{m} + \frac{\sigma_2^2}{m\bar{n}} + \lambda(mD_1 + m\bar{n}D_2 - \bar{D}^*)$$

$$\frac{\partial L}{\partial \bar{n}} = -\frac{\sigma_2^2}{m\bar{n}^2} + \lambda m D_2 = 0$$

which yields

$$\frac{\sigma_2^2}{m\bar{n}} = \lambda(\bar{D}^* - mD_1)$$

or

$$m\bar{n} = \frac{\sigma_2^2}{\lambda(\bar{D}^* - mD_1)} \quad (18)$$

Then

$$\frac{\partial L}{\partial m} = -\frac{\sigma_1^2}{m^2} - \frac{\sigma_2^2}{m^2\bar{n}} + \lambda(D_1 + \bar{n}D_2) = 0$$

Since from equation (16)

$$D_1 + \bar{n}D_2 = \frac{\bar{D}^*}{m}$$

we have

$$\lambda\bar{D}^* = m\left[\frac{\sigma_1^2}{m^2} + \frac{\sigma_2^2}{m^2\bar{n}}\right]$$

$$= \frac{\bar{n}\sigma_1^2 + \sigma_2^2}{m\bar{n}} \quad (19)$$

Substituting for  $m\bar{n}$  in equation (19) from equation (18), and simplifying, we obtain

$$\frac{\bar{n}\sigma_1^2 + \sigma_2^2}{\sigma_2^2} = \frac{\bar{D}^*}{\bar{D}^* - mD_1} = \frac{mD_1 + m\bar{n}D_2}{m\bar{n}D_2}$$

Hence

$$\bar{n} \left( \frac{\sigma_1^2}{\sigma_2^2} \right) = \frac{D_1}{\bar{n} D_2}$$

Thus

$$\bar{n}^0 = \sqrt{\frac{D_1 \sigma_2^2}{D_2 \sigma_1^2}}, \quad m^0 = \frac{\bar{D}^*}{D_1 + \bar{n}^0 D_2}$$

and the optimum allocation is given by

$$n_r^0 = \bar{n}^0 \frac{\sigma_{2r}}{P_r \sum_{i=1}^M \sigma_{2i}} \quad (19a)$$

or

$$n_r^0 = \frac{\sigma_{2r}}{P_r \sigma_1} \sqrt{\frac{D_1}{D_2}}$$

As it can be seen above, the evaluations of  $m^0$ ,  $\bar{n}^0$ , and  $n_r^0$  depend on  $\sigma_1^2$ ,  $\sigma_2^2$  and  $\sigma_{2r}$ . Since these would not ordinarily be known ahead of time, estimates would have to be obtained from similar previous surveys or from a pilot survey. The estimating equations would be

$$\hat{\sigma}_{2r}^2 = \left\{ \frac{1}{n_r(n_r-1)} \left[ \sum_{j=1}^{n_r} \left( \frac{v_{rj}}{p_{rj}} \right)^2 - n_r v_{r-}^2 \right] \right\}^{1/2} \quad (20)$$

$$\hat{\sigma}_2^2 = \frac{1}{m} \sum_{i=1}^m \frac{\hat{\sigma}_{2i}^2}{p_i}$$

and

$$\hat{\sigma}_1^2 = m(\text{var}(v)) - \frac{1}{m} \sum_{i=1}^m \frac{1}{n_i} \frac{\hat{\sigma}_{2i}^2}{p_i}$$

where  $\text{var}(v)$  is obtained from equation (4) and the  $\hat{\sigma}_{2i}^2$ 's are obtained from equation (20).

### Three-Stage Sampling

From equation (12) we obtain the variance of the three-stage pps estimator

$$\begin{aligned} \text{Var}(v) &= \frac{\sigma_1^2}{m} + \frac{1}{m} \sum_{i=1}^M \frac{1}{n_i} \frac{\sigma_{2i}^2}{p_i} + \frac{1}{m} \sum_{i=1}^M \frac{1}{n_i} \sum_{j=1}^{N_i} \frac{1}{t_{ij}} \frac{\sigma_{3ij}^2}{p_i p_{ij}} \\ &= \frac{\sigma_1^2}{m} + \frac{1}{m} \sum_{i=1}^M \frac{\tilde{\sigma}_{2i}^2}{n_i} + \frac{1}{m} \sum_{i=1}^M \frac{1}{n_i} \sum_{j=1}^{N_i} \frac{\tilde{\sigma}_{3ij}^2}{t_{ij}} \end{aligned} \quad (21)$$

in which  $\tilde{\sigma}_{2i}^2 = \frac{\sigma_{2i}^2}{p_i}$ ,  $\tilde{\sigma}_{3ij}^2 = \frac{\sigma_{3ij}^2}{p_i p_{ij}}$ ,  $m$  and  $n_i$  are as defined above, and  $t_{ij}$  is the number of third stage units in the  $j^{\text{th}}$  second stage unit within the  $i^{\text{th}}$  first stage unit. We then introduce the simple linear cost constraint

$$D = mD_1 + \left( \sum_{i=1}^m n_i \right) D_2 + \left( \sum_{i=1}^m \sum_{j=1}^{n_i} t_{ij} \right) D_3$$

in which  $D_1$ ,  $D_2$ , and  $D_3$  are the costs attributable to measuring the first, second and third stage units respectively;

$$E(t_{ij}) = \sum_{i=1}^M \sum_{j=1}^{N_i} p_i p_{ij} t_{ij} = \bar{t}$$

and

$$E(n_i) = \sum_{i=1}^M p_i n_i = \bar{n}$$

The expected cost is

$$\bar{D}^* = E(D) = mD_1 + m\bar{n}D_2 + m\bar{n}\bar{t}D_3$$

We seek first the optimal values of  $t_{ij}$  and  $\bar{t}$  in the third stage and then progress to the second stage values of  $n_j$  and  $\bar{n}$ . Let  $T_i = N_i\bar{t}$  be the total number of third stage units in the  $i^{\text{th}}$  first stage unit. Then

$$L = \sum_{j=1}^{N_i} \frac{\tilde{\sigma}_{3ij}^2}{t_{ij}} + \lambda \left( N_i \sum_{i=1}^M \sum_{j=1}^{N_i} P_i P_{ij} t_{ij} - T_i \right)$$

Differentiating with respect to a particular  $t_{ij}$ , we have

$$\frac{\partial L}{\partial t_{ir}} = - \frac{\tilde{\sigma}_{3ir}^2}{t_{ir}^2} + \lambda N_i P_i P_{ir} = 0$$

and

$$t_{ir}^2 = \frac{\tilde{\sigma}_{3ir}^2}{\lambda N_i P_i P_{ir}} = \frac{\sigma_{3ir}^2}{\lambda N_i P_i^2 P_{ir}^2}$$

Hence

$$t_{ir} = \frac{1}{\sqrt{\lambda}} \frac{\sigma_{3ir}}{P_i P_{ir} \sqrt{N_i}}$$

$$\bar{t} = \sum_{i=1}^M \sum_{j=1}^{N_i} P_i P_{ij} t_{ij} = \frac{1}{\sqrt{\lambda}} \sum_{i=1}^M \sum_{j=1}^{N_i} \frac{\sigma_{3ij}}{\sqrt{N_i}}$$

and

$$\frac{1}{\sqrt{\lambda}} = \frac{\bar{t}}{\sum_{i=1}^M \sum_{j=1}^{N_i} \frac{\sigma_{3ij}}{\sqrt{N_i}}}$$

Hence the optimum number of third stage units in the  $r^{\text{th}}$  second stage unit is given by

$$t_{ir}^o = \frac{\bar{t}}{\sum_{i=1}^M \sum_{j=1}^{N_i} \left( \frac{\sigma_{3ij}}{\sqrt{N_i}} \right)} \frac{\sigma_{3ir}}{p_i p_{ir} \sqrt{N_i}}$$

Thus in the third term of the variance, we have

$$\begin{aligned} \sum_{j=1}^{N_i} \frac{\sigma_{3ij}^2}{p_i p_{ij} t_{ij}^o} &= \sum_{j=1}^{N_i} \frac{\sigma_{3ij}^2 p_i p_{ij} \sqrt{N_i}}{p_i p_{ij} \bar{t} \sigma_{3ij}} \left( \sum_{i=1}^M \sum_{j=1}^{N_i} \frac{\sigma_{3ij}}{\sqrt{N_i}} \right) \\ &= \frac{1}{\bar{t}} \left( \sum_{i=1}^M \sum_{j=1}^{N_i} \frac{\sigma_{3ij}}{\sqrt{N_i}} \right) \sum_{j=1}^{N_i} \sigma_{3ij} \sqrt{N_i} \\ &= \frac{A_i}{\bar{t}} \end{aligned} \quad (22)$$

Thus

$$\begin{aligned} \text{Var}(v) &= \frac{\sigma_1^2}{m} + \frac{1}{m} \sum_{i=1}^M \frac{\sigma_{2i}^2}{n_i} + \frac{1}{m \bar{t}} \sum_{i=1}^M \frac{A_i}{n_i} \\ &= \frac{\sigma_1^2}{m} + \frac{1}{m} \sum_{i=1}^M \frac{\sigma_{2i}^2 + \frac{A_i}{\bar{t}}}{n_i} \end{aligned} \quad (23)$$

Working with the second stage units, let  $N = M\bar{n}$ . Then we wish to minimize the total variance,

$$L = \sum_{r=1}^M \frac{\sigma_{2r}^2 + \frac{A_r}{\bar{t}}}{n_r} + \lambda (M \sum_{r=1}^M p_r n_r - N)$$

with respect to  $n_r$ . Accordingly, we have

$$\frac{\partial L}{\partial n_r} = -\frac{\tilde{\sigma}_{2r}^2 + \frac{A_r}{\bar{t}}}{n_r^2} + \lambda MP_r = 0$$

Hence

$$\lambda MP_r n_r^2 = \tilde{\sigma}_{2r}^2 + \frac{A_r}{\bar{t}} = \frac{\sigma_{2r}^2 + \frac{A_r P_r}{\bar{t}}}{P_r}$$

Solving for  $n_r$  we obtain

$$n_r = \frac{1}{\sqrt{\lambda}} \frac{(\sigma_{2r}^2 + \frac{A_r P_r}{\bar{t}})^{1/2}}{P_r \sqrt{M}} \quad (24)$$

which then yields

$$\bar{n} = \frac{M}{\sum_{i=1}^M P_i n_i} = \frac{1}{\sqrt{\lambda}} \frac{\sum_{i=1}^M (\sigma_{2i}^2 + \frac{A_i P_i}{\bar{t}})^{1/2}}{\sqrt{M}}$$

or

$$\frac{1}{\sqrt{\lambda}} = \frac{\bar{n} \sqrt{M}}{\sum_{i=1}^M (\sigma_{2i}^2 + A_i P_i / \bar{t})^{1/2}} \quad (25)$$

Then using equations (24) and (25) we can express the minimizing (optimum) value of  $n_r$  as

$$n_r^0 = \frac{\bar{n}}{P_r} \frac{(\sigma_{2r}^2 + A_r P_r / \bar{t})^{1/2}}{\sum_{i=1}^M (\sigma_{2i}^2 + A_i P_i / \bar{t})^{1/2}} \quad (26)$$

By substituting equation (26) into equation (23) and simplifying, we obtain

$$\text{Var}(v) = \frac{\sigma_1^2}{m} + \frac{\left[ \sum_{i=1}^M (\bar{t}\sigma_{2i}^2 + A_i p_i) \right]^{1/2}}{m\bar{t}}^2$$

The above solution assumes that no serious "stability" problems arise from having  $\bar{t}$  within the radical. However, should this be a problem, the sample size can be held constant at the second stage so as to eliminate this problem. In the class of estimators discussed in this paper, a three-stage design would entail space and aerial photo interpretation in the first and second stages. The field data would be obtained in the third stage only. Since it is the field samples which usually are more costly than photo samples in forest surveys, it is important to have a near optimal allocation of field plots to photo plots, taking advantage of the variable sizes of the photo units if possible. On the other hand, the allocation of second stage photo plots to first stage photo plots that accounts for the exact variations in the size of the primary units may not be of extreme importance. Therefore, to keep the complexity of the problem within reasonable bounds, we will hold the second stage sample size ( $n$ ) constant and proceed from there. In this simplified case, we express the variance as

$$\begin{aligned} \text{Var}(v) &= \frac{\sigma_1^2}{m} + \frac{1}{mn} \sum_{i=1}^M \frac{\sigma_{2i}^2}{p_i} + \frac{1}{mn} \sum_{i=1}^M \sum_{j=1}^{N_i} \frac{1}{t_{ij}} \frac{\sigma_{3ij}^2}{p_i p_{ij}} \\ &= \frac{\sigma_1^2}{m} + \frac{1}{mn} \sum_{i=1}^M \tilde{\sigma}_{2i}^2 + \frac{1}{mn} \sum_{i=1}^M \sum_{j=1}^{N_i} \frac{\tilde{\sigma}_{3ij}^2}{t_{ij}} \end{aligned} \quad (27)$$

The accompanying cost function is

$$D = mD_1 + mnD_2 + \left( \sum_{i=1}^m \sum_{j=1}^n t_{ij} \right) D_3$$

with

$$E(t_{ij}) = \sum_{i=1}^M \sum_{j=1}^{N_i} P_i P_{ij} t_{ij} = \bar{t}$$

and

$$\bar{D}^* = E(D) = mD_1 + mnD_2 + mn\bar{t}D_3$$

As before, let  $T_i = N_i \bar{t}$ . Then allocating "optimally" gives

$$t_{ir}^0 = \frac{\bar{t}}{\sum_{i=1}^M \sum_{j=1}^{N_i} \left( \frac{\sigma_{3ij}}{\sqrt{N_i}} \right)} \cdot \frac{\sigma_{3ir}}{P_i P_{ir} \sqrt{N_i}} \quad (28)$$

and from formula (27)

$$\begin{aligned} \sum_{j=1}^{N_i} \frac{\tilde{\sigma}_{3ij}^2}{t_{ij}} &= \frac{1}{\bar{t}} \left( \sum_{i=1}^M \sum_{j=1}^{N_i} \frac{\sigma_{3ij}}{\sqrt{N_i}} \right) \sum_{j=1}^{N_i} \sigma_{3ij} \sqrt{N_i} \\ &= \frac{A_i}{\bar{t}} \end{aligned}$$

as before. Hence

$$\begin{aligned} \text{Var}(v) &= \frac{\sigma_1^2}{m} + \frac{1}{mn} \sum_{i=1}^M \tilde{\sigma}_{2i}^2 + \frac{1}{mn\bar{t}} \sum_{i=1}^M A_i \\ &= \frac{E_1}{m} + \frac{E_2}{mn} + \frac{E_3}{mn\bar{t}} \end{aligned} \quad (29)$$

Minimizing  $\text{Var}(v)$  with respect to  $m, n$  (constant) and  $\bar{t}$  subject to the cost constraint gives

$$\bar{t}^0 = \sqrt{\frac{E_3 D_2}{E_2 D_3}} \quad (30)$$

$$n^0 = \sqrt{\frac{E_2 D_1}{E_1 D_2}} \quad (31)$$

$$m^0 = \frac{\bar{D}^* \sqrt{\frac{E_1}{D_1}}}{\sqrt{E_1 D_1} + \sqrt{E_2 D_2} + \sqrt{E_3 D_3}} \quad (32)$$

These results, although arrived at differently, agree with Murthy (1967, p. 347). The variable allocation to third stage units would be according to equation (28) and an approximation of the variable allocation of second stage units to first stage units can be made according to equation (26). However, these two equations require population values that are interconnected through all stages of the design and would not normally be available. Therefore, approximate estimators for these values are given below.

In order to use a variable allocation which depends on unit sizes, we shall need estimators for the optimum values of  $n_r^0$  and  $t_{ir}^0$ . Incorporated within these are the requirements for estimators of the  $A_r$ 's, the  $\sigma_{3ir}$ 's and the  $\sigma_{2r}^2$ 's. Accordingly, we have the estimates

$$\hat{n}_r^0 = \frac{n}{P_r} \cdot \frac{(\hat{\sigma}_{2r}^2 + \hat{A}_r P_r / \bar{t}^0)^{1/2}}{\frac{1}{m} \sum_{i=1}^m \frac{1}{p_i} (\hat{\sigma}_{2i}^2 + \hat{A}_i p_i / \bar{t}^0)^{1/2}}$$

$$\hat{t}_{ir}^0 = \frac{\bar{t}}{\frac{1}{m} \sum_{i=1}^m \frac{1}{p_i n_i} \sum_{j=1}^{n_i} \frac{1}{p_{ij}} \left( \frac{\hat{\sigma}_{3ij}}{\sqrt{N}} \right)} \cdot \frac{\hat{\sigma}_{3ir}}{p_i p_{ir} \sqrt{N}}$$

and

$$\hat{A}_r = \left( \frac{1}{m} \sum_{i=1}^m \frac{1}{p_i n_i} \sum_{j=1}^{n_i} \frac{1}{p_{ij}} \frac{\hat{\sigma}_{3ij}}{\sqrt{N_i}} \right) \cdot \frac{1}{n_r} \sum_{j=1}^{n_r} \frac{1}{p_{rj}} \hat{\sigma}_{3rj} \sqrt{N_r}$$

The third stage variances in the above formula can be estimated from a pilot sample or previous survey using the same form of estimator given in equations (4) and (20). To obtain estimates of the  $\sigma_{2r}^2$ 's, consider the second stage samples and their respective third stage subsamples as  $m$  two-stage samples. Then

$$\hat{\sigma}_{2r}^2 = n_r(\text{var}(v)_r) - \frac{1}{n_r} \sum_{j=1}^{n_r} \frac{1}{t_{rj}} \frac{\hat{\sigma}_{3rj}^2}{p_{rj}}$$

in which  $\text{var}(v)_r$  is the estimated total sample variance in the  $r^{\text{th}}$  first-stage unit.

Finally, to estimate  $m^0$ ,  $n^0$ , and  $\bar{t}^0$  estimates are first needed for  $\sigma_1^2$ ,  $\sum_{i=1}^M \tilde{\sigma}_{2i}^2$ , and  $\sum_{i=1}^M A_i$ . These may be obtained as follows:

$$\hat{\sigma}_1^2 = m[\text{var}(v)] - \frac{1}{mn} \sum_{i=1}^m \frac{\hat{\sigma}_{2i}^2}{p_i} - \frac{1}{m\bar{t}} \sum_{i=1}^m \frac{\hat{A}_i}{p_i}$$

$$\widehat{\sum_{i=1}^M \tilde{\sigma}_{2i}^2} = \frac{1}{m} \sum_{i=1}^m \frac{\hat{\sigma}_{2i}^2}{p_i}$$

and

$$\widehat{\sum_{i=1}^M A_i} = \frac{1}{m} \sum_{i=1}^m \frac{\hat{A}_i}{p_i}$$

## APPENDIX C

### DERIVATION OF THE VARIANCES

#### Two-Stage Variable Probability Sampling with Replacement

From the basic definition of variance, we have

$$\begin{aligned} \text{Var}(v) &= E[v - E(v)]^2 \\ &= E[v - V]^2 \\ &= E[v^2] - V^2 \end{aligned} \quad (33)$$

By substituting the sample estimate of  $v$  (equation 2) into (33), we obtain

$$\begin{aligned} \text{Var}(v) &= E\left[\left(\frac{1}{m} \sum_{i=1}^m \frac{v_i}{p_i}\right)^2\right] - v^2 \\ &= \frac{1}{m^2} E\left[\sum_{i=1}^m \frac{v_i^2}{p_i}\right] - v^2 \\ &= \frac{1}{m^2} E\left[\sum_{i=1}^m \frac{v_i^2}{p_i} + \sum_{i \neq i'}^m \frac{v_i}{p_i} \frac{v_{i'}}{p_{i'}}\right] - v^2 \end{aligned}$$

By expressing each of the  $v_i$ 's in terms of the second stage estimators, we have

$$\begin{aligned} \text{Var}(v) &= \frac{1}{m^2} E\left\{E_i\left[\sum_{i=1}^m \frac{1}{p_i n_i} \left(\sum_{j=1}^{n_i} \frac{v_{ij}}{p_{ij}}\right)^2\right.\right. \\ &\quad \left.\left.+ \sum_{i \neq i'}^m \left(\frac{1}{p_i n_i} \sum_{j=1}^{n_i} \frac{v_{ij}}{p_{ij}}\right) \left(\frac{1}{p_{i'} n_{i'}} \sum_{j=1}^{n_{i'}} \frac{v_{i'j}}{p_{i'j}}\right)\right]\right\} - v^2 \end{aligned}$$

in which  $E_i$  is the conditional expectation of second stage elements holding the first stage sample fixed. Before evaluating the

expectations in the second stage, however, we must first decompose  $(\sum_{j=1}^{n_i} \frac{v_{ij}}{p_{ij}})^2$  into its sums of squares and cross products. Hence

$$\begin{aligned} \text{Var}(v) &= \frac{1}{m^2} E\{E_i[\sum_{i=1}^m \frac{1}{p_i^2 n_i} \sum_{j=1}^{n_i} \frac{v_{ij}^2}{p_{ij}^2} + \sum_{i=1}^m \frac{1}{p_i^2 n_i} \sum_{j \neq j'}^{n_i} \frac{v_{ij}}{p_{ij}} \frac{v_{ij'}}{p_{ij'}} \\ &\quad + \sum_{i \neq i'}^m (\frac{1}{p_i n_i} \sum_{j=1}^{n_i} \frac{v_{ij}}{p_{ij}}) (\frac{1}{p_{i'} n_{i'}} \sum_{j=1}^{n_{i'}} \frac{v_{i'j}}{p_{i'j}})]\} - V^2 \\ &= \frac{1}{m^2} E[\sum_{i=1}^m \frac{1}{p_i^2 n_i} E_i \frac{v_{ij}^2}{p_{ij}^2} + \sum_{i=1}^m \frac{n_i-1}{p_i^2 n_i} E_i \frac{v_{ij}}{p_{ij}} \frac{v_{ij'}}{p_{ij'}} \\ &\quad + \sum_{i \neq i'}^m (\frac{1}{p_i} E_i \frac{v_{ij}}{p_{ij}}) (\frac{1}{p_{i'}} E_{i'} \frac{v_{i'j}}{p_{i'j}})] - V^2 \end{aligned} \tag{34}$$

The conditional expectations of the cross products in the second term within the brackets may be evaluated separately because subsampling within clusters is with replacement. The conditional expectations may be taken separately in the third term because subsampling within one cluster is independent of the subsampling within all other clusters. Hence,

$$\begin{aligned} \text{Var}(v) &= \frac{1}{m^2} E[\sum_{i=1}^m \frac{1}{p_i^2 n_i} \sum_{j=1}^{N_i} \frac{V_{ij}^2}{p_{ij}^2} + \sum_{i=1}^m \frac{n_i-1}{p_i^2 n_i} (\sum_{j=1}^{N_i} V_{ij}) (\sum_{j'=1}^{N_i} V_{ij'}) \\ &\quad + \sum_{i \neq i'}^m (\frac{1}{p_i} \sum_{j=1}^{N_i} V_{ij}) (\frac{1}{p_{i'}} \sum_{j'=1}^{N_{i'}} V_{i'j'})] - V^2 \\ &= \frac{1}{m^2} E[\sum_{i=1}^m \frac{1}{p_i^2 n_i} \sum_{j=1}^{N_i} \frac{V_{ij}^2}{p_{ij}^2} + \sum_{i=1}^m \frac{n_i-1}{p_i^2 n_i} V_i^2 + \sum_{i \neq i'}^m \frac{V_i V_{i'}}{p_i p_{i'}}] - V^2 \\ &= \frac{1}{m^2} E[\sum_{i=1}^m \frac{1}{p_i^2 n_i} \sum_{j=1}^{N_i} \frac{V_{ij}^2}{p_{ij}^2} + \sum_{i=1}^m \frac{V_i^2}{p_i^2} - \sum_{i=1}^m \frac{V_i^2}{p_i^2 n_i} + \sum_{i \neq i'}^m \frac{V_i V_{i'}}{p_i p_{i'}}] \\ &\quad - V^2 \end{aligned}$$

Now, evaluating the unconditional expectation over all population clusters, we have

$$\text{Var}(v) = \frac{1}{m^2} \left[ mE \frac{1}{P_i n_i} \sum_{j=1}^{N_i} \frac{V_{ij}^2}{P_{ij}} + mE \frac{V_i^2}{P_i} - mE \frac{V_i^2}{P_i n_i} + m(m-1)E \frac{V_i}{P_i} \frac{V_{i'}}{P_{i'}} \right] - V^2$$

Remembering that the expectations of the cross product in the third term are evaluated separately because of independence due to selecting the first stage clusters with replacement, we have

$$\begin{aligned} \text{Var}(v) &= \frac{1}{m^2} \left[ m \sum_{i=1}^M \frac{1}{P_i n_i} \sum_{j=1}^{N_i} \frac{V_{ij}^2}{P_{ij}} + m \sum_{i=1}^m \frac{V_i^2}{P_i} - m \sum_{i=1}^M \frac{V_i^2}{P_i n_i} \right. \\ &\quad \left. + m(m-1) \left( \sum_{i=1}^M V_i \right) \left( \sum_{i'=1}^m V_{i'} \right) \right] - V^2 \\ &= \frac{1}{m} \sum_{i=1}^M \frac{1}{P_i n_i} \sum_{j=1}^{N_i} \frac{V_{ij}^2}{P_{ij}} + \frac{1}{m} \sum_{i=1}^M \frac{V_i^2}{P_i} - \frac{1}{m} \sum_{i=1}^M \frac{V_i^2}{P_i n_i} \\ &\quad + \frac{(m-1)}{m} V^2 - V^2 \\ &= \frac{1}{m} \sum_{i=1}^M \frac{1}{P_i n_i} \sum_{j=1}^{N_i} \frac{V_{ij}^2}{P_{ij}} + \frac{1}{m} \sum_{i=1}^M \frac{V_i^2}{P_i} - \frac{1}{m} \sum_{i=1}^M \frac{V_i^2}{P_i n_i} + V^2 \\ &\quad - \frac{V^2}{m} - V^2 \end{aligned}$$

Finally, by rearranging terms and factoring, we obtain  $\text{Var}(v)$  for two stage sampling with replacement, i.e.

$$\begin{aligned} \text{Var}(v) &= \frac{1}{m} \sum_{i=1}^M \frac{V_i^2}{P_i} - \frac{V^2}{m} + \frac{1}{m} \sum_{i=1}^M \frac{1}{P_i n_i} \sum_{j=1}^{N_i} \frac{V_{ij}^2}{P_{ij}} - \frac{1}{m} \sum_{i=1}^M \frac{V_i^2}{P_i n_i} \\ &= \frac{1}{m} \left( \sum_{i=1}^M \frac{V_i^2}{P_i} - V^2 \right) + \frac{1}{m} \sum_{i=1}^M \frac{1}{P_i n_i} \left( \sum_{j=1}^{N_i} \frac{V_{ij}^2}{P_{ij}} - V_i^2 \right) \\ &\quad \text{1st stage} \qquad \qquad \qquad \text{2nd stage} \end{aligned}$$

### Three-Stage Variable Probability Sampling with Replacement

In deriving  $\text{Var}(v)$  for three stage probability sampling, we return to equation (34), substitute the third stage estimators in place of the  $v_{ij}$ 's, and proceed as before:

$$\begin{aligned}
 \text{Var}(v) &= \frac{1}{m^2} E\{E_i[E_{ij}[\sum_{i=1}^m \frac{1}{p_i^2 n_i^2} \sum_{j=1}^{n_i} \frac{1}{p_{ij}^2 t_{ij}^2} (\sum_{k=1}^{t_{ij}} \frac{v_{ijk}}{p_{ijk}})^2 \\
 &+ \sum_{i=1}^m \frac{1}{p_i^2 n_i^2} \sum_{j \neq j'}^{n_i} (\frac{1}{p_{ij} t_{ij}} \sum_{k=1}^{t_{ij}} \frac{v_{ijk}}{p_{ijk}}) (\frac{1}{p_{ij'} t_{ij'}} \sum_{k=1}^{t_{ij'}} \frac{v_{ij'k}}{p_{ij'k}}) \\
 &+ \sum_{i \neq i'}^m (\frac{1}{p_i n_i} \sum_{j=1}^{n_i} \frac{1}{p_{ij} t_{ij}} \sum_{k=1}^{t_{ij}} \frac{v_{ijk}}{p_{ijk}}) \\
 &\cdot (\frac{1}{p_{i'} n_{i'}} \sum_{j=1}^{n_{i'}} \frac{1}{p_{i'j} t_{i'j}} \sum_{k=1}^{t_{i'j}} \frac{v_{i'jk}}{p_{i'jk}})]\}} - v^2 \\
 &= \frac{1}{m^2} E\{E_i[E_{ij}[\sum_{i=1}^m \frac{1}{p_i^2 n_i^2} \sum_{j=1}^{n_i} \frac{1}{p_{ij}^2 t_{ij}^2} \\
 &\cdot (\sum_{k=1}^{t_{ij}} \frac{v_{ijk}^2}{p_{ijk}^2} + \sum_{k \neq k'}^{t_{ij}} \frac{v_{ijk}}{p_{ijk}} \frac{v_{ij'k'}}{p_{ij'k'}}) \\
 &+ \sum_{i=1}^m \frac{1}{p_i^2 n_i^2} \sum_{j \neq j'}^{n_i} (\frac{1}{p_{ij} t_{ij}} \sum_{k=1}^{t_{ij}} \frac{v_{ijk}}{p_{ijk}}) (\frac{1}{p_{ij'} t_{ij'}} \sum_{k=1}^{t_{ij'}} \frac{v_{ij'k}}{p_{ij'k}}) \\
 &+ \sum_{i \neq i'}^m (\frac{1}{p_i n_i} \sum_{j=1}^{n_i} \frac{1}{p_{ij} t_{ij}} \sum_{k=1}^{t_{ij}} \frac{v_{ijk}}{p_{ijk}}) \\
 &\cdot (\frac{1}{p_{i'} n_{i'}} \sum_{j=1}^{n_{i'}} \frac{1}{p_{i'j} t_{i'j}} \sum_{k=1}^{t_{i'j}} \frac{v_{i'jk}}{p_{i'jk}})]\}} - v^2
 \end{aligned}$$

In evaluating the expectation, we first find the conditional expectation of the third stage, holding the units of the first two stages constant. Secondly, we find the conditional expectation over all second stage units, holding the first stage units constant. Finally, we evaluate the unconditional expectation over

all first stage units. During the process, we keep in mind that all cross product terms contain independent random variables due to sampling with replacement at all levels and independently selected subsamples. In evaluating the expectations, we have

$$\begin{aligned}
 \text{Var}(v) &= \frac{1}{m^2} E\left\{ E_i \left[ \sum_{i=1}^m \frac{1}{p_i n_i} \sum_{j=1}^{n_i} \frac{1}{p_{ij} t_{ij}} E_{ij} \frac{v_{ijk}^2}{p_{ijk}^2} \right. \right. \\
 &+ \sum_{i=1}^m \frac{1}{p_i n_i} \sum_{j=1}^{n_i} \frac{t_{ij}-1}{p_{ij} t_{ij}} E_{ij} \frac{v_{ijk} v_{ijk'}}{p_{ijk} p_{ijk'}} \\
 &+ \sum_{i=1}^m \frac{1}{p_i n_i} \sum_{j \neq j'}^{n_i} \left( \frac{1}{p_{ij}} E_{ij} \frac{v_{ijk}}{p_{ijk}} \right) \left( \frac{1}{p_{ij'}} E_{ij'} \frac{v_{ij'k}}{p_{ij'k}} \right) \\
 &+ \sum_{i \neq i'}^m \left( \frac{1}{p_i n_i} \sum_{j=1}^{n_i} \frac{1}{p_{ij}} E_{ij} \frac{v_{ijk}}{p_{ijk}} \right) \\
 &\left. \left. \cdot \left( \frac{1}{p_{i'j'}} \sum_{j=1}^{n_{i'}} \frac{1}{p_{i'j'}} E_{i'j'} \frac{v_{i'jk}}{p_{i'jk}} \right) \right] \right\} - v^2 \\
 &= \frac{1}{m^2} E \left[ \sum_{i=1}^m \frac{1}{p_i n_i} E_i \frac{1}{p_{ij} t_{ij}} \sum_{k=1}^{T_{ij}} \frac{v_{ijk}^2}{p_{ijk}^2} \right. \\
 &+ \sum_{i=1}^m \frac{1}{p_i n_i} E_i \frac{t_{ij}-1}{p_{ij} t_{ij}} \left( \sum_{k=1}^{T_{ij}} v_{ijk} \right) \left( \sum_{k'=1}^{T_{ij}} v_{ijk'} \right) \\
 &+ \sum_{i=1}^m \frac{n_i-1}{p_i n_i} E_i \left( \frac{1}{p_{ij}} \sum_{k=1}^{T_{ij}} v_{ijk} \right) \left( \frac{1}{p_{ij'}} \sum_{k=1}^{T_{ij'}} v_{ij'k} \right) \\
 &\left. + \sum_{i \neq i'}^m \left( \frac{1}{p_i} E_i \frac{1}{p_{ij}} \sum_{k=1}^{T_{ij}} v_{ijk} \right) \left( \frac{1}{p_{i'}} E_{i'} \frac{1}{p_{i'j'}} \sum_{k=1}^{T_{i'j'}} v_{i'jk} \right) \right] - v^2
 \end{aligned}$$

$$\begin{aligned}
&= \frac{1}{m^2} [mE \frac{1}{p_i n_i} \sum_{j=1}^{N_i} \frac{1}{p_{ij} t_{ij}} \sum_{k=1}^{T_{ij}} \frac{V_{ijk}}{p_{ijk}} + mE \frac{1}{p_i n_i} \sum_{j=1}^{N_i} \frac{t_{ij}-1}{p_{ij} t_{ij}} V_{ij}^2 \\
&\quad + mE \frac{n_i-1}{p_i n_i} (\sum_{j=1}^{N_i} V_{ij}) (\sum_{j'=1}^{N_i} V_{ij'}) \\
&\quad + m(m-1)E (\frac{1}{p_i} \sum_{j=1}^{N_i} V_{ij}) (\frac{1}{p_{i'}} \sum_{j=1}^{N_i} V_{i',j})] - V^2 \\
&= \frac{1}{m^2} [m \sum_{i=1}^M \frac{1}{p_i n_i} \sum_{j=1}^{N_i} \frac{1}{p_{ij} t_{ij}} \sum_{k=1}^{T_{ij}} \frac{V_{ijk}^2}{p_{ijk}} + m \sum_{i=1}^M \frac{1}{p_i n_i} \sum_{j=1}^{N_i} \frac{t_{ij}-1}{p_{ij} t_{ij}} V_{ij}^2 \\
&\quad + m \sum_{i=1}^M \frac{n_i-1}{p_i n_i} V_i^2 + m(m-1) (\sum_{i=1}^M V_i) (\sum_{i'=1}^M V_{i'})] - V^2 \\
&= \frac{1}{m} \sum_{i=1}^M \frac{1}{p_i n_i} \sum_{j=1}^{N_i} \frac{1}{p_{ij} t_{ij}} \sum_{k=1}^{T_{ij}} \frac{V_{ijk}^2}{p_{ijk}} + \frac{1}{m} \sum_{i=1}^M \frac{1}{p_i n_i} \sum_{j=1}^{N_i} \frac{1}{p_{ij}} V_{ij}^2 \\
&\quad - \frac{1}{m} \sum_{i=1}^M \frac{1}{p_i n_i} \sum_{j=1}^{N_i} \frac{V_{ij}^2}{p_{ij} t_{ij}} + \frac{1}{m} \sum_{i=1}^M \frac{V_i^2}{p_i} - \frac{1}{m} \sum_{i=1}^M \frac{V_i^2}{p_i n_i} + V^2 - \frac{V^2}{m} - V^2
\end{aligned}$$

Finally, by rearranging terms and factoring, we have

$$\begin{aligned}
&\text{Var}(v) \\
&= \frac{1}{m} \sum_{i=1}^M \frac{V_i^2}{p_i} - \frac{V^2}{m} + \frac{1}{m} \sum_{i=1}^M \frac{1}{p_i n_i} \sum_{j=1}^{N_i} \frac{V_{ij}^2}{p_{ij}} - \frac{1}{m} \sum_{i=1}^M \frac{V_i^2}{p_i n_i} \\
&\quad + \frac{1}{m} \sum_{i=1}^M \frac{1}{p_i n_i} \sum_{j=1}^{N_i} \frac{1}{p_{ij} t_{ij}} \sum_{k=1}^{T_{ij}} \frac{V_{ijk}^2}{p_{ijk}} - \frac{1}{m} \sum_{i=1}^M \frac{1}{p_i n_i} \sum_{j=1}^{N_i} \frac{V_{ij}^2}{p_{ij} t_{ij}} \\
&= \frac{1}{m} \left( \sum_{i=1}^M \frac{V_i^2}{p_i} - V^2 \right) + \frac{1}{m} \sum_{i=1}^M \frac{1}{p_i n_i} \left( \sum_{j=1}^{N_i} \frac{V_{ij}^2}{p_{ij}} - V_i^2 \right) \\
&\quad \text{1st stage} \qquad \qquad \qquad \text{2nd stage} \\
&\quad + \frac{1}{m} \sum_{i=1}^M \frac{1}{p_i n_i} \sum_{j=1}^{N_i} \frac{1}{p_{ij} t_{ij}} \left( \sum_{k=1}^{T_{ij}} \frac{V_{ijk}^2}{p_{ijk}} - V_{ij}^2 \right) \\
&\quad \qquad \qquad \qquad \qquad \qquad \qquad \text{3rd stage}
\end{aligned}$$

## Derivation of the Estimate of the Variance

It was stated earlier (in Appendix A) that regardless of the number of stages in variable probability sampling, an unbiased estimate of  $\text{Var}(v)$  can be obtained from the estimates at the first stage. The formula may be written as

$$\widehat{\text{Var}}(v) = \text{var}(v) = \frac{1}{m(m-1)} \left( \sum_{i=1}^m \frac{v_i^2}{p_i} - mv^2 \right) \quad (35)$$

in which,

$v$  is the estimated population total obtained by pps sampling,

$v_i$  is the estimated total of the  $i^{\text{th}}$  first stage unit,

$p_i$  is the probability of selecting the  $i^{\text{th}}$  first stage unit, and

$m$  is the number of primary units in the sample.

The proof of equation (35) is given below for two-stage variable probability sampling to illustrate the principle, i.e.

$$\begin{aligned} E[\widehat{\text{Var}}(v)] &= E \left[ \frac{1}{m(m-1)} \left( \sum_{i=1}^m \frac{v_i^2}{p_i} - mv^2 \right) \right] \\ &= \frac{1}{m(m-1)} E \left[ \sum_{i=1}^m \frac{v_i^2}{p_i} - \frac{1}{m} \left( \sum_{i=1}^m \frac{v_i}{p_i} \right)^2 \right] \\ &= \frac{1}{m(m-1)} E \left[ \sum_{i=1}^m \frac{v_i^2}{p_i} - \frac{1}{m} \left( \sum_{i=1}^m \frac{v_i}{p_i} + \sum_{i \neq i'} \frac{v_i}{p_i} \frac{v_{i'}}{p_{i'}} \right) \right] \\ &= \frac{1}{m(m-1)} E \left[ \left( \frac{m-1}{m} \right) \sum_{i=1}^m \frac{v_i^2}{p_i} - \frac{1}{m} \sum_{i \neq i'} \frac{v_i}{p_i} \frac{v_{i'}}{p_{i'}} \right] \end{aligned}$$

$$= E\left[\frac{1}{m^2} \sum_{i=1}^m \frac{v_i^2}{p_i} - \frac{1}{m^2(m-1)} \sum_{i \neq i'}^m \frac{v_i v_{i'}}{p_i p_{i'}}\right]$$

Substituting the second stage estimates for the  $v_i$ 's, we have

$$\begin{aligned} E[\text{var}(v)] &= E\left\{E_i\left[\frac{1}{m^2} \sum_{i=1}^m \frac{1}{p_i n_i} \left(\sum_{j=1}^{n_i} \frac{v_{ij}}{p_{ij}}\right)^2\right.\right. \\ &\quad \left.\left.- \frac{1}{m^2(m-1)} \sum_{i \neq i'}^m \left(\frac{1}{p_i n_i} \sum_{j=1}^{n_i} \frac{v_{ij}}{p_{ij}}\right) \left(\frac{1}{p_{i'} n_{i'}} \sum_{j'=1}^{n_{i'}} \frac{v_{i'j'}}{p_{i'j'}}\right)\right]\right\} \\ &= E\left\{E_i\left[\frac{1}{m^2} \sum_{i=1}^m \frac{1}{p_i n_i} \left(\sum_{j=1}^{n_i} \frac{v_{ij}^2}{p_{ij}^2} + \sum_{j \neq j'}^{n_i} \frac{v_{ij} v_{ij'}}{p_{ij} p_{ij'}}\right)\right.\right. \\ &\quad \left.\left.- \frac{1}{m^2(m-1)} \sum_{i \neq i'}^m \left(\frac{1}{p_i n_i} \sum_{j=1}^{n_i} \frac{v_{ij}}{p_{ij}}\right) \left(\frac{1}{p_{i'} n_{i'}} \sum_{j'=1}^{n_{i'}} \frac{v_{i'j'}}{p_{i'j'}}\right)\right]\right\} \end{aligned}$$

We now take the conditional expectation of the second stage sample holding the first stage sample fixed.

$$\begin{aligned} &E\{E_i[\text{var}(v)]\} \\ &= E\left[\frac{1}{m^2} \sum_{i=1}^m \frac{1}{p_i n_i} E_i \frac{v_{ij}^2}{p_{ij}^2} + \frac{1}{m^2} \sum_{i=1}^m \frac{n_i-1}{p_i n_i} E_i \frac{v_{ij} v_{ij'}}{p_{ij} p_{ij'}}\right. \\ &\quad \left.- \frac{1}{m^2(m-1)} \sum_{i \neq i'}^m \left(\frac{1}{p_i} E_i \frac{v_{ij}}{p_{ij}}\right) \left(\frac{1}{p_{i'}} E_{i'} \frac{v_{i'j'}}{p_{i'j'}}\right)\right] \\ &= E\left[\frac{1}{m^2} \sum_{i=1}^m \frac{1}{p_i n_i} \sum_{j=1}^{N_i} \frac{v_{ij}^2}{p_{ij}^2} + \frac{1}{m^2} \sum_{i=1}^m \frac{n_i-1}{p_i n_i} \left(\sum_{j=1}^{N_i} v_{ij}\right) \left(\sum_{j'=1}^{N_{i'}} v_{i'j'}\right)\right. \\ &\quad \left.- \frac{1}{m^2(m-1)} \sum_{i \neq i'}^m \left(\frac{1}{p_i} \sum_{j=1}^{N_i} v_{ij}\right) \left(\frac{1}{p_{i'}} \sum_{j'=1}^{N_{i'}} v_{i'j'}\right)\right] \end{aligned}$$

$$= E\left[\frac{1}{m^2} \sum_{i=1}^m \frac{1}{p_i n_i} \sum_{j=1}^{N_i} \frac{v_{ij}^2}{P_{ij}} + \frac{1}{m^2} \sum_{i=1}^m \frac{v_i^2}{p_i} - \frac{1}{m^2} \sum_{i=1}^m \frac{v_i^2}{p_i n_i} - \frac{1}{m^2(m-1)} \sum_{i \neq i'}^m \frac{v_i}{p_i} \frac{v_{i'}}{p_{i'}}\right].$$

The unconditional expectation over all first stage samples is then

$$\begin{aligned} E[\text{var}(v)] &= \frac{1}{m} \sum_{i=1}^M \frac{1}{p_i n_i} \sum_{j=1}^{N_i} \frac{v_{ij}^2}{P_{ij}} - \frac{1}{m} \sum_{i=1}^M \frac{v_i^2}{p_i n_i} + \frac{1}{m} \sum_{i=1}^M \frac{v_i^2}{p_i} - \frac{v^2}{m} \\ &= \frac{1}{m} \left( \sum_{i=1}^M \frac{v_i^2}{p_i} - v^2 \right) + \frac{1}{m} \sum_{i=1}^M \frac{1}{p_i n_i} \left( \sum_{j=1}^{N_i} \frac{v_{ij}^2}{P_{ij}} - v_i^2 \right) \\ &\quad \text{1}^{\text{st}} \text{ stage} \qquad \qquad \qquad \text{2}^{\text{nd}} \text{ stage} \end{aligned}$$

Q.E.D.

END

## REFERENCES

- Aldred, A.H. 1971. A planning model for forest inventories based on combined photo and ground sampling methods. Ph.D. thesis, School of Forestry and Conservation, University of California, Berkeley, California. pp. 192.
- Cochran, W.G. 1963. Sampling techniques. Second edition. John Wiley & Sons, N.Y.
- Colwell, R.N. 1965. The extraction of data from aerial photographs by human and mechanical means. *Photogrammetria*, 20 (1965). pp. 211-228.
- Grosenbaugh, L.R. 1958. Point sampling and line sampling: probability theory, geometric implications, synthesis. USDA Forest Service, Southern For. Exp. Sta. Occas. Paper 160. pp. 34.
- Hansen, M.H. and W.N. Hurwitz. 1949. On the determination of the optimum probabilities in sampling. *Ann. Math. Statis.* 20. pp. 426-342.
- Langley, P.G. 1961. Can forest photo-interpretation be automated? *Amer. Soc Photogram., Columbia River Sect. Proc.* pp. 17-24.
- \_\_\_\_\_. 1971. Earth resources information systems using satellites, aircraft, and ground teams. *In Proceedings of the 21st International Astronautical Congress, Constance, West Germany.* pp. 819-829.
- \_\_\_\_\_. 1971. Multistage sampling of earth resources with aerial and space photography. *In Monitoring Earth Resources from Aircraft and Spacecraft.* NASA. SP-275, Washington, D.C. pp. 129-141.
- \_\_\_\_\_, R.C. Aldrich, and R.C. Heller. 1969. Multistage sampling of forest resources by using space photography - an Apollo 9 case study. Volume 2: Agr., Forest., and Sensor Studies. *Proc. 2nd Annual Earth Resources Aircraft Program Review*, pp. 19-1 to 19-21. NASA MSC, Houston, Texas.
- \_\_\_\_\_, D.A. Sharpnack, R.M. Russell, and J. van Roessel. 1970. The development of an earth resources information system using aerial photographs and digital computers. Report on Remote Sensing Applications in Forestry, Univ. of California, Berkeley, California, for Earth Resources Survey Program, OSSA, NASA.
- Murthy, M.N. 1967. Sampling theory and methods. Calcutta, Statistical Publishing House. 684 pp.

- Schreuder, H.T. 1966. Unequal probability and double sampling in forestry. Ph.D. thesis, Iowa State Univ., Amex. 139 pp. Univ. Microfilms, Ann Arbor, Michigan (Diss. Abstract 27:3739 B).
- Shiue, C.J. and H.H. John. 1962. A proposed sampling design for extensive forest inventory: double systematic sampling for regression with multiple random starts. J. Forest. 60. pp. 607-616.
- Wear, J.F., et al. 1964. Estimating beetle killed douglas-fir by aerial photo and field plots. J. Forest. 62. pp. 309-315.
- Wert, S.L. and B. Roettgering. 1968. Douglas-fir beetle survey with color photos. Photogrammetric Eng., December 1968. pp. 1243-1248.
- Zarkovic, S.S. 1964. On the efficiency of sampling with varying probabilities and the selection of units with replacement. Biometrika 3.